THE ROLE OF HYDROLOGICAL PROCESSES IN OCEAN-ATMOSPHERE INTERACTIONS

Peter J. Webster
Program in Atmospheric and Oceanic Sciences
University of Colorado
Boulder, Colorado

Abstract. Earth is unique among the planets of the solar system in possessing a full hydrological cycle. The role of water in the evolution of planetary atmospheres is discussed. As the atmospheres of the planets developed and modified the early climates of the planets, only the climate trajectory of Earth intercepted the water phase transitions near the triple point of water, thus allowing the full gamut of water forms to coexist. As a result, transitions between the water phases pervade the entire system and probably are responsible for the creation of a unique climate state. The interactions between the components of the climate system are enriched by the nonlinearity of the water phase transitions. The nonlinear character of the phase transitions of water suggests that the climate should be particularly sensitive to hydrological processes, especially in the tropics. Signatures of the nonlinearity are found in both the structure of the oceans and the atmosphere. Specific processes that determine the character of ocean-atmosphere interaction, including the role of ambient water vapor and clouds, the selective absorption of radiation by the ocean, the distribution of total heating in the ocean-atmosphere system, and the role of the flux of freshwater, are discussed in detail. Models of the ocean and atmospheric and oceanic data and models of the coupled system are used to perform systematic analyses of hydrological processes and their role in system interaction. The analysis is extended to consider the role of hydrological processes in the basic dynamics and thermodynamics of oceanic and atmospheric systems. The role hydrological processes play in determining the scale of the major atmospheric circulation patterns is investigated. Explanations are offered as to why large-scale convection in the tropical atmosphere is constrained to lie within the 28°C sea surface temperature contour and how hydrological processes are involved in interannual climate variability. The relative roles of thermal and haline forcing of the oceanic thermohaline circulation are discussed. Hydrological processes are considered in a global context by the development of a conceptual model of a simple planetary system. The constancy and maintenance of the very warm tropical sea surface temperatures are seen to be critical for the stability of climate. However, within the confines of the simplicity of the theory, the climate system, dominated by hydrological processes, conspires to maintain the temperature of the tropical warm pools.

1. INTRODUCTION

Earth appears in stark contrast to its inner solar system neighbors both in its abundance of water and in the multiple forms in which water is present on the planet. Earth exhibits a complex geographic configuration and a multifaceted and dynamic climate structure. In addition to large land masses, the surface of the planet exhibits vast reservoirs of water and large expanses of ice. In the atmosphere, large evolving areas of clouds appear at many heights through its deep structure. Moreover, the movement of the clouds indicates a wide range of dynamic and thermodynamic timescales ranging from diurnal to interannual and motions that link geographically remote regions.

The climate system of Earth can be broken down into a number of components: the ocean, the atmosphere, the lithosphere, the cryosphere, and the biosphere. The biosphere is considered to be an important component of the climate system as it possesses the ability to modify the climate of the Earth, especially by changing the surface characteristics of the planet, the gaseous composition of the atmosphere, and the turbidity of the ocean. However, permeating all of the climate components is water. Water pervades all of the physical and dynamic structures within the Earth system through a myriad of hydrological processes.

The most rapid timescale of hydrological processes in Earth's climate system occurs in clouds. Clouds and the ambient water vapor mass, within which clouds reside, dominate the radiative budget of the planet. Clearly, accurate weather forecasting and climate modeling require a very careful simulation of these cloud processes. Yet the simulation and depiction of

8755-1209/94/94RG-01873$15.00

Reviews of Geophysics, 32, 4 / *November 1994*
pages 427–476
Paper number 94RG01873

clouds in models remain an elusive problem and the largest sources of errors. On longer timescales, details of the evolving dynamic and thermodynamic structure of the ocean must be considered in a description of climate variability. How the ocean and the atmosphere interact, though, and how higher-frequency hydrological processes rectify to help produce the observed lower-frequency climate are difficult to understand. Furthermore, in attempts to assess the impact of the anthropogenic increase of CO_2 on the global climate, it is the role of water that remains the greatest mystery. In an increased CO_2-induced climate change, only water has the potential of enhancing or mitigating global warming. A warming atmosphere would lead to an increase of water vapor (from increased evaporation) and an enhancement of the greenhouse effect. By increasing the emission of infrared radiation, water vapor, thus enhanced, would lead to further warming and an increased thermal emission. On the other hand, a warming planet may lead to an increase of cloudiness that, in turn, would modulate the global temperature by an increased reflection of solar radiation. Thus net radiative effects of an increase in CO_2 remain uncertain. However, what is certain is that hydrological processes stand at the center of the climate of the Earth system.

The central theme of this paper is to discuss the influence of hydrological processes on the interaction of the components of the climate system and on their functional role in stabilizing the climate state. There will be considerable concentration on processes that occur in the tropical regions. This emphasis arises from the nonlinear properties of water (section 3) that suggest the signal of hydrological processes will be easiest to discern where the temperature is warmest and also because of the large amount of data that exist at the tropical ocean-atmosphere interface. At the same time, there is considerable speculation on the role of hydrological processes at higher latitudes in influencing deepwater formation in the different ocean basins and determining the deep low-frequency, interbasin circulation. These global roles of hydrological processes will be discussed in section 7.

The tropical regions of Earth possess the warmest sea surface temperatures (SSTs), the deepest atmospheric convection, the most copious precipitation, and, some 17 km above the surface, the coldest air temperatures on the planet. Within the tropics, strong radiative and latent heating gradients exist that drive vigorous circulations. Between the equator and the poles the ocean and the atmosphere are connected over wide spatial and temporal scales by fluxes of heat, water, and momentum. It will be argued that probably all of these features result directly from hydrological processes. In particular, the equator-to-pole heating gradients are magnified by the nonlinear properties of water.

In section 2 of this paper, the hydrological characteristics of Earth and its planetary neighbors are discussed. In section 3 the fundamental physical properties of water and their impact on planetary atmosphere evolution are considered. In section 4, geophysical signatures of hydrological processes are sought in both the ocean and the atmosphere. In section 5 the generic classes of interaction between the ocean and the atmosphere are discussed. A detailed description of the processes involved in the interaction of the ocean and the atmosphere is considered in section 6. A simple model of the upper ocean and a comprehensive ocean-atmosphere data set obtained from the recent Tropical Ocean–Global Atmosphere Coupled Ocean-Atmosphere Response Experiment (TOGA COARE) [*Webster and Lukas*, 1992] held in the tropical western Pacific Ocean are used. The role that moist processes play in oceanic and atmospheric dynamics and especially how these processes determine scales of motion and the basic character of such phenomena as the monsoons and the equatorial Walker Circulation [see *Webster*, 1983b] are considered in section 7. Finally, the hypothesis is posed that the climate regime of the Earth and the stability of its climate are determined by the coexistence of the three forms of water (vapor, liquid, and ice) on the planet. Furthermore, the notion is advanced that in the very long term the abundance of the three phases of water on planet Earth acts as a climatic governor or stabilizer, restricting Earth's climate to remain within fairly narrow bounds.

2. WATER IN THE SOLAR SYSTEM

Two thirds of Earth's surface area is covered by ocean, and at any one time over half of the planet is covered with cloud. The polar regions are dominated by vast areas of permanent ice, and, globally, water vapor is an abundant constituent of the atmosphere. About 80% of the freshwater on the planet is in ice form [*Untersteiner*, 1984]. Sea ice in both hemispheres waxes and wanes seasonally. For example, the sea ice extent in the southern hemisphere changes from a summer minimum of about 2.5×10^6 km^2 to 15×10^6 km^2 in winter. In its myriad forms, water permeates the thermodynamic and dynamic structure of the planet and imparts an indelible signature on the climatic structure.

Earth is not the only planet in the solar system to possess water but is unique because of the total amount of water and the coexistence of the three phases of water over the entire planet. Only Earth possesses vast reservoirs of liquid water and regions of surface ice both over the continents and the oceans. Water vapor is an important constituent of the atmosphere ($\approx$1% by mass) and is the only atmospheric constituent that changes phase in the range of conditions existing on Earth. Besides water vapor, suspended ice and liquid droplets coexist in clouds.

TABLE 1. Physical Properties of the Inner Planets

	Mercury	*Venus*	*Earth*	*Mars*
		Specifications		
Planetary mass, 10^{23} kg	3.4	48.7	59.8	6.43
Planetary radius, km	2439	6049	6371	3390
Gravitation, m s^{-2}	3.8	8.9	9.8	3.7
Solar distance, 10^6 km	58	108	150	228
Solar irradiance, W m^{-2}	9200	2600	1393	596
		State		
Mean surface temperature, K	442	700	288	210
Mean planetary albedo, %	6	71	33	17
Surface pressure, hPa	0	7900	1010	6
		Atmospheric Composition, %		
CO_2	0	95	3×10^{-2}	>50
N_2, A	0	<5	79	<50
O_2	0	$<4 \times 10^{-3}$	21	1×10^{-1}
H_2O	0	1×10^{-2}	1	≤1.0E − 1
HCl	0	1×10^{-4}	0	0
HF	0	2×10^{-6}	0	0
CO	0	2×10^{-2}	1×10^{-5}	1×10^{-1}
		Water Disposition, kg		
Atmospheric mass	0	4.2×10^{20}	5.3×10^{18}	2.4×10^{16}
Liquid	0	0	1.4×10^{21}	0
Ice	0	0	4.3×10^{19}	$1. \times 10^{17}$
Gas	0	4.2×10^{16}	1.6×10^{16}	2×10^{13}

Though water exists on Earth in all phases, the majority of the total mass of water is in liquid form. The liquid water content of the system is three orders of magnitude greater than the mass of the total atmosphere (Table 1).

Water is also present on Venus and Mars [*Hartmann*, 1983; *Lewis and Prinn*, 1984]. On Mars, water vapor is an atmospheric constituent and water ice (together with solid CO_2) occurs permanently in the northern hemisphere polar cap and, possibly, in the form of permafrost below the surface of the planet. Water vapor exists on Venus probably with a mass equivalent to that in Earth's atmosphere. However, when all the phases of water are taken into account, Venus's water mass is smaller than Earth's by about 5 orders of magnitude (Table 1). In fact, the vastness of Earth's liquid reservoir can be appreciated by noting the equivalent surface pressure that would result if the oceans were to evaporate. Simple calculations from Table 1 show that the oceans are equivalent to about 1000 Earth atmospheres.

Earth's diverse water forms appear to be of fundamental importance to the planet's climate. Water acts as the major modifier of the planetary radiation balance by influencing both the infrared and shortwave radiative fluxes (see sections 4 and 6 for quantitative assessments). Cloud liquid water and ice act as the major scatterers and reflectors of solar radiation and, with atmospheric water vapor, absorb efficiently in the infrared range. Clouds and the developing biosphere were responsible for raising the albedo of Earth from its primitive levels. Without these factors the albedo of Earth might be similar to that of Mars (0.17) rather than the current value of about 0.3.

Atmospheric water vapor is the major greenhouse gas on the planet. With the other major greenhouse gases (CO_2, CH_4, and O_3) and the infrared absorption by liquid water and ice in clouds, water vapor is responsible for increasing the surface temperature of the planet and modulating diurnal temperature variations [e.g., *Paltridge and Platt*, 1976].

The collective albedo and greenhouse effects of clouds and gases produce a global average surface temperature of Earth that is greater than the freezing point of water. By remaining above freezing, the oceans retain their fluid characteristics which allow heat stored deeply in the oceans to ameliorate the global climate on extremely long timescales. Thus perhaps through the agency of water in its many forms, the mean temperature of Earth has remained within rather narrow bounds. Without an abundance of water and the variety of its forms in the Earth system, the average global temperature would probably reside near to −10°C (i.e., 20°C less than present) and would probably replicate a somewhat warmer version of Mars.

The liquid and ice forms of water influence planetary climate in a variety of ways. Snow- and ice-covered regions possess large albedos; some $2\frac{1}{2}$ times larger than the global average surface albedo, which reduces the amount of solar radiation absorbed at the surface. The oceans, on the other hand, have a much

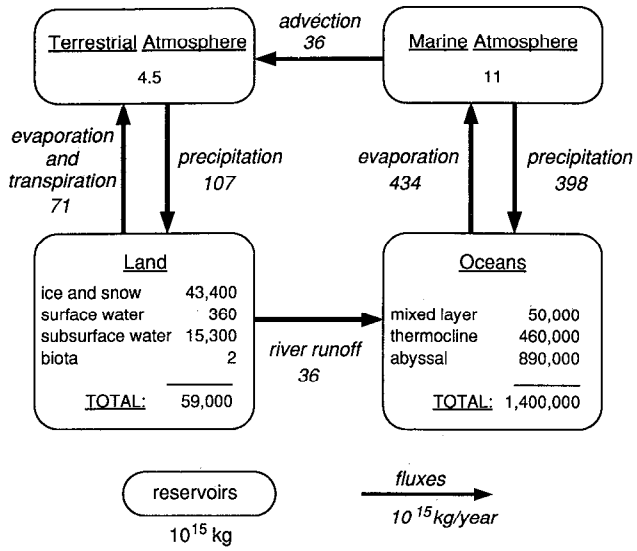

Figure 1. The global water cycle and the reservoirs of water. Arrows indicate fluxes of water from one reservoir to another. Note that water in the atmosphere over the ocean and the land accounts for only 0.0001% of the total water in the system. Data are from *Chahine* [1992].

lower albedo and thus absorb solar radiation more readily than the more highly reflecting continental regions. Furthermore, oceans store vast quantities of heat both by possessing a higher heat capacity than the land areas and by being able to mix heat downward through convective and turbulent processes. The impact of the ocean heat storage is to build a thermal lag into the planetary climate system. For example, extrema in the annual cycle temperature of the upper ocean occur nearly 3 months after the solstices. Over land the extrema in surface temperature lag by only a few weeks. Sea ice also insulates the ocean from the atmosphere, thus slowing down their dynamical and thermodynamical interaction [*Untersteiner*, 1984]. Thus sea ice, although it is an efficient reflector of solar radiation, also minimizes the cooling of the polar ocean.

The existence of the oceans on the Earth appears to be a critical factor in determining the character of its climate. Without abundant liquid water both Mercury and Mars have climates that are very strongly tied to an instantaneous radiation balance with outer space. This results in a diurnal temperature variation that is far greater than on Earth. Earth has a climate system that is tempered both by the strong greenhouse atmosphere and by the heat stored within the oceans. However, this longer-term memory can only be realized if the stored heat is accessible. Accessibility depends on the oceans remaining liquid. It will be argued later that the narrow physical bounds within which Earth resides, and within which the stored heat remains accessible, are the result of the proximity of Earth to the triple point of water.

Figure 1 (adapted from *Chahine* [1992]) shows the main reservoirs of water in the Earth system and the fluxes of water between these reservoirs. The atmosphere contains only about 0.001% of the total water in the system, mainly in vapor form. The oceanic water content exceeds land water by a factor of 30. About half of the land-based water is subterranean. Assuming that the land areas constitute 30% of the surface area of the planet, the oceanic rain rate is about 25% greater than over land. Furthermore, over the ocean, evaporation exceeds, but almost balances, precipitation. The loss of net water vapor over the oceans is balanced by river runoff.

The data in Figure 1 allow the calculation of residence times of water in the various reservoirs. The total evaporation over the oceans is 434 pkg resulting from a global evaporation average of 1.2 m yr^{-1} from the world's oceans. Using the value of mass of liquid water from Table 1, the residence time of water in the oceans is about 3000 years. The atmospheric residence time (mass of water vapor divided by total precipitation) is about 11 days. That is, the atmosphere recycles its water over 30 times per year. Surface water over land has a residence time of about 5 years, although the residence time for soil moisture is about 1 year.

The residence times calculated from the data in Table 1 and Figure 1 can be misleading. For example, not all parts of the ocean recycle at the same rate. In the ocean surface layers the timescales may be much more rapid, perhaps of the order of days to weeks in highly convective regions of the tropical warm pools. However, deep bottom water may take thousands of years to recycle [e.g., *Woods*, 1984]. Furthermore, the residence time of ice is about 6000 years. However, this does not indicate the timescales of sea ice that evolve on annual and decadal timescales. In the Arctic, sea ice has a recycling time of 1–6 years, while in the Antarctic it is about 1 year [*Untersteiner*, 1984]. The total residence time for global ice (i.e., 6000 years) is strongly biased by the slow evolution of land ice, particularly in Antarctica and Greenland.

In summary, whereas the data contained in Figure 1 are informative, it does not help us understand the physical processes involved in the transfer of water from one reservoir to another or explain how the various reservoirs are maintained in their observed state. To help answer these questions, the hydrological cycle is considered using fundamental governing laws.

3. CLAUSIUS-CLAPEYRON AND PLANETARY EVOLUTION

Figure 2a shows phase transitions of water as a function of temperature and partial pressure. The solid lines represent temperatures and water vapor partial pressures where two water phases coexist in equilib-

rium. The triple point of water occurs where the three phase lines of water meet and where all phases of water coexist in equilibrium. Important phase transitions occur at the surface of the planet between the ocean and the atmosphere, the ocean and the sea ice, and the ice and the atmosphere. The triple point of water exists in all atmospheric columns on the Earth, except perhaps in the polar regions during winter.

The complexity of hydrological processes in the Earth system is evident from the nonlinearity of the phase equilibrium lines. For example, the phase transition between liquid and vapor increases in an exponential fashion with temperature. The Clausius-Clapeyron equation that describes the nonlinear dependency of the saturated vapor pressure e_s on temperature T may be written as [e.g., *Wallace and Hobbs*, 1977]

$$\frac{d \ln e_s}{dT} = \frac{L_{c,s}}{R_v T^2} \tag{1}$$

where L_c and L_s are the latent heats of evaporation and sublimation, respectively. R_v is the specific gas constant for water vapor. If it is assumed that the parameters $L_{c,s}$ are constant with temperature (L_c actually varies by about 10% over the temperature range 0° to 100°C), (1) can be solved to give an expression for the saturation vapor pressure over liquid water or an ice surface as a function of temperature, that is,

$$e_s(T) = e_s(T_0) \exp\left[\frac{L_{c,s}}{R_v}\left(\frac{1}{T_0} - \frac{1}{T}\right)\right], \tag{2}$$

where $e_s(T_0)$ is the saturation vapor pressure at temperature T_0. Equation (2) shows that the saturation vapor pressure is only a function of temperature and increases almost exponentially with increasing temperature. This nonlinear thermodynamic effect, often referred to as the Clausius-Clapeyron effect, will be shown to be of fundamental importance to the climate of Earth.

The nonlinearity of water phase transitions may also have been crucial in setting the climatic regimes of each of the inner planets. *Goody and Walker* [1972] argued that prior to the evolution of an atmosphere, the initial surface temperature of a planet would be the same as the equivalent blackbody temperature of the planet. This primitive temperature of Earth is given by

$$T_E = \left(\frac{S_0(1-a)}{4\sigma}\right)^{1/4} \tag{3}$$

where S_0 is the solar irradiance (in watts per square meter), a is the planetary albedo of the primitive planet (i.e., before the development of a water mass capable of producing a biosphere, oceans, and clouds), and σ is the Stefan-Boltzmann constant (5.67×10^{-8} W m^{-2} K^{-4}). T_E may be thought of as the radiating

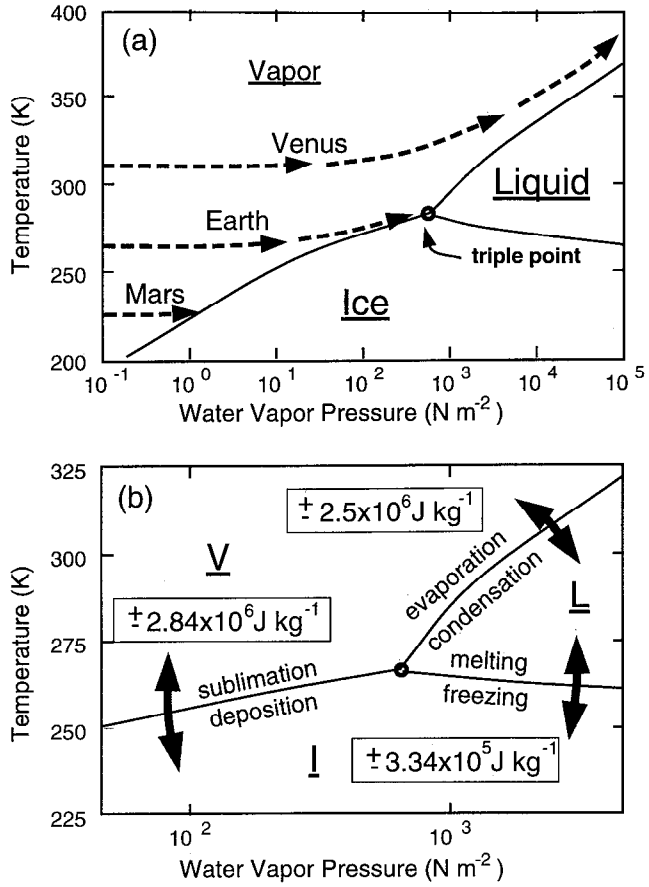

Figure 2. (a) The phases of water as a function of the partial pressure and temperature. The solid curves are the phase transition curves between water, vapor, and solid phases, defined by (1) and (2). The triple point of water occurs where the three phases of water coexist in equilibrium. The dashed curves are hypothetical climate trajectories of Venus, Earth, and Mars as they may have evolved through time [*Rasool and de Bergh*, 1970]. The trajectories emanate from the primitive effective temperatures of the planets defined in (3). As an atmosphere develops on each planet, the climate is constrained by interception of the climate trajectory with a phase transition line and the radiative properties of the developing atmosphere. (b) The water phase diagram in the vicinity of the triple point of water and within the physical parameters define Earth. Six possible phase transformations of water and their associated transitional or latent energies occur on Earth.

temperature of the planet calculated by simply setting the total incoming solar energy equal to the blackbody emission of the planet (i.e., $\pi r^2 S(1-a) = 4\pi r^2 \sigma T_E^4$). Assuming that a planetary atmosphere evolves through the volcanic outgassing, the partial pressure of water vapor is presumed to increase with time, allowing the atmosphere to become more absorbing of outgoing surface radiation. Downward reradiation of this absorbed radiation toward the planetary surface creates an atmospheric greenhouse effect. Thus as the atmospheres of the primitive planets evolved, the surface of the planet slowly warmed. The evolution of the

atmospheres of Venus, Mars, and Earth, according to this simple model, is shown in Figure 2a.

As the water vapor concentration increases, secondary effects also influence the planetary climate trajectories. For example, the planetary albedo could increase with the formation of liquid water droplets or highly reflective ice in the atmosphere. Ultimately, though, the basic climate regime is determined by whether or not the planetary climate trajectories collide with a Clausius-Clapeyron phase transition curve. In this simple conceptual model, Venus missed all phase transition lines and evolved to its present state as a water vapor–driven "runaway" greenhouse planet [*Rasool and De Bergh*, 1970]. Mars, on the other hand, collided with the vapor-ice transition line so that subsequent water vapor added to the atmosphere would be in ice form. The trajectory of Earth, though, encounters the phase transition lines near the triple point of water.

Proximity to the triple point substantially increases the degrees of freedom of Earth's climate. In the case of Mars, water transitions are limited to either vapor or ice such that the only processes possible are deposition (vapor to ice) and sublimation (ice to vapor). The situation is slightly more complicated because sublimation and deposition of carbon dioxide is also possible. About 10% of the atmospheric mass deposits at the winter pole. Together with the strong surface heating of the large orographic features, the CO_2 mass source and sink forces a vigorous annual cycle on Mars [*Webster*, 1977]. However, on Earth there are two other phase transitions possible, giving a total of six thermodynamic phase transitions. In addition to sublimation and deposition, there are freezing, melting, evaporation, and condensation. Figure 2b shows the possible water phase transitions on Earth. These added degrees of freedom of water state have a number of major effects. First, there is substantial heating (cooling) of the medium as transitions from a higher to a lower (lower to higher) phase state occur. Second, the three phases of water impinge substantially on the shortwave and longwave radiative streams of the planet. Third, the liquid and solid phases of water add variability to the fluid dynamical structure of the system.

Given a specific atmospheric composition, it is the mass of the planet and its distance from the Sun that determine the final mass and disposition of water on the planets [*Goody and Walker*, 1972; *Kastings*, 1988]. The solar distance and the planetary albedo determine the primitive temperature of the planets and, to a large degree, the kinetic velocity distribution of each constituent gas. On the other hand, the mass of the planet determines the velocity required for a molecule or atom, under the action of gravity, to escape the planet's gravitational field. As the mean kinetic velocity distribution of light gases (e.g., H, He) is greater than heavier gases (e.g., N_2, O_2) for a given temperature, it is expected that the smaller planets closest to the Sun will shed their lightest gases first. Mercury is sufficiently small and so close to the Sun that all gases have been shed. Earth, on the other hand, is far enough from the Sun and sufficiently large that it can retain all of its atmospheric constituents except, perhaps, hydrogen [*Goody and Walker*, 1972]. As water vapor will be photodissociated by ultraviolet radiation in the upper atmosphere, it should be expected that a continual diminution of hydrogen to space would occur, constituting a sink of water for the planet. However, Earth appears to retain a stable water content.

As a planetary atmosphere develops, the temperature defined in (3) changes its meaning. The equation now defines the infrared radiating temperature of the planet, or the effective temperature. As the albedo of the planet has increased since the time of formation, the effective temperature will have decreased from its primitive values.

Finally, it should be mentioned that the volcanic outgassing theory for the source of water possesses some problems. From Table 1 the necessary rate of outgassing to explain the present total water mass would be about 3×10^{11} kg yr^{-1}. However, present rates of water outgassing are estimated to be about 2 orders of magnitude greater. Thus, assuming that present volcanic activity is representative of the entire life of the planet (probably a serious underestimate), the present hydrosphere is about 2 orders of magnitude smaller than it should be. However, this estimate ignores the recycling of water back into the solid earth through leakage in the deep ocean trenches. Whereas most of this water will be eventually outgassed through volcanoes, it is possible that some of the water is stored within the Earth's crust by binding into the rock matrix in hydrous minerals. Also, it assumes that the loss of water through photodissociation is linear with time. Perhaps in a less dense primitive atmosphere the loss may have been substantially greater. The maintenance of Earth's water mass is discussed in section 7.4.3.

4. SIGNATURES OF HYDROLOGY IN THE EARTH SYSTEM

The Clausius-Clapeyron relationship (equation (1)) states that the saturation vapor pressure is only a function of temperature. The global distribution of water vapor is determined by the distribution of the sources and sinks of water vapor which occur when dynamic and thermodynamic influences (e.g., radiative heating or cooling) cause an encounter with the phase transition curves shown in Figure 2. Here geophysical signatures of the hydrological cycle in the Earth's climate are sought. Both the ocean and the atmosphere are examined.

The modulation of atmospheric climate by the

ocean arises from thermal and dynamic properties and processes within the ocean. If the ocean were immobile, only the surface characteristics of the ocean would be important to the atmosphere and the modulation of the climate would only be a function of the ratio of the heat capacities per unit mass of the atmosphere and ocean which differ by a factor of 4. As the transfer of heat downward in these circumstances could only be accomplished by slow conductive processes, such an ocean would appear to be something like a slowly evolving swamp. However, as the real ocean has the ability to mix vertically through advective and turbulent processes, the mass of ocean that actually influences the atmosphere is determined by the oceanic vertical mixing scales. On annual timescales the vertical mixing scale of the tropical oceans is of the order of 50–100 m. On the timescale of hundreds to thousands of years the vertical mixing is throughout the entire depth and extent of the global ocean, of order 4–5 km [*Woods*, 1984]. Thus the difference in the effective heat capacities of the ocean and the atmosphere is very much greater than the ratio of the specific heats of air and water. In fact, the difference extends to many orders of magnitude even if the entire mass of the atmosphere is taken into account. Thus it is equally important that subsurface characteristics of the ocean are discussed as well as those of the ocean surface.

4.1. Atmospheric Signatures

Figure 3 plots the vertical distribution of water vapor at different latitudes. The Clausius-Clapeyron relationship is evident in the structure of all atmospheric columns irrespective of location. Even in winter, the surface vapor pressure in the tropics is almost a factor of 2 greater than that in the middle latitudes and an order of magnitude greater than in the polar regions. What is interesting is that all of the environmental curves are parallel to the saturated vapor pressure curve (dotted line). Thus even though the parcels are not saturated, their water vapor content follows the shape of the Clausius-Clapeyron vapor-liquid curve.

The implications of the strong temperature dependency of atmospheric water vapor pressure are important from both radiative and latent heating perspectives. Atmospheric radiative absorption is a strong function of water vapor, and the liquid water and ice concentration in clouds and infrared emission depends on the concentration and temperature of the absorbing gas or substance. The single scattering properties of cloud particles (i.e., optical depth, single scattering albedo, and phase function) are a function of the amount of condensed water phase (i.e., solid or liquid) and particle size distribution. Collectively, these factors determine the albedo and emissivity of the atmosphere. Thus, from the moisture distributions shown in Figure 3, the radiative effects of water in the atmosphere may be expected to possess a strong geographical bias determined principally by the variation of temperature on the planet.

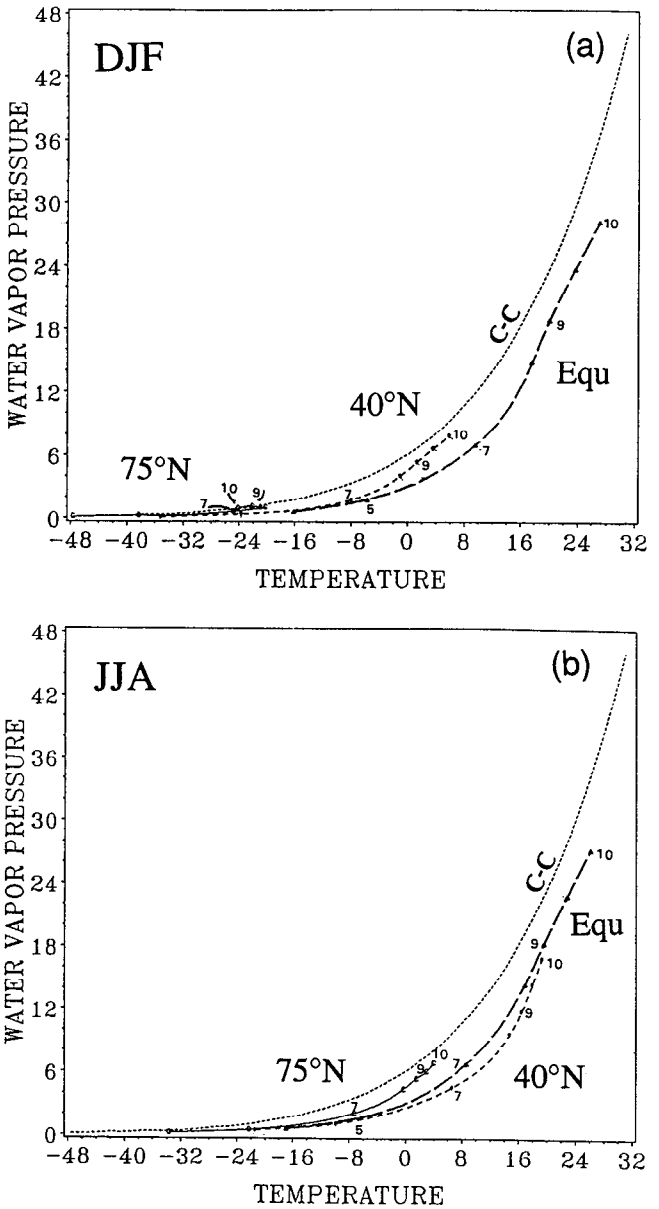

Figure 3. Atmospheric vapor pressure (in millibars) as a function of temperature (in degrees Celsius) for mean atmospheres located at the equator (large dashes), 40°N (small dashes), and 75°N (solid curve) as a function of pressure levels in the vertical (marked in hundreds of millibars on curves) for (a) the boreal winter December-January-February (DJF) and (b) the boreal summer June-July-August (JJA). The dotted curve (marked C-C) is the Clausius-Clapeyron saturation vapor pressure curve. Note how the environmental curves are consistently parallel to C-C at all temperatures.

Thermodynamic considerations suggest that the amount of latent heat released in lifting a saturated parcel of air through a column is a function of the initial temperature of the saturated parcel [e.g., *Wal-*

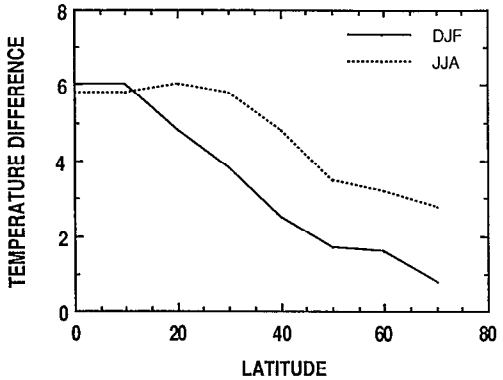

Figure 4. The temperature difference occurring between saturated moist ascent and dry adiabatic ascent for a parcel lifted 1 km from 900 mbar. The temperature difference is plotted as a function of latitude. Climatological temperature values are used as initial data. Profiles are shown for the boreal winter (DJF; solid curve) and summer (JJA; dotted curve). The large differences at low latitudes compared to higher latitudes are due to the exponential increase of saturated vapor pressure as a function of temperature and hence latitude. The nonlinear properties of water allow 5 times the temperature gain for the same amount of work in lifting a tropical air parcel compared to a polar parcel through the same height.

lace and Hobbs, 1977]. From Figure 3 it can be seen that if a tropical parcel, initially residing in the lower troposphere, is raised 1 km in the vertical, the amount of latent heat released will be very much greater than for the same vertical displacement of a parcel of saturated air at higher latitudes. These latitudinal differences follow from the Clausius-Clapeyron relationship (Figure 2), which governs the shape of the saturated vapor pressure curve as a function of temperature. Figure 4 shows the net temperature increase (i.e., the moist adiabatic temperature change minus the adiabatic cooling) for saturated parcels initially residing at 900 mbar that are raised vertically by 1 km. The relative temperature changes induced by the latent heat release for an equivalent amount of work in raising an air parcel the same vertical distance are at least a factor of 2 larger in the tropics than in the middle latitudes. By extension of these thermodynamic arguments, it can be expected that convection in the warm pool regions of the tropical oceans will be deeper and more intense and associated with the greater rainfall than convection at higher latitudes.

Figure 5 shows the latitudinal distribution of vertically integrated water vapor and the cloud liquid ice water in nonprecipitating clouds extracted from the Special Sensor Microwave Imager (SSM/I) satellite data of August 1987 [*Greenwald et al.*, 1993]. The latitudinal distributions of the two water forms are very different. For the most part the integrated water vapor distribution almost follows the saturation vapor pressure curve associated with the sea surface temperature [*Stephens*, 1990]. Note, though, where the SST is between 18° and 23°C, and also at higher latitudes, the total integrated water vapor is slightly depressed, indicating that other influences are acting to move the curve away from thermodynamic equilibrium. Dynamic influences produce atmospheric subsidence in the subtropical high-pressure belt, and the resultant lower tropospheric inversion does not permit moisture to be mixed throughout the troposphere.

The liquid water–ice concentration, on the other hand, is almost independent of SST and appears to be determined by the atmospheric circulation. The peaks in the liquid water distribution are associated with net

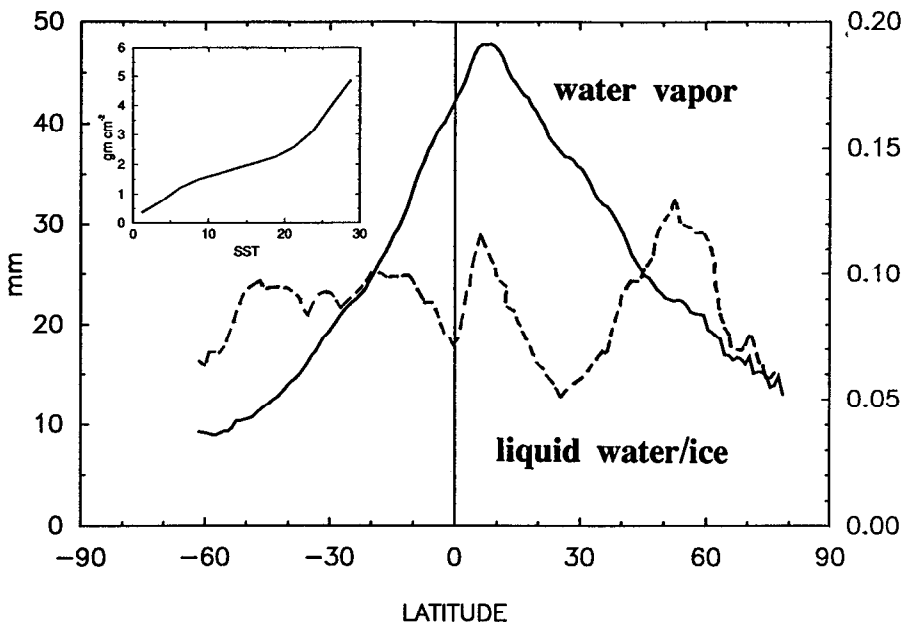

Figure 5. Satellite estimates of the total liquid water content in vapor form (solid curve; in millimeters) and liquid and ice form (dashed curve; in millimeters) as a function of latitude [*Greenwald et al.*, 1993]. All forms of water derived from the satellite data are transformed into equivalent liquid state for easy comparison. Water vapor almost follows the sea surface temperature (SST) distribution, as shown in the inset [*Stephens*, 1990]. The liquid and ice forms are correlated with atmospheric circulation features.

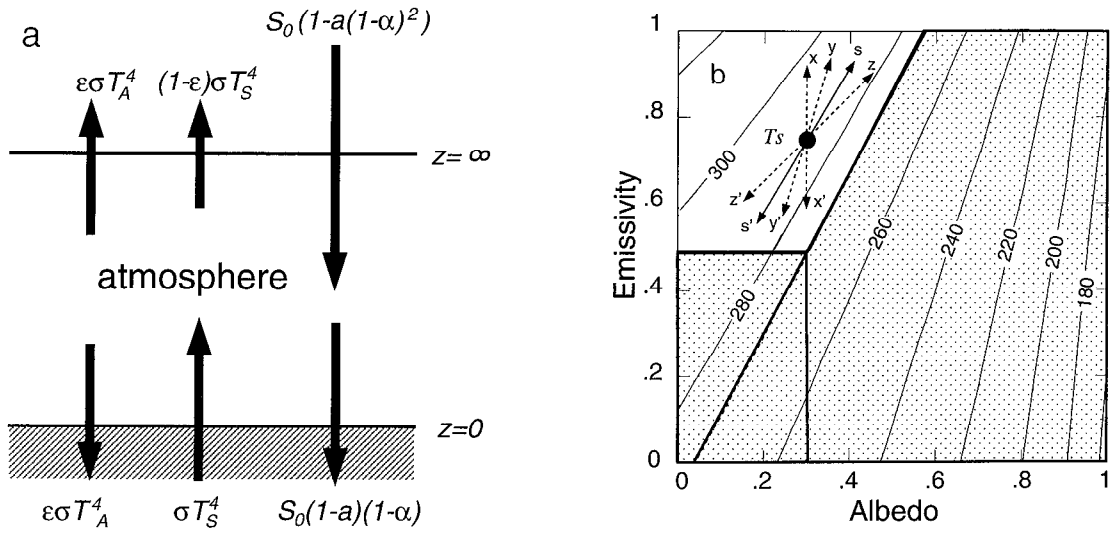

Figure 6. (a) Radiative structure of a simple gray atmosphere of emissivity ε, albedo a, and solar absorptivity α. The arrows indicate the net shortwave and longwave radiative fluxes at the surface and the top of the atmosphere. T_s and T_A are the ground and atmospheric temperatures, respectively. (b) The surface radiative temperature T_s as a function of albedo a and emissivity ε. The stippled region to the right of the diagonal solid line (the 273 K isotherm) denotes the values of albedo and emissivity for which the mean radiative surface temperature would be less than the freezing point of water. Using the generally accepted value of planetary albedo of 0.3, the results show that the emissivity must be greater than 0.5 for the mean radiating temperature of Earth to be greater than freezing. A mean planetary emissivity of 0.75 and a planetary albedo of 0.3 give a mean global radiative temperature of 284 K. A value of 10% is used for the solar absorptivity. The arrows indicate various temperature trends associated with various albedo-emissivity scenarios described in the text.

rising motion in the intertropical convergence zone (ITCZ) [see *Webster*, 1983b] and the belt of extratropical cyclonic storms, both of which are characterized by strong vertical motions. The adiabatic cooling associated with rising air parcels induces saturation and increases the liquid water concentration in the atmosphere. However, the system is highly nonlinear because these same vertical motions depend on the release of latent heat. Thus while phase change and latent heating in the atmosphere are the result of the dynamic convergence of the water vapor, the convergence itself is dependent on heating.

The various forms of water influence climate in different ways. For example, all forms of atmospheric water warm the atmosphere by infrared absorption. However, cloud liquid and ice water tends to cool the atmosphere by the reflection of solar radiation. The net radiative impact of water may be shown using a simple model (Figure 6a) of the long-term mean radiative balance of the planet. Consider a single-layer absorbing atmosphere of temperature T_A, infrared emissivity ε, infrared transmission $(1 - \varepsilon)$, and shortwave absorptivity α. The atmospheric emissivity, or the degree to which the atmosphere emits infrared radiation, depends on the concentration of greenhouse gases in the atmosphere. Besides water (liquid, vapor, and ice) and CO_2, methane, nitrous oxide, ozone, and chlorofluorocarbons (i.e., CH_4, N_2O, O_3, and CFCs) are important greenhouse gases. For simplicity it is assumed that the albedo of the planet is represented by an average planetary albedo a. Furthermore, the planetary surface is assumed to be in radiative equilibrium at temperature T_s. The long-term mean radiation energy balances at the top of the atmosphere and at the planetary surface can be written as

$$\varepsilon\sigma T_A^4 + (1 - \varepsilon)\sigma T_s^4 - S_0(1 - a(1 - \alpha)^2) = 0 \qquad (4a)$$

$$\sigma T_s^4 - \varepsilon\sigma T_A^4 - S_0(1 - a)(1 - \alpha) = 0, \qquad (4b)$$

respectively [*Wallace and Hobbs*, 1977]. If S_0 is the globally averaged insolation (i.e., $S_0 = S/4$ or 345 W m^{-2}), then T_s is the global average surface radiative equilibrium temperature. Solving for T_s gives

$$T_s = \left\{ S_0 \frac{(1 - a)(1 - \alpha) + (1 - a(1 - \alpha)^2)}{\sigma(2 - \varepsilon)} \right\}^{1/4}. \qquad (5)$$

In the limit, when there is no atmosphere (i.e., α, ε = 0), the radiative surface temperature reduces to the effective temperature T_E defined in (3). However, when the planetary albedo is unity (i.e., $a = 1$), the surface temperature is nonzero even though the surface flux of solar radiation is zero. In this case, (4) reduces to $T_s^4 = \varepsilon T_A^4$, which shows that the surface temperature will be nonzero as long as the solar ab-

sorptivity and the longwave emissivity of the atmosphere are finite.

Figure 6b shows the mean global surface radiative equilibrium temperature as a function of planetary albedo a and atmospheric emissivity ε calculated from (4) and (5). The solar absorptivity is assumed to be 10% (i.e., $\alpha = 0.1$). In general, the radiative surface temperature tends to increase with increasing emissivity (e.g., greater water vapor concentrations) but decreases with increasing albedo (increased cloud or greater sea ice). Thus, for the mean surface temperature to remain above freezing, the albedo of the planet must be relatively low and the mean infrared emissivity rather high. Using the generally accepted value of $a = 0.3$, the emissivity must be greater than 0.5 for $T_s > 273$ K. In fact, using *Goody*'s [1964] estimate of global emissivity of 0.75, a mean planetary surface radiation temperature of 285 K results, which is fairly close to the observed average surface temperature value. However, small variations of emissivity or albedo will cause significant changes in temperature. The various phases of water thus tend to impose strong, but very different, controls on the radiative equilibrium of the planet.

It is not difficult to realize why the two cloud radiation parameters, the albedo a and emissivity ε, are related, as both cloud albedo and cloud emissivity increase with increasing cloud thickness. As these two radiative properties have the opposite effect on surface temperature, they tend to partially compensate each other. The degree and sign of the compensation are very important and are at the center of the problems of trying to understand the potential changes of climate in an atmosphere with increasing greenhouse gases such as CO_2. As the greenhouse gas–related emissivity increases, it is generally thought that the water vapor will also increase as a result of increased evaporation accompanying the initial radiative warming of the surface. In turn, the increase in water vapor will increase the atmospheric emissivity considerably and may increase cloud amount and thus planetary albedo. The final outcome of CO_2 increase, for example, depends on the emissivity and albedo response of the system. For example, if a remains constant as ε increases, the climate would follow trajectory $x - x'$ in Figure 6b, and a strong planetary heating would ensue. On the other hand, if the albedo were to increase as ε increases but at a rate less than the emissivity, the climate would follow trajectory $y - y'$, and a smaller warming would result. If the albedo were to increase faster than the emissivity, the climate would follow $z - z'$, and a slight cooling would occur. If the albedo were to exactly compensate for the increase in emissivity, then the mean planetary temperature would not change, and the climate would follow trajectory $s - s'$. Most climate models predict a slight warming somewhere between the $s - s'$ and $y - y'$ lines. However, such results generally depend on very crude parameterizations of radiative and physical properties of clouds in the models.

The actual infrared emittance to space is much more complicated than the integrated flux considered in the simple model. Top-of-the-atmosphere radiation is made up of a combination of emittances from the surface of the planet and from infrared absorbing materials in the atmosphere; principally, water vapor, ice, and liquid, and CO_2 and the other greenhouse gases listed earlier. If the column contains sufficient infrared absorbers, the emittance may just be from the absorbers in the column and would be representative of their temperature. On the other hand, if the column is particularly dry (e.g., over deserts or at high latitudes, in general) the emittance sensed at the top of the atmosphere may originate at the planetary surface.

Figure 7 shows the satellite-measured outgoing longwave radiation (OLR) distribution (in watts per square meter) for long-term winter conditions (December-January-February [*Yang and Webster*, 1990]). A minimum in OLR indicates emission by cold radiatively active gases or substances. A reasonable interpretation of the diagram is that the emitters are located in the upper troposphere and that the OLR minima located in the equatorial western Pacific and eastern Indian Oceans characterize emission from very high clouds. Minima at higher latitudes, though, provide an ambiguous signature. Emission may come from either the very cold surface or from cold cloud tops. In general, the OLR values increase substantially in the eastern equatorial Pacific Ocean and the subtropics. Higher values of OLR indicate infrared emission sources lower in the atmosphere. In effect, in regions of minimal cloud cover and relatively low water vapor amount, the principal emitter to space is the moist oceanic boundary layer and the ocean surface itself. Furthermore, there is considerable longitudinal structure in the OLR.

Because deep convective clouds are associated with precipitation, OLR minima in the tropics convey information about precipitation [*Arkin and Meisner*, 1987]. In Figure 7 the majority of deep convection occurs within the 28°C boreal winter SST isotherm, indicating a strong relationship between precipitation processes and tropical SST. This relationship will be discussed at length in section 7.2. Farther poleward, subtropical minima in precipitation (OLR maxima) are evident even though the SST is still warmer than the more rainy extratropics. The local failure of the SST-precipitation relationship indicates that subsidence constrains precipitation. On the other hand, precipitation in the higher latitudes is induced by rising air in strong dynamical systems.

4.2. Oceanic Signatures

Figure 8a shows the temperature and salinity distribution by volume (in cubic kilometers) of Earth's oceans [after *Worthington*, 1981]. Overall, the temper-

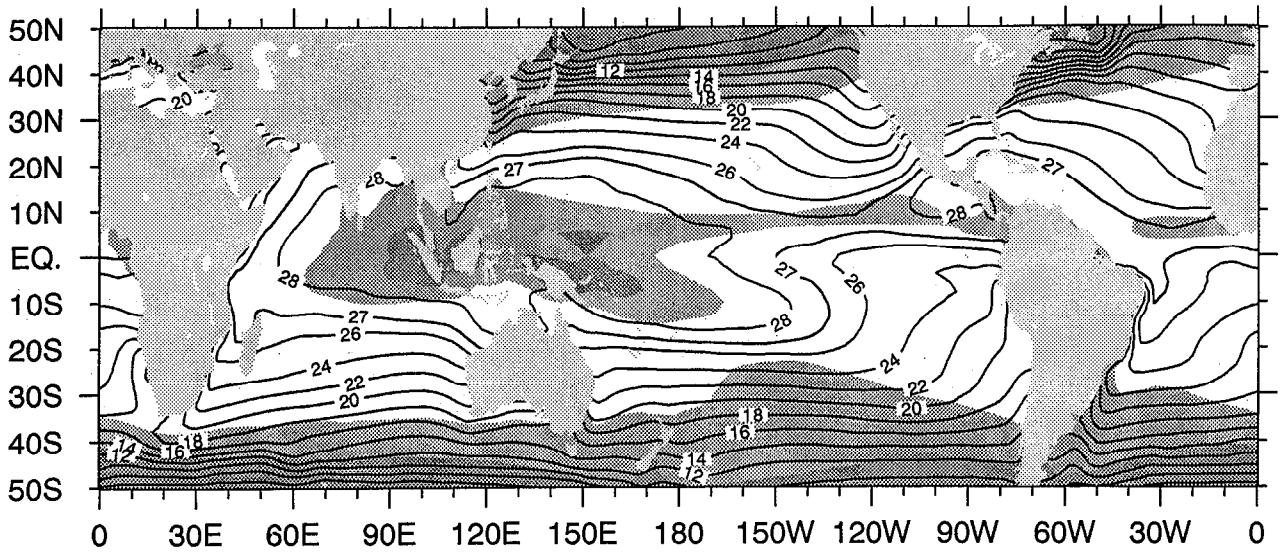

Figure 7. The geographic distribution of mean winter SST (solid contours). The shaded regions show the outgoing longwave radiative flux between 240 and 220 W m^{-2} (light shading) and 220 and 200 W m^{-2} (darker shading) and less than 200 W m^{-2} (heaviest shading). In the tropics the locations of the OLR minima indicate a strong correlation between warm SST (>28°C) and convection.

ature of the oceans is quite cool with a mean temperature of only 277 K (4°C), or approximately the mean radiative surface temperature of Earth as deduced in Figure 6b. The mean salinity of the ocean is about 35.5‰. Water with temperatures >301 K (28°C) occupies only 0.05% of the total water mass! Thus the warm tropical water associated with deep convection and precipitation in the tropical atmosphere (see Figure 7) constitutes only an extremely small part of the total ocean mass.

Figure 8b shows the SST and sea surface salinity (SSS) distribution as a function of area covered (in square kilometers). The mean SST is 292 K (19°C) while the mean SSS is 35.2‰. In comparison with the distribution by volume, there is a considerably larger proportion of warmer and less saline water covering the planetary oceans. About 11% of the surface is covered by water ≥28°C, 31% ≥26°C, and 57% ≥20°C. Thus the surface water, so critical for forcing the atmosphere, is a relatively warm, fresh, and very thin skin overlaying a cold and saline deep ocean. In fact, if the warm water were spread around the globe it would be only 2 m thick compared to the average ocean depth of 4 km. Although the warm water is generally contained within the tropics (see Figure 7), how the warm water is maintained becomes a critically important question. Ideas related to the maintenance of the tropical warm water skin and the manner in which it extends its influence to the global climate are presented in section 7.

The distributions of ocean temperature and salinity change their vertical structures with latitude. Vertical profiles of temperature and salinity are shown in Figure 9a at the equator, 30°N, and 60°N averaged over all longitudes [from *Levitus*, 1982]. Except in the upper ocean regions (i.e., above 400 m), the equatorial and subtropical profiles are remarkably similar, differing mainly by a warm and fresh layer near the surface of the equatorial profile. The greatest differences occur in the higher latitudes, which is the region where deep cold water is formed.

Figure 9b shows temperature and salinity profiles from the Bismarck Sea region of the western Pacific Ocean. The rapid decrease of density with depth (i.e., temperature decreases while salinity increases with depth) indicates a very stable density stratification. However, even against this stable density stratification there are indications of substantial diurnal mixing through the first 50 m of the column. The Bismarck Sea area (which is fairly typical of the tropical western Pacific Ocean) receives about 5 m yr^{-1} of precipitation and about 2 m yr^{-1} excess of precipitation over evaporation. The stable layers of the tropical warm pool are, at least in part, a direct result of the precipitation excess and are a distinct signature of atmospheric hydrological processes in the ocean.

5. MODES OF OCEAN-ATMOSPHERE INTERACTION

Evidence of the influence of hydrological signatures in the ocean structure indicates that the ocean is forced to some degree by atmospheric hydrological processes. However, the ocean is also forced by atmospheric winds and direct thermal forcing, and to a large degree the climate system is the integration of these two responses. An attempt is now made to de-

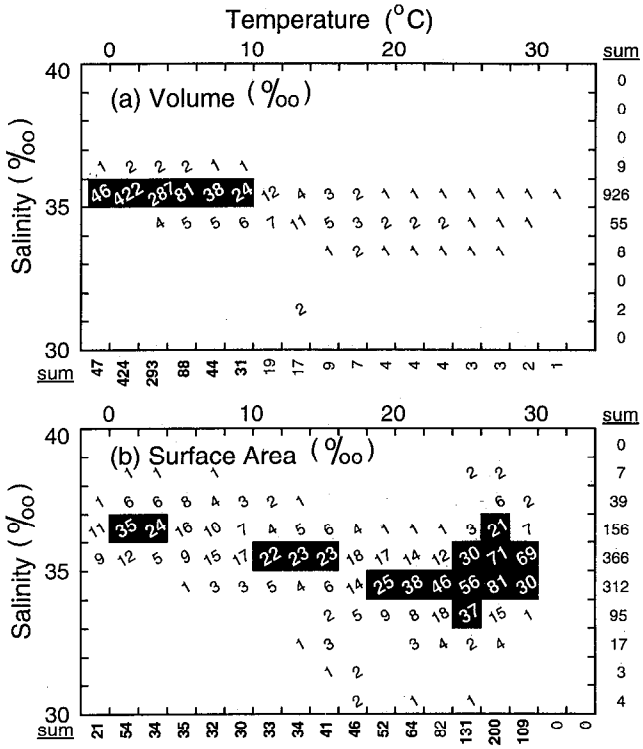

Figure 8. The distribution of the ocean waters as a function of temperature (in degrees Celsius) and salinity (in per mil). The distributions are shown as (a) per mil (i.e., ‰) of volume and (b) per mil of surface area. The summed temperature and salinity are shown on the abscissas and ordinates. The boxed areas enclose temperature and salinity pairs occupied by more than 2% volume or area. Over 70% of water by volume is less than 3°C. However, by surface area, nearly 60% of the water has a temperature greater than 18°C compared to less than 2% by volume. Thus the oceans may be thought of as a very cold body of water surmounted by a skin of relatively warm water. The mean temperature and salinity values by volume and surface area are marked on Figure 11.

cipher the relative roles of all of these forcing functions and modes of interaction.

5.1. Basic Driving Mechanisms of the Global System

The ultimate forcing mechanism of oceanic and atmospheric motions is the pole-to-equator gradient of radiative heating of the planet. Atmospheric motions are produced by fluxes of heat at the lower boundary and by radiative cooling to space generally from higher levels in the atmosphere. The ocean, on the other hand, is driven by a combination of wind stress from the atmosphere, a horizontal heating gradient, and a freshwater flux resulting from precipitation, evaporation, the formation and melting of ice, and runoff from rivers. In both systems the forcing is manifested as pressure gradient force fields or body forces that do work on fluid parcels, thus producing fluid motion. The ultimate purpose of the motion is to keep the planet in thermal balance. Excessive heat collected in the equatorial regions is transported to the polar regions. The transport is equally partitioned between the atmosphere and the ocean [e.g., *Peixoto and Oort*, 1992; *Trenberth and Solomon*, 1994]. Fluid motions transport heat, moisture, and momentum between the equator and the poles in order to maintain balances within the system. The heat transport is almost equally partitioned between the atmosphere and the ocean [*Peixoto and Oort*, 1992; *Trenberth and Solomon*, 1994].

The atmospheric winds drive ocean currents by applying a wind stress at the ocean-atmosphere interface. The momentum flux is transported vertically into the ocean until the density stratification below the mixed layer inhibits further penetration. Thus the wind-driven circulation over much of the ocean is restricted to the mixed layer above the ocean thermocline. The resulting upper ocean currents are strong and often basin wide and form an important part of the ocean general circulation. However, in the lower three quarters of the ocean mass, motions are generated from energy diffused from the upper ocean or from large-scale density variations resulting from differential heating and surface freshwater flux [*Niiler*, 1992].

The strength of a thermal circulation depends on the efficiency of the thermal heat engine. Despite the commonality of the basic thermal driving of the atmosphere and the ocean, the thermal circulation produced in each system is very different. In the atmosphere the majority of heating takes place at the tropical lower boundary of the atmosphere (i.e., through the ocean and continental surfaces) and in the lower and middle tropical troposphere through the release of latent heat. The distribution of heating results from the effective transparency of the atmosphere to solar radiation and from condensational phase changes requiring vertical displacement. Thus, in the atmosphere, heating and expansion occur at moderately high pressures and generally in the warm part of the planet. Radiative cooling to space and contraction, on the other hand, occur in the upper troposphere at low pressures and low temperatures. The result is a relatively efficient heat engine which produces a moderately strong equator-to-pole, thermodynamically direct circulation that converts potential energy to kinetic energy. Despite the configuration of the heating in the atmosphere, the thermal efficiency is only about 8% [*Peixoto and Oort*, 1992]. Figure 10a shows a schematic of the atmospheric thermal circulation. Because of angular momentum considerations and subsequent hydrodynamic instabilities, the circulation observed in nature is considerably more complicated, especially poleward of the subtropics. There, because of the inefficiency of the atmospheric thermal circulation in transporting heat poleward, large-scale eddies are produced in the vicinity of the jet stream. These eddies rapidly transfer heat poleward to satisfy global energy balances.

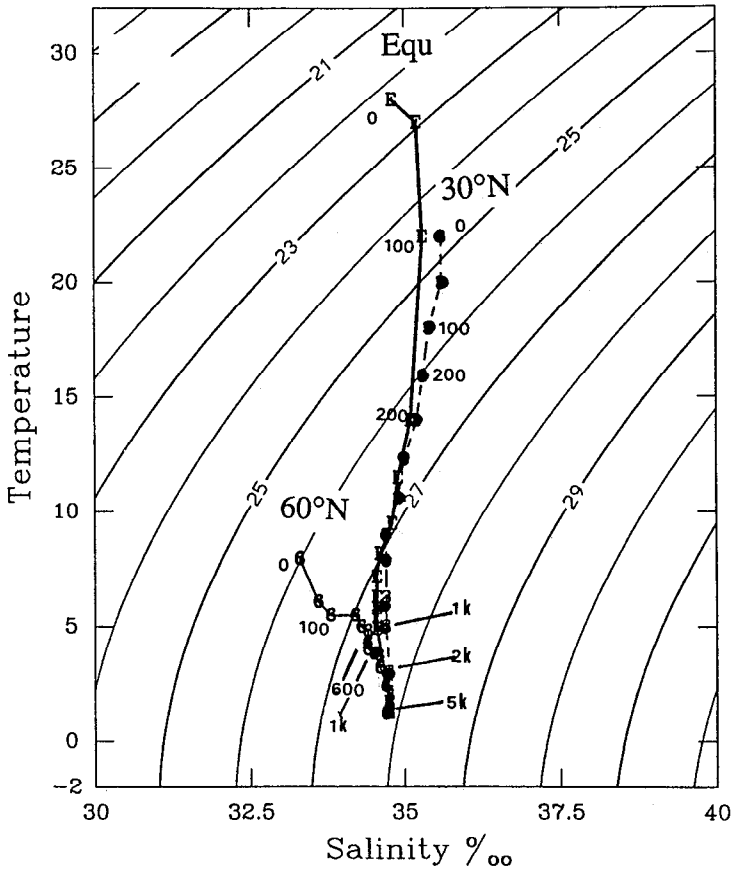

Figure 9a. The temperature and salinity of three typical northern hemisphere water columns (equator, 30°N, and 60°N) plotted as a function of temperature and salinity. Curves represent lines of constant density (curved solid contours; density (in kilograms per cubic meter) less 1000) are shown. Depths (100, 200 m, · · · , 1, 2, · · · , 5 km) are shown on the profiles. Most of the difference between ocean columns occurs in the first few hundred meters. In particular, the tropical profile is capped by a warm and fresh surface layer. At depths greater than 400 m the characteristics of all profiles are similar. Data are from *Levitus* [1982].

The oceanic thermal efficiency is much lower and does not appear favorable for the production of a strong thermal circulation. Heating occurs near the surface of the ocean or within the region of lowest pressure and warmest temperature. The majority of solar radiation is absorbed in the first few meters of the ocean (see Figure 18). On the other hand, surface radiational cooling occurs at high latitudes at the lowest ocean pressures. The cooling is destabilizing and, depending on the stratification of the ocean, mixing processes can extend the cooling downward into the ocean depths. However, because tropical surface heating creates a stable density stratification, the tropical heating cannot extend into the deeper ocean at all. Although the overall ocean thermal circulation produced is direct, the containment of heating in the upper tropical ocean renders the ocean thermal circulation weak and sluggish.

It is also necessary to consider the ocean density circulations induced by the surface freshwater flux due to the difference of precipitation and evaporating ($P - E$) and by freezing and melting processes at higher latitudes. The ($P - E$) distribution is quite complicated. Precipitation exceeds evaporation in the tropics and higher latitudes. In these regions a positive ($P - E$) will freshen and stabilize the upper layers of the ocean. In the subtropics, ($P - E$) is negative and works to increase the salinity of the upper ocean, which is a destabilizing process. In addition, ice formation at higher latitudes increases or decreases salinity depending on the season. The thermal and the haline forcing functions are shown in Figure 10b.

The impact of the thermal and haline forcing is shown schematically in Figure 10c. In the middle latitudes (20°–60°) the thermal and haline circulations are opposed. In the equatorial zone, thermal and haline forcing works together to create an extremely stable fresh warm pool at the surface. In the subtropics the strong evaporation causes the sinking of dense saline water which is subducted below the equatorial warm pool. *Neumann and Pierson* [1966] noted that this tropical cell does not extend deeply into the ocean. At very high latitudes the thermal and haline components of the circulation are again in phase. During the summer, solar heating of the surface occurs with a surface freshening from ice melting. In the winter, extreme radiational surface cooling coincides with ice formation and increases in salinity. The consequent increase in surface density allows extremely deep mixing and, in some regions, the formation of deep water.

Given the weakness of the thermohaline circulation it would appear from first consideration that it might be of minor importance. Indeed, *Peixoto and Oort* [1992] suggest that the thermal efficiency of the ocean is about an order of magnitude less than that of the atmosphere. However, a number of recent studies

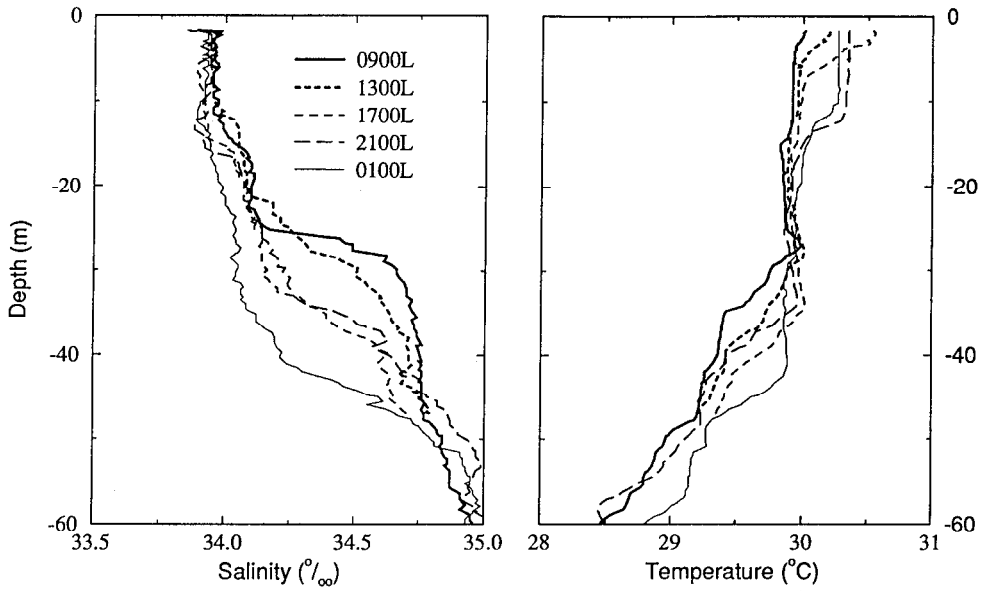

Figure 9b. Details of tropical ocean profiles taken in the Bismarck Sea to the northeast of Papua New Guinea. The (left) salinity and (right) temperature are plotted as functions of depth. The profiles were taken at 0900, 1300, 1700, 2100, and 0100 local time (see legend). During the day a shallow warm thermocline develops near the surface. Evidence of vigorous vertical mixing can be seen in both the salinity and temperature profiles during the evening as the surface cools. (J. S. Godfrey, private communication, 1993).

have theorized that the slow deep ocean circulation may have a critical function in long-term climate variability and in the maintenance of the present climate. This issue will be discussed in section 7.1.

In summary, the ocean and the atmosphere respond very differently to the same basic external forcing. Perhaps the reason for the difference in response of the two systems is their respective radiative properties. The differing responses combine to produce complicated modes of interaction between the two systems. To understand this interaction, the concept of buoyancy flux is introduced.

5.2. Buoyancy Concepts

The density of seawater (solid curves in Figure 11) is a complex nonlinear function of temperature and salinity [e.g., *Gill*, 1982]. The form of the nonlinearity suggests that density will be more sensitive to temperature changes in some regimes but to salinity in others. Consider two water masses marked "W" (warm) and "C" (cold) in Figure 11 that are assumed to be representative of equatorial and higher-latitude surface waters, respectively. Consider the variation of temperature and salinity of the two parcels for equivalent changes in density. Clearly, $\Delta T_W < \Delta T_C$ for a given $\Delta\rho$, while $\Delta S_W \approx \Delta S_C$ for a given $\Delta\rho$. These coefficients can be calculated directly from Figure 11. Thus it is generally assumed that the tropical oceans are controlled by factors that change temperature (e.g., heat flux). At higher latitudes it is assumed that factors that control salinity (e.g., precipitation, evaporation, ice formation and melting, and river runoff) control density on an equal basis with processes that affect temperature.

These regional sensitivities to heat and freshwater fluxes are evident in the thermal (α) and salinity (β) expansion coefficients of seawater which may be defined as

$$\alpha = \left(-\frac{1}{\rho_0}\frac{\partial\rho}{\partial T}\right)_S \tag{6a}$$

$$\beta = \left(\frac{1}{\rho_0}\frac{\partial\rho}{\partial S}\right)_T, \tag{6b}$$

respectively. Overall, the thermal coefficient (α) changes most drastically as a function of temperature, with a factor of 4 difference in magnitude between 2.5°C and 30°C (781×10^{-7} to 3413×10^{-7} K^{-1}). The salinity expansion coefficient, on the other hand, varies little over the range of water masses found in the ocean (8010×10^{-7} to 7490×10^{-7}). In the tropics it is generally thought that processes that affect temperature are much larger than processes that affect salinity. *Gill* [1982], for example, suggests that heating effects are about a factor of 4 greater than salinity effects. However, in the tropical warm pools and the polar regions, this factor will be shown to be much smaller.

To assess the influence of the atmosphere on the ocean, the concept of the buoyancy of the upper ocean layer is adopted [e.g., *Gill*, 1982]. The buoyancy B is a

function of the relative density of an ocean parcel compared with its neighbor and is defined as

$$B = \alpha T - \beta S \tag{7}$$

where S represents salinity, and α and β are the thermal and salinity expansion coefficients, defined in (6). Changes in the buoyancy of a parcel occur when the temperature or the salinity changes from fluxes of heat or freshwater. The total heat flux into the ocean Q_T is defined as

$$Q_T = Q_{lh} + Q_s + Q_r \tag{8}$$

where Q_{lh} and Q_s represent the turbulent latent and sensible heat fluxes and Q_r the net radiative heat flux. There are two components of sensible heat: the turbulent transfer of heat conducted from the ocean surface to the atmosphere (i.e., Q_{ts}) and the cooling of the ocean by the mixing of cooler precipitation into the ocean (Q_p). That is,

$$Q_s = Q_{ts} + Q_p \tag{9}$$

Careful estimates have been made of the second component (R. Gosnell, C. W. Fairall, and P. J. Webster, The sensible heat of rain in the tropics, manuscript submitted to the *Journal of Geophysical Research*, 1994; hereinafter referred to as Gosnell et al., submitted manuscript, 1994). Using data from the tropical western Pacific Ocean collected during the TOGA COARE experiment, it was found that the contribution was very small (-3 W m^{-2}) averaged over a number of weeks. However, during precipitation events, the contribution of cold rain to the sensible heat flux can be greater than -100 W m^{-2}.

The net radiative heat flux may be divided into solar and longwave components:

$$Q_r = S_s + I_{\downarrow} - I_{\uparrow} \tag{10}$$

where S_s represents the net solar radiation reaching the surface of the ocean (i.e., incident minus reflected), and $I_{\downarrow}$ and $I_{\uparrow}$ are the downward and upward longwave radiation fluxes at the surface, respectively. The flux of freshwater into the ocean, F_w, is defined as

$$F_w = (P - E) \tag{11}$$

where P and E represent precipitation and evaporation.

Communication between the ocean and the atmosphere (and vice versa) may be thought of in terms of a buoyancy flux [e.g., *Gill*, 1982] defined as

$$F_B = \alpha g Q_T + \beta g S(P - E). \tag{12}$$

F_B is written in such a manner as to delineate thermal and haline effects. That is, (12) appears as an aggregate of the heat flux and the freshwater flux into the ocean. As E appears in both Q_T (through Q_{lh} in (8)) and in the freshwater flux (11), the two components are not independent.

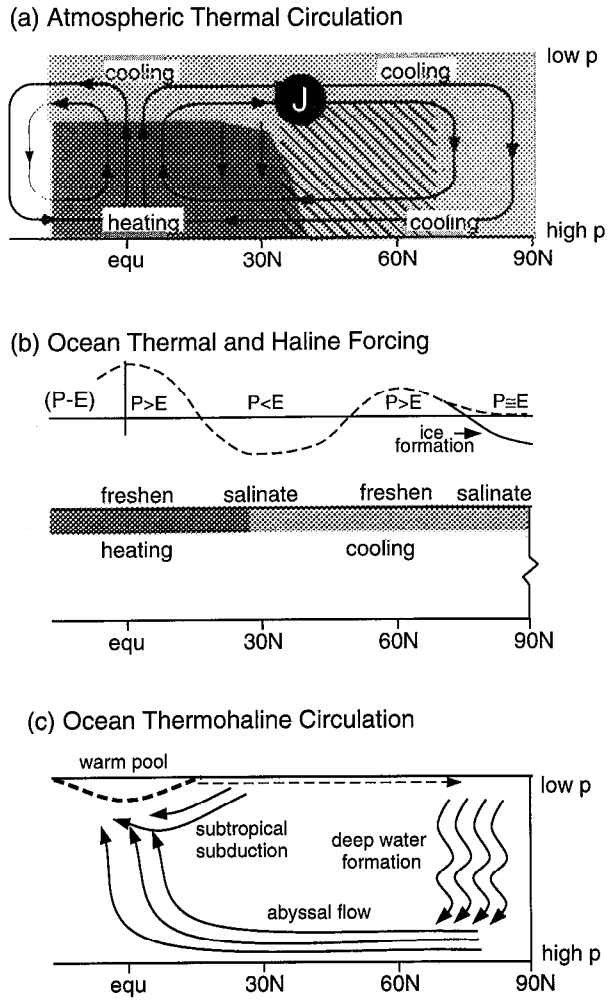

Figure 10. Forcing and resultant circulations in the atmosphere and the oceans. (a) The atmospheric forcing and resulting circulation. (b) The thermal and haline forcing of the ocean. (c) The resulting thermohaline ocean circulation.

If it is assumed that the freshwater flux is small in comparison to the net heat flux, (12) reduces to

$$F_B \approx \alpha g Q_T. \tag{13}$$

Since the density of seawater is controlled more by temperature effects when the temperature is warm, it is expected that the heat flux should determine most of the buoyancy fluctuations in the tropics. On the other hand, at high latitudes, the local freshwater flux, induced by sea ice melting or freezing, in addition to precipitation and evaporation differences, determines buoyancy. Thus it would appear that (13) should be a good approximation in tropical ocean-atmosphere models used in the forecasting of the El Niño–Southern Oscillation phenomena [e.g., *Cane and Zebiak*, 1985; *Anderson and McCreary*, 1985]. However, as the tropical ocean warm pools are also regions of considerable rainfall and only moderate evaporation (i.e., large positive F_w), it is worth determining whether the complete

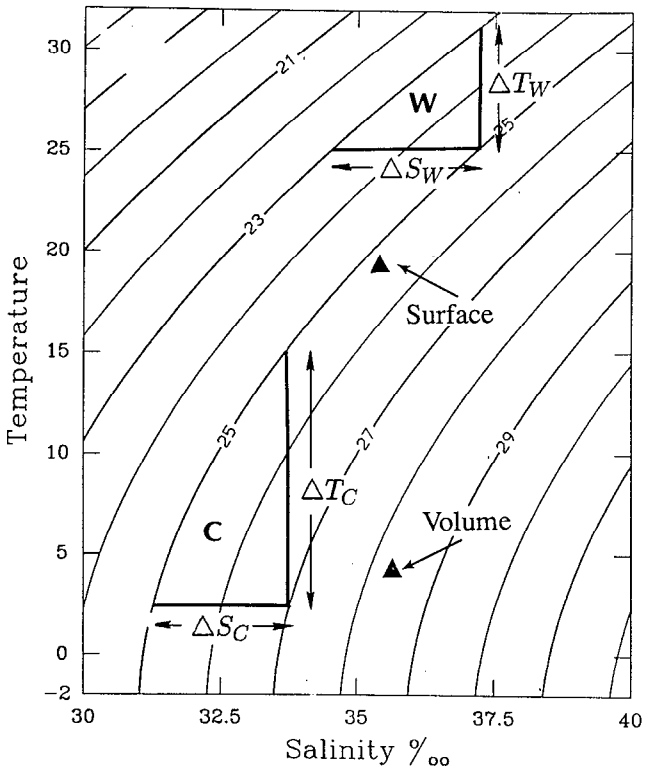

Figure 11. The relative sensitivity of the density of seawater to changes in temperature and salinity for different water masses. The relative sensitivity can be determined by noting the relative scales of temperature and salinity changes for the same change in density for typical tropical surface water (marked W) and high-latitude water (C). The two solid triangles marked "surface" and "volume" show the mean surface and volume temperatures and salinities of the world's oceans calculated from Figure 9.

buoyancy flux expression (i.e., expression (12) rather than (13)) is more representative of the tropics.

Table 2 provides estimates of the components of the mean ocean surface heat budget from (8) and (10), the freshwater flux from (11), and the buoyancy flux from (12). Data from *Oberhuber* [1988] were used to compute the zonally averaged quantities at northern hemisphere latitudes over the oceans during the boreal winter and summer. Except for the higher northern latitudes during winter, the net radiation budget is generally positive. However, at all latitudes the latent heat flux is negative, indicating heat loss due to evaporation. Thus, as solar radiation is absent at high latitudes during the winter, the net heat flux is strongly negative. In the winter and summer subtropics, at the equator, and even in the summer higher latitudes, the net radiative flux generally compensates for the latent heat loss, resulting in positive net surface heat flux values.

The situation is slightly different in the tropical warm pools of the Pacific and Indian Oceans. Given that these are regions of high cloud amount (see Figure 7), there is a considerable depletion of radiative heating. Thus the positive freshwater fluxes at the equator accompanying the depleted radiative fluxes produce a small negative buoyancy flux. That is, the buoyancy of the upper ocean increases slightly. In the winter subtropics, evaporation so dominates over precipitation that the buoyancy flux is reversed even though the radiative flux has increased from its warm pool values. Similarly, at higher latitudes, although principally because of the net heat flux deficit, the buoyancy flux is also strongly positive. It should be remembered, though, that in these arguments the decrease in buoyancy due to salt rejection during ice formation during the winter has not been taken into account. This process would further increase the positive buoyancy flux in the winter high latitudes. On the other hand, ice melting would enhance the negative buoyancy flux during the summer.

The global distributions of the total heat and freshwater fluxes from *Oberhuber* [1988] are shown in Figures 12a and 12b, respectively. There are three major domains in each of the fields. Both Q_T and $(P - E)$ are positive in the equatorial oceans but negative at higher latitudes. In the positive regions of Figure 12a, the radiative heating effects at the surface tend to dominate. In the negative regions, evaporative processes dominate the net heating and evaporation exceeds precipitation. Using the Oberhuber values from Figure 12 and the expansion coefficients defined in (6), the ratio of the heat flux and freshwater flux components of the buoyancy flux F_B can be calculated. The ratio R given by

$$R = \left| \frac{\alpha Q_T}{\beta S(P - E)C_w} \right|, \tag{14}$$

TABLE 2. Components of the Ocean Surface Energy Budget and Freshwater Flux at Latitudes in the Northern Hemisphere During the Boreal Winter and Boreal Summer

Component	*DJF 60°N*	*DJF 25°N*	*0°*	*JJA 25°N*	*JJA 60°N*
		Fluxes			
S_g, W m^{-2}	12	142	203	237	153
$(I\downarrow - I\uparrow)$, W m^{-2}	−43	−65	−48	−50	−30
Q_{th}, W m^{-2}	−100	−160	−80	−107	−25
Q_s, W m^{-2}	−70	−17	−8	−5	0
Q_p, W m^{-2}	?	0	−3	0	?
$(P - E)$, 10^{-3} m/yr^{-1}	80	−1200	760	−320	200
		Net Fluxes			
Radiation: Q_r, W m^{-2}	−3	77	155	187	123
Total heat: Q_T, W m^{-2}	−201	100	70	75	98
Buoyancy: F_B, 10^{-8} m^2 s^{-3}	5.3	8.2	−5.5	−6	−5

The boreal winter is December, January, and February (DJF), and the boreal summer is June, July, and August (JJA). The net radiation (10), the total heat flux (8), and the buoyancy flux (12) are listed at the bottom of the table. Data are from *Oberhuber* [1988].

is plotted in Figure 13 as a function of latitude and longitude. R is order unity at high latitudes (i.e., heat flux and freshwater fluxes are of the same magnitude) and generally increases in value toward the equator. The tropical oceanic warm pool regions are exceptional because the very large freshwater flux is the same order as the depleted net heat flux.

In summary, Figure 13 indicates that both heat and freshwater fluxes are important in influencing the state of the tropical ocean and, together with the momentum flux, determine the state of the upper ocean. Thus, wherever the freshwater flux is large and the salinity component of the buoyancy flux is comparable with the heat flux component, the thermodynamic influence of the atmosphere on the ocean is described by (12) rather than (13).

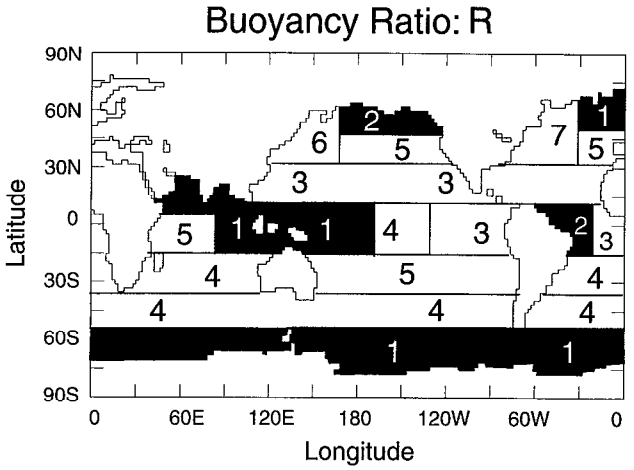

Figure 13. Ratio (R from equation (14)) of the relative impact on upper ocean buoyancy of heating (numerator) and salinity effects (denominator). Data from Figures 11a and 11b were used in the calculations. Regions where R is order unity are shaded. In general, at higher latitudes, the buoyancy appears to be equally effected by heating and buoyancy. At all other latitudes the buoyancy is much more sensitive to variations in heating (i.e., $R \ll 1$). Exceptions are in the western Pacific Ocean, the northeastern Indian Ocean, and the western Atlantic Ocean. In these tropical warm pools the freshwater flux is so great that the heating and salinity effects are at or near parity.

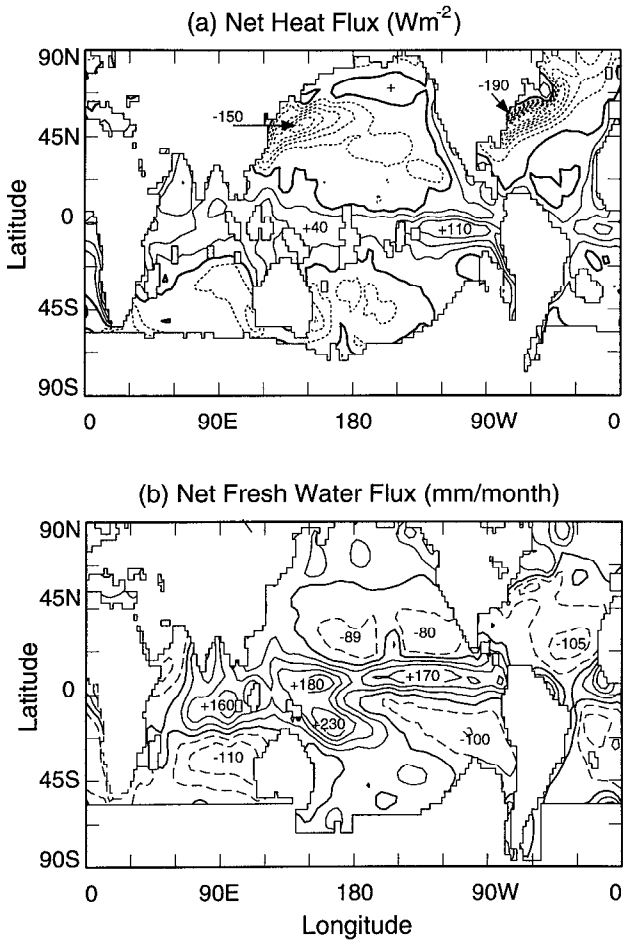

Figure 12. (a) The annual mean net heat flux into the ocean (Q_T from equation (8)). Dashed curves indicate net heat loss by the ocean; solid curves represent net heat gain. The oceans are divided into three major regions: the tropics, which are regions of net positive Q_T; the subtropics and higher latitudes, which are regions of moderate heat loss; and the western parts of the northern hemisphere ocean basins, which are regions of major heat loss to the atmosphere. Contour intervals are 25 W m^{-2}. (b) The annual mean net fresh water into the ocean (F_w from equation (10)). Solid contours ($P - E > 0$) dominate the tropical regions, especially where the SST is largest (see Figure 7). Dashed contours ($P - E < 0$) fill the subtropics. Contour intervals are 50 mm month^{-1}. Blank regions denote insufficient data. Data are from *Oberhuber* [1988].

Finally, as the coupled ocean-atmosphere system is being considered, it is necessary to determine the consequences of negative and positive buoyancy fluxes on the atmosphere as well as the ocean. For example, if the buoyancy of the upper ocean decreases because of an increase in the latent heating, will the buoyancy of the adjacent atmospheric column increase or decrease? A description of the buoyancy effects of various physical processes on the joint ocean-atmosphere system is given in Table 3. The table demonstrates that the buoyancy concept is a useful tool in understanding the interaction of the joint system.

6. PROCESSES OF OCEAN-ATMOSPHERE INTERACTION

6.1. Observed Surface Fluxes

A vivid example of the processes that affect sea surface temperature is shown in Figure 14 [*Lukas*, 1990]. The diagram shows SST plotted against SSS using data collected in the western Pacific Ocean warm pool during a 24-day period of the Western Equatorial Pacific Ocean Circulation Study (WEPOCS) I experi-

TABLE 3. Summary of Interface Processes Influencing the Oceanic (B_O) and Atmospheric B_A) Buoyancy

Processes	*Oceanic*	*Atmospheric*	*Comments*
			Q_T: Heat Flux
S	+	+	B_A increases through solar absorption. B_O increases through near-surface absorption (*e*-folding depth: 5 m) (sections 6.3, 6.5).
$I\uparrow$	−	+	B_A increases from greenhouse absorption by ambient water vapor and cloud liquid water and ice. B_O decreases by cooling of surface skin layer. The enhanced greenhouse effect of clouds in the tropics is about one third of the effect of latent heating in the atmosphere (sections 6.3, 6.5).
$I\downarrow$	+	−	Radiative emission from the ambient water vapor and clouds reduces B_A. Absorption of the downwelling IR increases B_O (sections 6.3, 6.5).
Q_{lh}	−	+	Ocean evaporation causes surface cooling and loss of B_O. Vapor entering the atmosphere will eventually increase B_A after condensation occurs. Unlike the loss of B_O, the gain of B_A may not be local. In that sense, B_A should be referred to as latent buoyancy (sections 6.5, 7.2).
Q_s	−	+	The turbulent transfer of heat from the ocean surface decreases B_O and increases B_A. Similar for the ocean surface by cold rain (sections 6.5, 7.2).
			F_w: Freshwater Flux
$(P - E) > 0$	+		Freshening of the upper ocean layer decreases the density and thus increases B_O (sections 6.4, 7.1).
$(P - E) < 0$	−		Increase in salinity increases the density and reduces B_O (sections 6.4, 7.1).
			Wind
	−		Wind stress creates turbulence in the ocean. If the wind is sufficiently strong, the turbulence can mix through the subthermocline and introduce cooler, saline water to the surface layer, thus reducing B_O. Strong winds are also associated with enhanced turbulent fluxes and thus further decreases in B_O (sections 7.1, 7.2).

ment [e.g., *Lukas and Lindstrom*, 1987, 1991]. A number of regimes are evident, each indicated by a line superimposed on the data. Axis A shows the diurnal heating and cooling of the surface layers. During these diurnal changes the salinity remains constant irrespective of the initial surface salinity, indicating that the strongest diurnal variations occur when the winds are lightest. Axis B illustrates the effect of rainfall. Here both SST and SSS decrease. The decrease in SSS results from the freshening effect of the surface layers by rainfall. The cooling results from two effects: the physical cooling of the surface layers by the cooler raindrops (e.g., Gosnell et al., submitted manuscript, 1994) and the reduced net radiation flux at the surface as cloudiness increases during rain events. Axis C shows the impact of two further processes: entrainment and evaporative cooling. Strong winds cause deep ocean mixing and the entrainment from below of cooler, saltier water into the surface layer. Evaporation, on the other hand, also a strong function of wind strength, cools the surface and increases the salinity.

Figures 15 and 16 display the components of the total heat and freshwater flux at the ocean surface observed in the western Pacific Ocean warm pool [*Young et al.*, 1992]. The weather during the observation period was generally clear interspersed with a few intense periods of convection and precipitation. Figure 15 shows the components of the surface radiation flux (from equation (8)) and the total surface heat flux (equation (10)). In general, $Q_T > 0$ during the day (solar radiation dominating) but negative during the night (evaporation dominating) so that the daily average of the total heat flux is small and positive. The upwelling and downwelling infrared radiation fluxes remain fairly constant throughout the period. The constancy in the upwelling flux represents an almost constant SST. Constancy in the downwelling radiation (the flux actually displays a variability of about 20–40 W m^{-2}) displays a relative independence to cloud amount and suggests that the extremely moist boundary layer dominates the downward emission to the ocean surface. The solar radiation, on the other hand, changes substantially from day to day, varying from less than 100 W m^{-2} during disturbed periods to greater than 1000 W m^{-2} during clear times. Thus during disturbed periods the ocean is losing heat to the atmosphere, but it is gaining heat when the system is undisturbed.

Figure 16 shows details of the surface processes during a 5-day period (specifically, hours 72–192). Figure 16a shows the radiative fluxes. Of the five days, the first, second, and fifth are convectively active with severely depleted solar radiation, periods of heavy precipitation, and relative high wind (Figure 16c). During these periods the difference in the SST and the 10-m atmospheric temperature is as much as 5°C (Figure 16b) because of the injection of cold, dry midtropospheric air into the boundary layer. The relaxation period is about 24 hours or much longer than most precipitation events, and during this period the surface

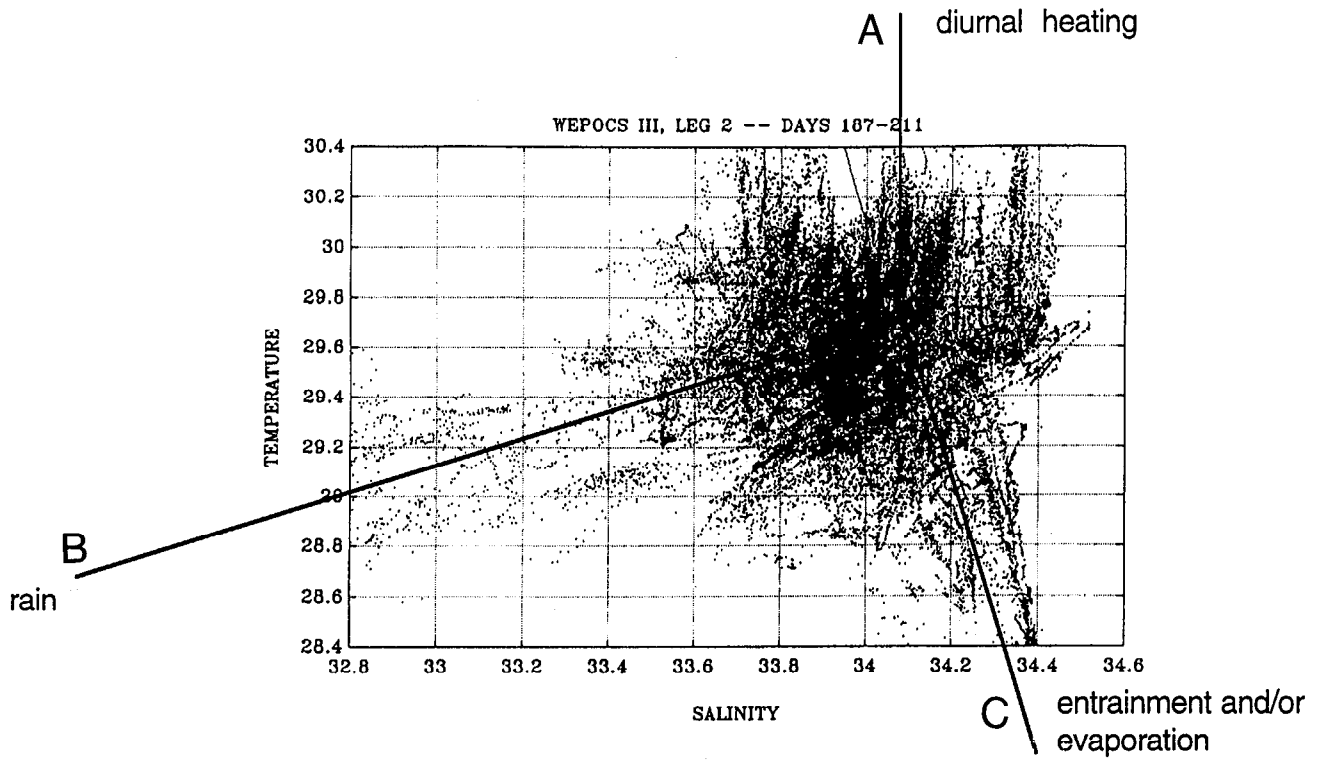

Figure 14. Scatter plot of SST and sea surface salinity pairs obtained from a 25-day period during the Western Equatorial Pacific Ocean Circulation Study (WEPOCS) experiment in the western Pacific Ocean. The heavy lines indicate the expected conditions from the different processes affecting the TS relationship. From *Lukas* [1990].

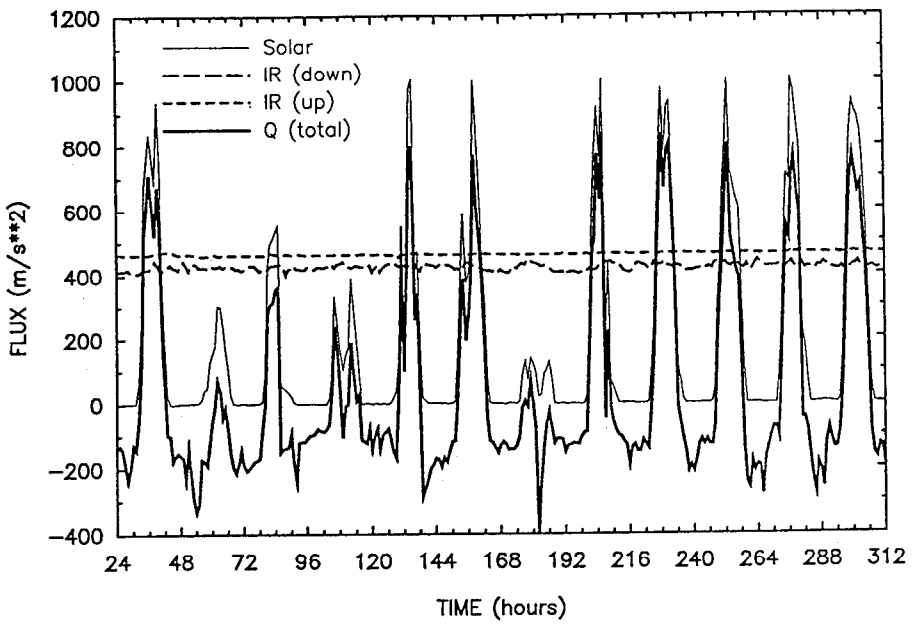

Figure 15. Surface flux data from the western Pacific Ocean for the 12-day period February 19 to March 3, 1990. The diurnal cycle is clearly apparent through the record. However, on disturbed days the solar radiation is reduced from a normal 800–1000 W m^{-2} to 200–300 W m^{-2} or between hours 168 and 192 to about 100 W m^{-2}. On disturbed days the total heat flux remains near zero during the daylight hours and negative averaged over a 24-hour period. Note that the downwelling surface radiation is almost constant (420 ± 20 W m^{-2}). The upwelling infrared radiation is even more steady indicating an almost constant SST during the observational period. Data are from *Young et al.* [1992].

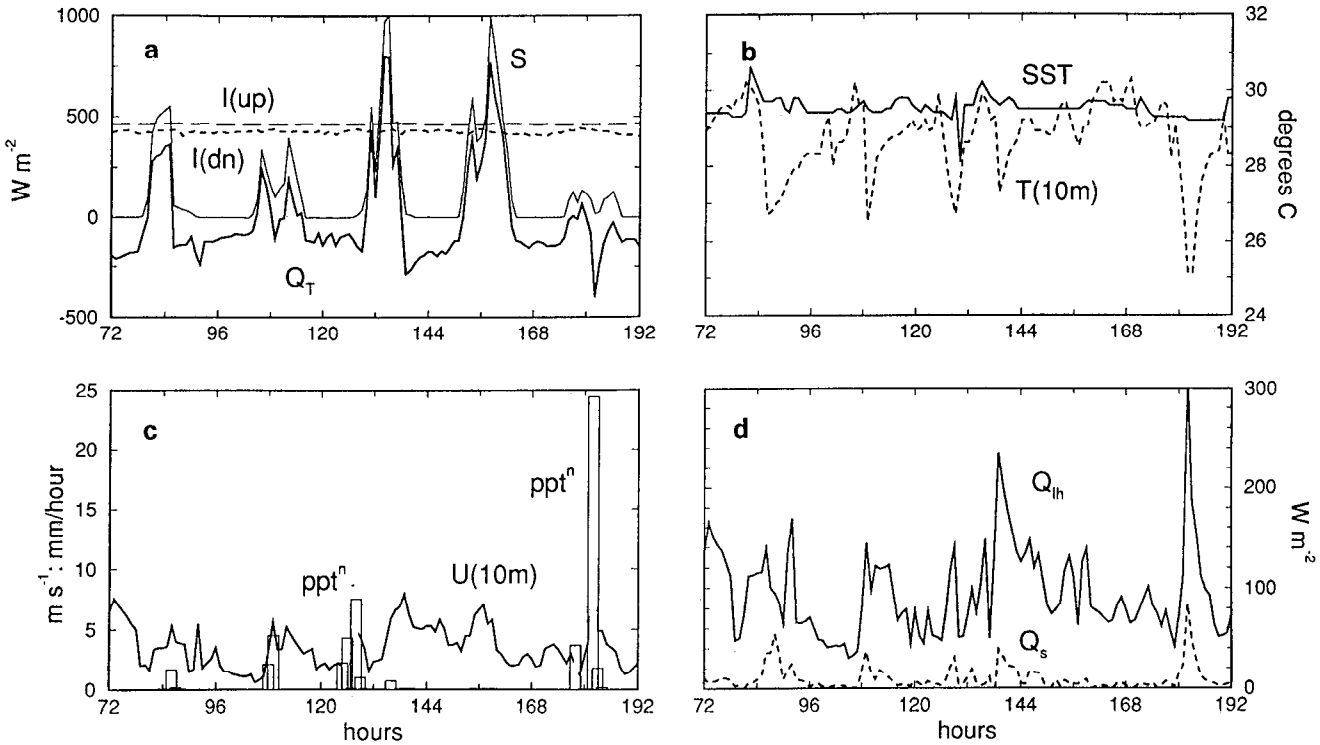

Figure 16. Detail of the disturbed period between hours 72 and 192 of Figure 15. (a) Components of the surface radiation balance and the total heat flux into the ocean. (b) Variation of the SST and the 10-m atmospheric temperature. Whereas the SST remains fairly constant throughout the period, the air temperature shows considerable variability. During rainfall events the air temperature drops by as much as 4° cooler than the SST responding to periods of rainfall and may remain so for up to 24 hours following the convection. (c) Variation of the 10-m wind (in meters per second) through the period and the precipitation (bars; in millimeters per hour). (d) Surface latent heat and sensible heat fluxes. The latent heat flux, in particular, is highly variable and is strongly correlated with the wind variations and convective activity.

fluxes grow substantially. The latent heat flux (Figure 16d) increases well beyond its average value of 110 W m^{-2} to values as high as 300 W m^{-2}. Also, the sensible heat flux, with values that average less than 10 W m^{-2}, increases by a factor of 4 or 5. Note, though, that the relationship between the fluxes and the weather is not altogether straightforward. Fluxes do increase with convection on the second and fifth day. But they also increase substantially on the third day when the wind increases with no convection. Thus during convective periods the depletion of total heating into the oceans is contributed to by reductions in solar radiation and increases in latent and sensible heating.

6.2. Ambient Water Vapor, Cloud, and Surface Radiation

Stephens [1978] related cloud infrared emissivity ε_c and cloud albedo a_c of a cloudy atmospheric column to the liquid water path l of the column, which is expressed in terms of mass of water per unit volume through a vertical slab. The ε_c and a_c relationship with l is shown in Figure 17a [*Stephens and Webster*, 1983]. The cloud types associated with specific water paths are plotted along the upper abscissa. Cirrus clouds possess equivalent liquid water paths generally less than 20 g m^{-2}. Lower tropospheric stratocumulus and stratus clouds usually fall within the 20–200 g m^{-2} range. Large cumulus, nimbostratus, and cumulonimbus clouds generally have liquid water paths greater than 200 g m^{-2} and even in excess of 1000 g m^{-2}. According to Stephens's parameterization, cloud albedo tends to increase to a maximum of 0.8 for very deep clouds. Infrared emissivity, on the other hand, behaves very nonlinearly with increasing liquid water path and approaches unity (blackbody) for quite small values of liquid water content. Thus thin clouds such as cirrus, which have small albedos and are thus fairly transparent to solar radiation, may be black in the infrared. Thicker clouds, though, while optically black, have larger albedos. *Stephens and Webster* [1979] argue that the different rates of change of cloud albedo and infrared emissivity are very important in the overall impact of cloudiness on climate through their influence of the surface radiation balance. Thin clouds (i.e., small a_c, moderate to large ε_c) tend to warm the surface of the planet even though their emitting temperature (i.e., cloud base temperature) is relatively low. Thicker clouds (i.e., large a_c, large ε_c)

tend to cool the surface even though their effective radiating temperature is relatively high.

If clouds existed in a perfectly dry environment, Stephens's parameterization would provide all the information necessary to determine the net downward flux of longwave radiation at the planetary surface. However, an atmospheric column contains varying amounts of water vapor above and below the cloud. Thus, as water vapor is very active in the infrared, it is necessary to consider the distribution of ambient water vapor in addition to cloud radiative properties in order to compute the surface radiation budget.

Intuitively, it might be expected that the ambient water vapor effect may be maximized in the tropics where water vapor is both plentiful and very warm. This is true, but it comes about in a rather unexpected manner. The high tropical water vapor concentration (Figure 3) renders the tropical atmospheric boundary layer optically black such that all upwelling surface infrared radiation will be completely absorbed close to the surface. The downwelling radiation from this absorbing layer occurs at a temperature only slightly cooler than the surface (see Figure 15). It is easy to calculate the effective radiating temperature of the tropical atmosphere. Using the Stefan-Boltzmann law, the net infrared balance at the surface can be written as

$$I_{\uparrow} - I_{\downarrow} = \sigma(T_s^4 - T_A^4), \qquad (15)$$

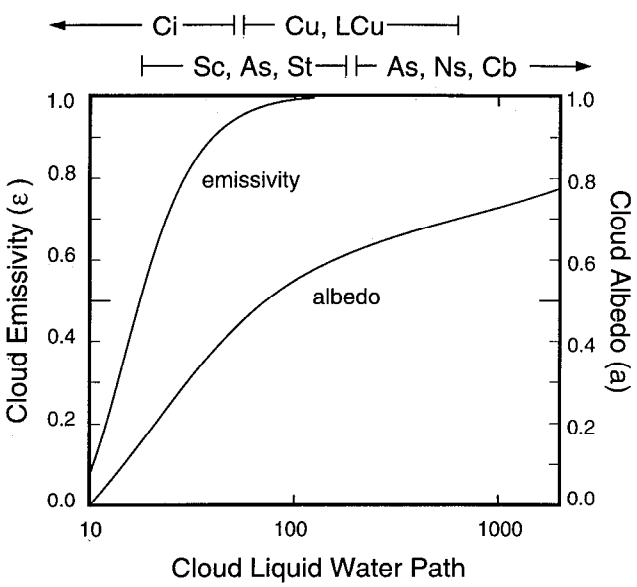

Figure 17a. Relationship of the cloud albedo a and emissivity ε as a function of the liquid water path l of a cloud [*Stephens*, 1978]. Cloud types associated with the values of liquid water path are shown on the upper abscissa. Whereas albedo increases relatively slowly with liquid water path, the emissivity increases rapidly. Thus, from the planetary surface, a cloud will appear to become optically black even for relatively thin clouds. The change in albedo grows at a slower rate with thickening clouds.

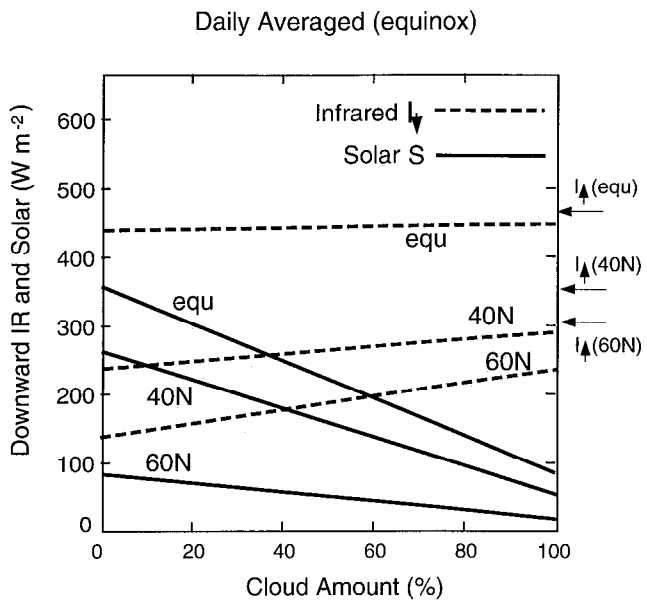

Figure 17b. The solar (solid curves) and downwelling infrared radiation (dashed curves) as a function of cloud amount for the warm pool regions of the tropics (equ), 40°N, and 60°N, at an equinox. Values of the upwelling surface infrared radiation ($I_{\uparrow}$) are shown on the right-hand ordinate.

where T_A is the atmospheric radiating temperature to the surface. Figure 15 provides the left-hand side of the equation. For the observed range of 30–50 W m^{-2}, the radiating temperature varies from 298 K to 296 K. That is, the effective radiating layer is within the first half to one kilometer above the surface or close to or slightly above the average cloud base height. A direct consequence, then, of the moist tropical boundary layer is reduction of the impact of clouds on the surface longwave radiation budget. Downwelling radiation from clouds is absorbed very close to the base of the clouds and reradiated successively down to the surface through the moist boundary layer. Thus the enhanced radiation from the clouds is only marginally felt at the ocean surface. Figure 15 shows that there appears to be little difference in the longwave fluxes between cloudy days (note, for example, the reduced solar radiation between hours 48–72 in Figure 16) and clear days (e.g., hours 24–48). Probably, the cloud effect is close to the instrumentation error.

At higher latitudes where the atmosphere is cooler and contains a smaller water vapor concentration than in the tropics (see Figure 3), the absorption of longwave radiation in the boundary layer is only partial. The upwelling radiation that is absorbed is reradiated back (at least partially) to the surface but from a higher elevation and at a much colder radiating temperature than in the tropics. As a consequence the magnitude of downwelling infrared radiation at the surface is much smaller than the tropics. However, as distinct from the tropics, downwelling radiation received at the surface is much more variable, and the existence of a cloud

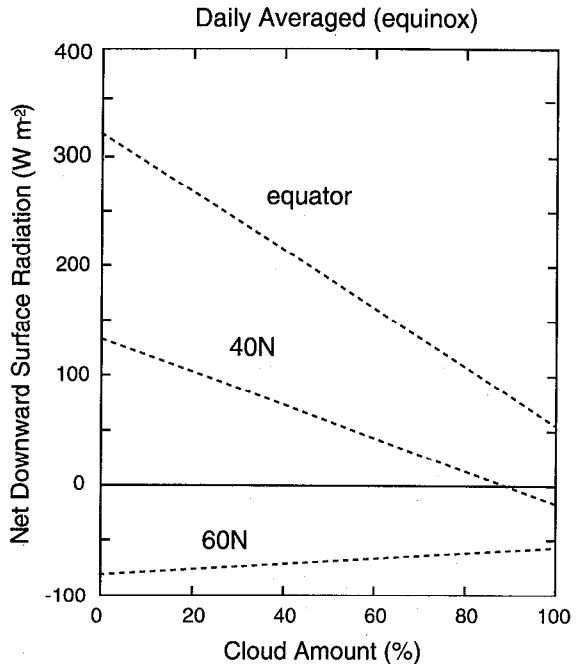

Figure 17c. The variation of the net radiation at the surface (i.e., downwelling solar radiation plus the net surface infrared radiation) as a function of cloud amount. The net effect of cloud at low latitudes is to cool the surface substantially. At 40°N the cooling with increasing cloud is less apparent. However, at high latitudes, increasing clouds tend to warm the surface slightly.

assumes a critical importance for the surface radiation balance. Most of the radiation passes through the relatively dry boundary layer with only moderate attenuation. Measurements of downwelling infrared radiation at the surface in the higher latitudes show a factor of 2 difference between cloudy and clear skies [e.g., *Paltridge and Platt*, 1976; *Liou*, 1980].

The effect of clouds and the ambient water vapor distribution on the components of the surface radiation budget is summarized in Figure 17b. Three latitudes are considered: the equator, 40°N, and 60°N. As cloudiness increases, the solar radiation reaching the ocean surface decreases in proportion to the liquid water content of the cloud and the value of the unattenuated solar radiation. As cloud amount increases, the downwelling infrared radiation from the cloud base ($I_{\downarrow}$) also increases, compensating somewhat for the depletion of the solar flux. However, as the ambient water vapor increases, the compensation between the two radiative streams diminishes. Overall, in both the tropics and extratropics, the solar radiation flux will be reduced by roughly the same percentage for a given cloud type assuming differences in cloud composition and solar zenith angles are ignored. On the other hand, the downwelling surface infrared radiative flux increases only slightly with increasing cloud amount in the tropics, although substantially at higher latitudes.

Figure 17c shows the impact of cloud amount on the net surface radiation flux (i.e., $S_s + I_{\downarrow}$). In general, the net downward surface radiation in the extratropics decreases slightly with increasing cloud because the reduced solar component is compensated to a large degree by the enhanced downwelling infrared flux. In the tropics the net downward radiation at the surface decreases substantially with increasing cloud simply because the decrease in solar radiation is only marginally compensated by the longwave flux. At very high latitudes the impact of clouds is entirely different. Because of a much lower solar flux at 60°N, the infrared radiation dominates the column. As cloudiness increases, the decrease in solar radiation is outweighed by the increase in downwelling infrared flux. Therefore an increase in cloudiness tends to warm the surface rather than cool it.

The role of the ambient water vapor content of the lower troposphere points toward remarkable regional differences in the processes that determine the net surface radiation flux. These differences create a paradox. The relative insensitivity of the downwelling infrared radiation in the tropics to cloud amount renders the tropical oceans particularly sensitive to variations in cloud amount. Indeed, Figure 15 shows that the net radiative flux at the surface can vary by 80–90% from one day to another. At higher latitudes, while the variations of the net radiative flux between clear and cloudy skies are substantial, they are proportionally much smaller than found in the tropics because of a greater infrared-solar radiation flux compensation.

Even though it has been established that the variation of the downwelling infrared radiative flux in the tropics is relatively small in percentage terms (i.e., about 10%), it translates into variations in $I_{\downarrow}$ of between 20 and 40 W m^{-2} at the surface. This is a large number in terms of the surface flux and about 4 times the estimated requirement for the initialization of coupled ocean-atmosphere models [*World Climate Research Program*, 1985] using monthly mean quantities. There are even more stringent requirements for climate models used to assess global warming. It is estimated that a CO_2 concentration doubling would increase the surface downwelling infrared flux by 5 W m^{-2}. Thus very careful modeling of cloud radiative properties is required.

6.3. The Distribution of Radiative Heating in the Upper Ocean

It is clear from the above discussion that clouds change the magnitude of the net radiation flux at the surface of the ocean. However, clouds also change the spectral distribution of the net radiative flux. This spectral format is important as it determines the vertical distribution of radiative heating in the upper ocean.

Expanding (10), the total radiative flux at the surface may be written as

$$Q_r = S_s + I_\downarrow - I_\uparrow$$
$$= S_0(1 - a_c)(1 - a_s)(1 - \alpha) + I_\downarrow - I_\uparrow + \Delta S' \quad (16)$$

where S_0, a_c, a_s, and α are the local solar irradiance at the top of the atmosphere, the cloud albedo, the surface albedo, and the solar absorption coefficient of the atmospheric column, respectively. $\Delta S'$ is the contribution to the surface solar radiation from multiple reflections from the surface and the cloud base. Over land areas, where both the shortwave and longwave radiation are rapidly attenuated with depth in the skin layer of the soil or in the biosphere, the heating of the surface is determined by Q_r directly, together with the turbulent surface fluxes of heat and moisture. In the upper ocean the situation is very different; turbulent fluxes are still important, although in different proportions to over land. Furthermore, vertical dynamic heat transfer and the horizontal advection of heat beneath the surface, absent in the land situation, become very important. Also, the attenuation coefficient of the radiation in the ocean is smaller than in soil and is a very strong function of the wavelength. The downwelling infrared radiation $I_\downarrow$ is absorbed in the first few micrometers and the upwelling infrared emission to the atmosphere $I_\uparrow$ occurs from an equally shallow layer. Ocean solar radiation absorption shows a strong spectral dependence, with the red and near-infrared radiation absorbed within a meter or so of the surface and the shorter wavelength radiation (i.e., the blue-green end of the spectrum) absorbed at greater depths.

Simpson and Dickey [1981] divided the solar radiation incident at the surface of the ocean into two streams representing, in turn, the longer-wave part of the spectrum (the "red" end) and the shortwave end (the "blue-green" end). They developed the following expression for the intensity of subsurface solar radiation:

$$S_{oce}(z) = S_s\left[r \exp\left(\frac{z}{\psi_1}\right) + (1 - r) \exp\left(\frac{z}{\psi_2}\right)\right] \quad (17)$$

where r is the proportion of the incident solar radiation following the red absorption characteristics (attenuation depth of ψ_1) while $(1 - r)$ is the proportion of blue-green solar radiation (ψ_2). Table 4 summarizes the relative absorption of radiation as a function of depth and wavelength. Here, ψ_1, ψ_2, and r are also strong functions of turbidity of the ocean which may, in turn, partly depend on S_{oce} through the stimulation of biospheric activity. The red end of the solar spectrum ($\lambda > 0.9$ μm) accounts for about 40% of the incoming flux with an e-folding depth of about 1 cm. The visible blue-green end of the spectrum ($\lambda < 0.9$ μm) represents about 60% of the incoming radiation and reduces to e^{-1} of its surface value within 8 m of the surface and 98% by 100 m. Figure 18 shows the attenuation of solar radiation in the ocean as a function of wavelength and depth. The downwelling atmospheric infrared radiation (i.e., $I_\downarrow$) is attenuated within a few micrometers of the surface of the ocean. The infrared emittance (i.e., $I_\uparrow$) emanates from the same shallow layer.

The largest modulator of radiative heating of the upper layer of the ocean is the diurnal cycle of solar heating. During the day the heating is spread through the ocean column according to Figure 18 together with the downwelling atmospheric radiation which is absorbed in the ocean skin layer. At nighttime the heating of the ocean is only a function of the net infrared radiation which is confined to the surface layer.

It is possible that radiation attenuation may be significant for longer-term climate variability if the radiation attenuation depth scale is greater than the depth of the ocean mixed layer. Dynamic processes above the thermocline occur on much more rapid timescales than below. If the attenuation depth (e.g., ψ_2) is greater than the mixed layer depth, then slower dynamic processes will have to adjust to the added heating. The lettering on Figure 18 shows the average thermocline depths for the summer extratropics (A), the average tropics (C), and the eastern (B) and western (D) equatorial Pacific Ocean, respectively. During warm events in the Pacific Ocean (i.e., during El Niño episodes), the average thermocline depth across the entire Pacific Ocean is somewhere between B and D. The importance of the magnitudes of the attenuation depths are now apparent. If $\psi_2 < z$ (A, $\cdots$, D), then the radiative heating of the column will be mixed rapidly by the rapid near-surface mixing processes. However, if $\psi_2 > z$ (A, $\cdots$, D), then the slower dynamics of the deeper ocean must compensate for the diurnal heating at depths greater than the thermocline depth. *Woods* [1984] suggested that during a period of rapid transition in the Pacific Ocean (e.g., during the onset of an El Niño event), a fraction of the solar heating may be absorbed below the thermocline. Woods felt that this anomalous heating could be significant in a climate sense as it could not be redistributed rapidly by mixed layer dynamics.

Care must be taken in interpreting Table 4 and Figure 18. During its transmission through the atmosphere, the solar beam is subject to substantial reflection and absorption by the ambient water vapor and clouds in the atmosphere. Reflection also takes place at the surface of the ocean. Reflection by clouds and the ocean surface is fairly uniform across all wavelengths and results in an overall reduction of intensity of the solar beam. However, absorption by clouds and water vapor is very spectrally dependent. The blue-green end of the spectrum is transmitted through the atmosphere and cloud (albeit at lower intensity due to reflection) with little absorption. Part of the solar radiation spectrum is in the near infrared, which is absorbed preferentially by atmospheric water vapor and cloud water droplets, water vapor, and ice crystals. The remainder of the visible spectrum is absorbed

TABLE 4. Energy Distribution With Depth of the Incoming Solar Beam Displayed as a Function of Wavelength

	Depth in Ocean, m									
Wavelength, μm	*0*	*10^{-5}*	*10^{-4}*	*10^{-3}*	*10^{-2}*	*10^{-1}*	*1*	*10*	*100*	*Proportion*
Blue-green										
0.2–0.6	237	237	237	237	236	229	207	172	14	60%
0.6–0.9	360	360	360	359	353	305	129	9		
Red										
0.9–1.2	179	179	178	172	123	8				40%
1.2–1.5	87	86	82	63	17					
1.5–1.8	80	78	64	27						
1.8–2.1	25	23	11							
2.1–2.4	25	24	19							
2.4–2.7	7	6	2							
Sum	1000	993	953	858	729	542	336	181	14	
Percent absorbed	0	.1	5	14	27	46	66	82	99	
Percent blue-green	0	0	0	.2	1.3	10.6	43.7	69.6	97.7	*e*-fold 8 m
Percent red	0	1	12	34	65	99	100	100	100	*e*-fold 8×10^{-3}m

An incident solar intensity of 1000 is assumed. The spectral dependency of absorption falls into two categories which are termed "blue-green" and "red" bands. The percent absorption of the total beam of the blue-green and red bands is shown together with the *e*-folding depths of the solar stream. (Adapted from *Simpson and Dickey*, [1981].)

equally as attested to by the white or gray color of the base of clouds. If absorption were preferential in any spectral band (say, red), then clouds would have a blue or greenish hue. Thus in addition to the diurnal heating cycle, clouds also alter the magnitude and spectral distribution of the solar heating of the ocean.

6.4. Freshwater Flux and Ocean-Atmosphere Interaction

Godfrey [1989] has made a careful estimate of the various contributions to the buoyancy flux in the warm pool regions of the tropical oceans. Using *Oberhuber*'s [1988] estimate of the $(P - E)$ of about 2 m, Godfrey estimated that the buoyancy flux due to freshwater flux is about 4–6 cm yr^{-1}. On the other hand, if it is assumed that the net heat flux is of order 20 W m^{-2}, then the modified buoyancy flux due to the surface heat flux is also about 4 cm yr^{-1}. Thus Godfrey confirms that salinity variations in the upper ocean of the tropics are probably just as important as temperature variations. Godfrey's estimates confirm the results shown in Figure 13. In fact, *Lukas* [1988] showed that the depth of the mixed layer is determined by salinity as often as by temperature. With this information it is possible to form a conceptual model of the tropics that allows the role of the freshwater flux to be understood in a general context.

Reference to Figures 26 and 27 shows that the low-level equatorial winds are made up of easterlies and westerlies that converge over the tropical warm pools. The impacts of easterlies and westerlies on the near-equatorial ocean are opposite: an anisotropicity introduced by the rotation of the planet. Westerly winds (e.g., in the eastern Indian Ocean of Figure 26a) are convergent at the equator due to Coriolis effects and produce moisture convergence and thus convective development. Also, they produce downwelling in the ocean through Ekman convergence [e.g., *Pond and Pickard*, 1983], which maintains the warm SSTs. In contrast, low-level easterlies sponsor Ekman divergence along the equator that results in cold water upwelling and, generally, an absence of convection. A clear example of the impact of equatorial upwelling can be seen in the eastern equatorial Pacific Ocean in Figure 7.

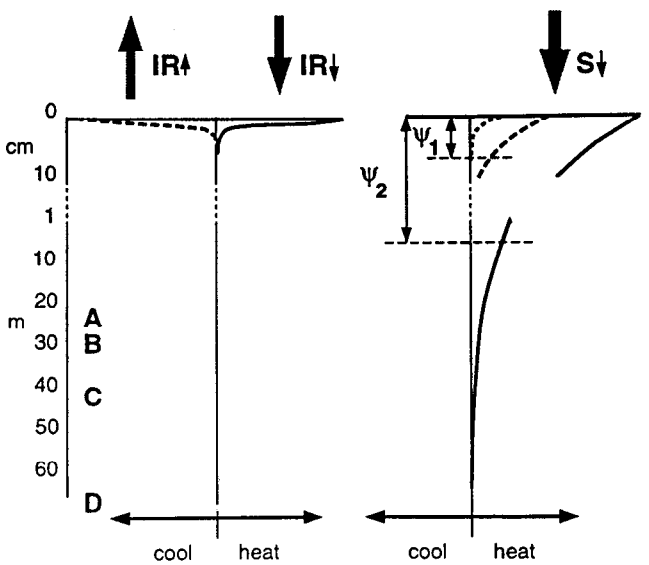

Figure 18. Attenuation of radiation in the upper ocean: (left) the infrared radiation and (right) the solar radiation. Here, ψ_1 and ψ_2 are the attenuation depths of the red and blue-green parts of the solar spectrum. The near-infrared and longwave components of the total stream are attenuated within a few microns of the surface of the ocean. The lettering (A–D) refers to the mean thermocline depths at various locations in the ocean and is discussed in the text.

It is the context of the different impacts of easterlies and westerlies on the ocean that gives precipitation added importance in the tropics. A freshwater flux into the ocean stabilizes the surface layer, inhibits the vertical penetration of wind-driven turbulence, and thus reduces the entrainment of the colder and saltier subthermocline water. In addition, a fresh stable surface layer will be heated by solar radiation, further increasing the stability. The layer between the fresh surface lens and the main thermocline has been termed the "barrier layer" by *Lukas and Lindstrom* [1991] as it inhibits vertical mixing between the surface and the thermocline. The extent of the barrier layer is not known, but it is probably safe to say that the layer exists in the vicinity of precipitation maxima and generally low winds. In the absence of other factors, the SST of the fresh, warm pools should increase without bound.

Natural governors may exist to curtail the warming. *Ramanathan and Collins* [1991] suggest that a first response to a warming ocean is the production of very deep clouds that reduce the radiation flux at the surface. As the warm pool increases in temperature, strong heating gradients develop between the warm pools and the cooler equatorial oceans. In response to the enhanced temperature gradients the speed of the surface wind increases. In the region of surface convergence, cloudiness increases and reduces the solar surface flux. As the wind stress does work on the ocean as the third power of the wind speed, the stronger winds will eventually erode through the stable surface layer and cool the upper ocean by entrainment at the same time as increasing evaporation. This enhanced mixing is manifested as gustiness associated with disturbances and periods of strong winds that occasionally exist over the warm pools.

Lukas [1988] confirmed the negative feedback between wind strength and upper ocean homogenization. He noted that the ubiquitous temperature and salinity profiles of the tropical warm pools were similar to those shown in Figure 9b that exhibited strong near-surface density surfaces. However, only after very strong surges of winds, usually from the west, did the fresh, warm lenses disappear. It would appear that the upper limit of SST is set by modulation of the net radiative heating by clouds and evaporation. The deep mixing by the strong winds and convective events responding to increasing temperature gradients sets the lower bound on SST. The few degree variability of the warm pool SST is probably an oscillation between these two sets of controls.

6.5. Distribution of Total Heating in the Ocean-Atmosphere System

Radiative, turbulent heat and freshwater fluxes at the ocean interface depend on both the SST and on events or processes occurring in the overlying atmosphere. Atmospheric motions are driven by a combination of radiative and latent heating. Gross estimates of the horizontal gradients of net radiative flux ∇F_r and latent heat flux ∇F_{lh} will now be made. In turn, these atmospheric forcing functions will be related to the heating of the upper ocean. The heating in four columns marked A, B, C, and D in Figures 27a, 27b, and 27c is calculated. These represent the desert regions of north Africa, the monsoon region of south Asia and the western Pacific Ocean, the South Indian Ocean, and the eastern Pacific Ocean, respectively.

A simple radiative model can be built to calculate the radiative flux divergence in each column. Essentially, the model is only a small extension of the global radiation model described in (4) and (5) and shown in Figure 6b. The net solar ($\Sigma S = S_\uparrow - S_\downarrow$) and longwave ($\Sigma I = I_\uparrow - I_\downarrow$) fluxes are calculated at the top and bottom of the atmospheric column. The net radiative flux in the atmospheric column is given by

$$F_r = (\Sigma S + \Sigma I)_{z=\infty} - (\Sigma S + \Sigma I)_{z=0} \qquad (18)$$

which may be expanded to give

$$F_r = S_0\alpha(1 - a_c)[1 + (1 - \alpha)a_s] - \sigma T_{ct}^4 + \sigma T_s^4 - \sigma\varepsilon_{bl}T_{bl}^4 - \sigma(1 - \varepsilon_{bl})T_{cb}^4. \qquad (19)$$

Besides the quantities defined in (4), (5), and (15), T_{ct}, T_{bl}, and T_{cb} represent the temperatures of the cloud top, the subcloud boundary layer, and the cloud base, respectively. If the emissivity of the atmospheric column is less than unity, it is assumed that the atmosphere radiates with an emissivity ε_a at radiating temperature T_a weighted relative to the moisture distribution of the column. Using the data from Table 5, the horizontal gradients of latent and radiational heating (e.g., $\nabla F_r(B \rightarrow A) = F_r(B) - F_r(A)$) between the various columns can be calculated. The magnitudes are listed in a footnote to Table 5.

Within the confines of this very simple model, the gradient of the net radiative flux across the Pacific Ocean is found to be within a factor of 2 to 3 of the latent heating gradient. Furthermore, significant gradients exist between the south Asian region and the north African deserts (i.e., between B and C) with magnitudes that parallel the latitudinal gradient across the equator. Radiative and latent heating effects, then, drive a transverse gradient of a similar magnitude to the cross-equatorial lateral monsoon. These estimates corroborate the observations of *Yang and Webster* [1990], who made similar calculations from the satellite-derived OLR data and the calculations of *Randall et al.* [1989], who used a complex general circulation model.

It is important to note that the latent and radiative heating gradients will always be of the same sign. That is, when the dynamics of the ocean-atmosphere coupled system conspire to provide moisture convergence and ascent and thus establish the horizontal gradient of

TABLE 5. Defining Parameters of the Four Columns Representing North Africa, South Asia and the Western Pacific Ocean, the South Indian Ocean, and the East Pacific Ocean

Quantity	*Parameter*	*Columns*			
		A	*B*	*C*	*D*
Surface Temperature, °K	T_s	308	303	298	298
Cloud base temperature, °K	T_{cb}	—	285	285	285
Boundary layer temperature	T_{bl}	300	290	289	289
Cloud top temperature, °K	T_{ct}	—	220	265	265
Mean atmospheric temperature, °K	T_a	275	275	270	270
Cloud albedo	a_c	0	0.3	0.2	0.15
Surface albedo	a_s	0.4	0.3	0.1	0.1
Absorbtion coefficient	α	0.05	0.15	0.1	0.1
Emissivity (atmosphere)	ε	0.6	1.0	0.8	0.6
Emissivity (boundary layer)	ε_{bl}	0.6	0.8	0.8	0.7
Precipitation rate, mm/d	r	0	10	3	2
Latent heating, W m^{-2}	Q_{lh}	0	289	82	58
Radiative heating, W m^{-2}	Q_r	−62	44	−65	−63

See Figure 26 for locations of A, B, C, and D. The differences of the latent, radiative, and total heating between the columns calculated using (18) are $\Delta F_{lh}(B \rightarrow A) = 289$; $\Delta F_{lh}(B \rightarrow C) = 207$; $\Delta F_{lh}(B \rightarrow D) = 231$; $\Delta F_r(B \rightarrow A) = 106$; $\Delta F_r(B \rightarrow C) = 109$; $\Delta F_r(B \rightarrow D) = 107$. Units are in watts per meter squared. Conditions are for the boreal summer.

latent heating, the resultant cloud mass will produce a same-signed radiative heating gradient. Thus, once a latent heating gradient is established, the resultant radiational heating gradient will continue and maintain the moisture convergence and latent heating.

Even though the horizontal scale of the two heating gradients is the same, the temporal characteristics of the latent and radiative heating are different. Latent heating requires upward motion which is usually constrained to be within the cores of deep cumulus clouds. For example, it has been shown using satellite data (G. Liu et al., Classification of clouds over the western equatorial Pacific Ocean using combined infrared and microwave satellite data, submitted to *Journal of Geophysical Research*, 1994) that only 25% of clouds in the tropics, at any one time, are precipitating. Net radiative heating of the troposphere merely requires the existence of cloud or a region of enhanced water vapor concentration. Therefore while only a small amount of the cloud mass precipitates and releases latent heat, all of the cloud mass is radiatively active. Net radiative heating extends over all regions where there is (or has been) extensive cloudiness and exists for a longer period than the precipitation event. As a result, the entire western Pacific Ocean region, for example, is probably dominated by radiatively forced broad-scale, slow ascent in addition to the more regional ascent associated with latent heating [*Randall et al.*, 1989].

There is an important caveat that must be attached to the above discussion. In section 5.1 it was pointed out that the vertical distribution of heating was important in determining the vigor of a direct circulation. Circulation strength is optimized by heating at the highest pressure and cooling at the lowest. The same constraints apply to the radiational driving of the system. If the radiative heating is to enhance the Walker Circulation, for example, the heating should be in the lower troposphere in the western Pacific and the cooling in the upper troposphere of the eastern Pacific. Only a minimal enhancement of the cell will occur if the heating and cooling were to change positions in the vertical.

The induced heating in the upper ocean between the cloudy and the clear regions can now be calculated. *Ramanathan* [1987] estimated that the heating gradient is about 0.5 to 1.5°C month^{-1} averaged over a 100-m layer of the ocean between the western and eastern Pacific. That is, he found that anomalous radiative flux convergence in the atmosphere (which produces an atmospheric heating) is accompanied by a reduced solar flux at the surface of the ocean (which results in an ocean cooling). Alternatively, increases (decreases) in atmospheric buoyancy are matched by decreases (increases) in ocean buoyancy. Therefore the interesting fact is that the heating gradient in the ocean is in the opposite sense to the radiational and latent heating gradient in the atmosphere!

Figure 19 shows a representation of the heating gradients within the coupled ocean-atmosphere system. Given a positive correlation between warm SST and cloudiness amount, it would seem that the ocean-atmosphere feedback is describing a natural governor on the system. With an increase of SST, cloudiness increases which, in turn, reduces the radiative heating of the ocean and modulates the SST increase. A decrease in cloud amount, though, will increase the heating of the ocean. *Ramanathan and Collins* [1991] argue that this feedback keeps the ocean temperature within rather narrow bounds.

The governing of ocean-atmosphere interaction is probably more complicated than a purely radiational regulation suggested by Ramanathan and Collins. Differential latent and radiative heating drive atmospheric

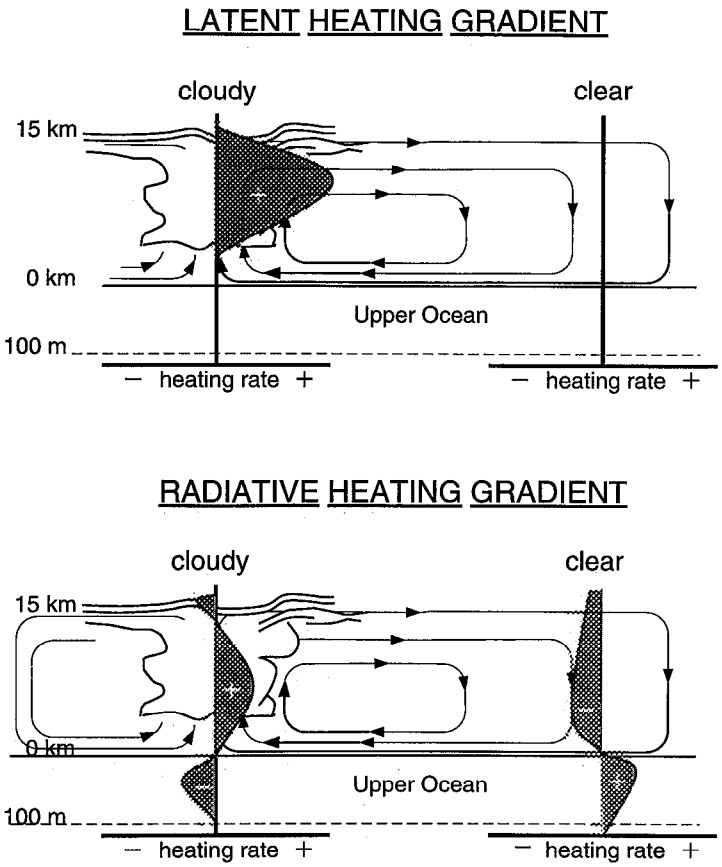

Figure 19. Comparison of the latent heating gradient and radiative flux divergence in the atmospheric and oceanic columns between clear and cloudy regions. The radiative and latent heating gradients in the atmosphere are in phase, although the radiative flux divergence probably exists on a broader scale than the latent heating. However, in the ocean the associated radiative heating is opposite in sign to that in the atmosphere. Clear regions are associated with radiative heating (cooling) of the ocean (atmosphere), while cloudy regions are associated with radiative cooling (heating) of the ocean (atmosphere). The heating rate differential in the upper ocean between the cloudy western and the less cloudy eastern Pacific Ocean is about 0.5 and 1°C month^{-1}. After *Ramanathan* [1987].

circulations which cause an increase in evaporation and deep ocean mixing. All these factors influence SST. Extensions of the Ramanathan-Collins hypothesis that take into account these factors have been suggested by *Fu et al.* [1992], *Stephens and Slingo* [1992], and *Hartmann and Michelson* [1993], among others.

Neither the Ramanathan and Collins model nor the extensions include the increasing stabilization resulting from the freshwater flux. For example, Ramanathan and Collins's hypothesis calls for an increase of convection to produce a greater cloud mass to reduce the surface radiative flux. However, increased convection is associated with increased precipitation and thus a greater freshwater flux. Thus while increased convection will lead to a reduction in the surface radiative flux, the radiative heating is constrained to remain in a fresher and shallower surface lens. Clearly, radiative controls alone cannot restrict SST increases. Thus a constraining mechanism of the increasing temperature of the warm pool must include the destruction of the warm, fresh lens.

6.6. Simulations and Observations of Upper Ocean–Atmosphere Interactions

To integrate the processes that couple the ocean and the atmosphere together, either a model or a complete data set that combines both ocean and atmospheric observations must be used. Both techniques have their own attributes and problems. Models allow control experiments and physical processes to be defined very precisely. On the other hand, the model is only as good as the interpretations of the physical processes that guide the building of the model. Studies using observations have the benefit of gathering actual data of natural events. The limitations here, though, are the quality of the data and the events that took place while instruments were in place. Both of these techniques will now be used to provide a synthesis of ocean-atmosphere interaction.

6.6.1. Simulation of ocean-atmosphere interaction. The model chosen for the upper ocean simulations is the one-dimensional model of *Kantha and Clayson* [1994] with a second-order turbulence closure scheme. The model has had some success in simulating a wide range of ocean conditions. The model belongs in a class of ocean models originated by *Kraus and Turner* [1967] and later refined by *Garwood* [1977]. A one-dimensional model allows sensitivity studies with some ease. On the other hand, its simplicity does not allow the calculation of the lateral response of the model to changes in the buoyancy flux and, consequently, the horizontal density gradient.

Figure 20a shows the initial conditions used for the simulation of the upper ocean structure. The profiles chosen closely match the characteristics of the tropical

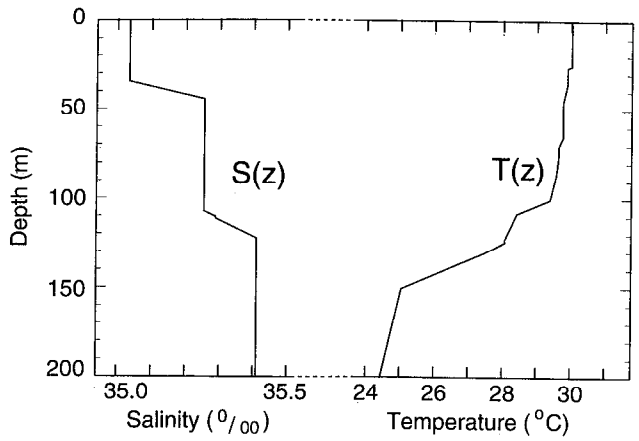

Figure 20a. The initial conditions used in the Kantha-Clayson mixed layer model. The profiles show salinity (per mil, left curve) and temperature (in degrees Celsius, right curve) as functions of depth. The data follow the western Pacific profiles shown in Figure 9b.

warm pools shown in Figure 9b, including a near-surface freshwater lens. The *e*-folding attenuation depth of solar radiation in the ocean is assumed to be 8 m. Cloudiness was incorporated into the model by utilizing the radiation scheme described by *Stephens and Webster* [1979]. With this scheme, solar and infrared radiation fluxes at the surface for arbitrary cloud distributions were supplied to the model relative to the emissivity-albedo parameterization used in Figure 17a. In all cases the climatological background moisture distribution from Figure 3 was used.

Figure 20b shows the results of three sets of experiments. In the first set of curves the evolution of the SST is plotted against surface wind speed with values ranging from 5 to 20 m s^{-1}. The speeds vary from the climatological average in the western Pacific Ocean to the extreme of a westerly wind burst [e.g., *Keen*, 1988]. The second set of curves represents the impact of precipitation on the SST evolution. Values range from 0 to 10 mm h^{-1}. The climatological precipitation rate for the warm pool region of the western Pacific Ocean is about 0.4 mm h^{-1}. However, precipitation rates during disturbed periods may average an order of magnitude larger for prolonged periods. Wind speed is assumed to be 5 m s^{-1} with zero cloudiness. The third set of curves shows the effect of cloud amount on SST. Cloud amounts step from 0% to 90%. In each of the cases run, the latent heat flux at the surface is governed by a bulk formula that sets the flux proportional to the product of the wind speed and the vapor pressure difference between the surface and 10 m altitude. Effectively, the latent heat flux increases from about 85 W m^{-2} at 5 m s^{-1} to about 300 W m^{-2} at 20 m s^{-1}.

The impact of varying the physical parameters is quite clear. Holding all other parameters constant, increasing wind speed tends to lower the SST. The effect is nonlinear as the wind does work on the ocean proportionally to the third power of the wind speed. Thus, with a prolonged period of strong winds (see, for example, Figures 21 and 22), the SST will rapidly approach thermocline temperatures. A positive freshwater flux, holding wind speed and insolation constant, increases the SST slightly over the 5-day period. Cloud increases, on the other hand, decrease the SST.

Diurnal variability is strongly evident in Figure 20b. Stronger winds decrease the amplitude of the diurnal SST oscillation by increasing mixing throughout the day. At low wind speeds, vertical mixing is maximized at night as the surface cools. A positive freshwater flux increases the amplitude of the diurnal maxima by retarding daytime mixing. For very large cloudiness amounts the diurnal variability decreases as the solar forcing diminishes.

The time sections of SST shown in Figure 20b are limited in value because only one parameter is changed at a time. Figure 20c plots 5-day changes in SST as a function of total heating of the ocean and the wind speed for three values of the freshwater flux. The results of the experiments may be summarized as follows. For a given surface radiation flux the SST decreases as wind increases. For a given wind speed the SST increases as radiation increases. In the strong

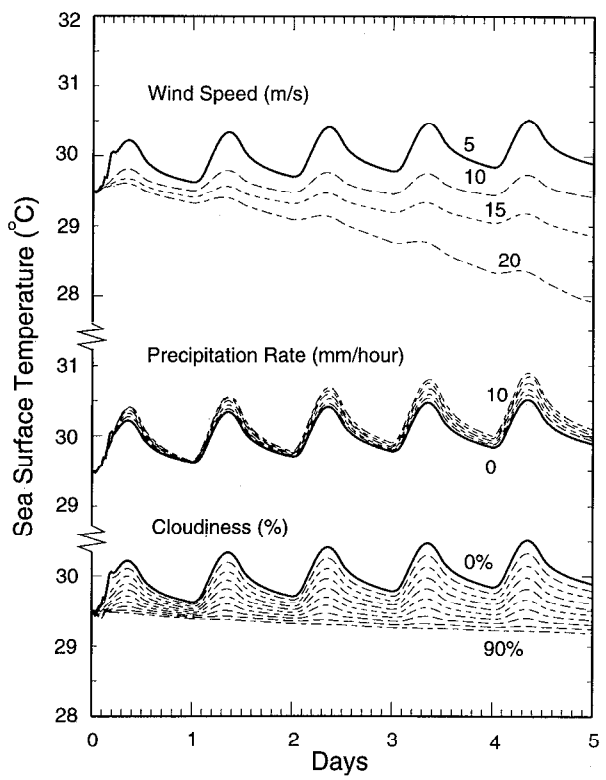

Figure 20b. Results with experiments using the Kantha-Clayson model. The SST evolution for different wind speeds with cloudiness and precipitation set to zero (top curves), for different precipitation rates with wind 5 m s^{-1} and zero cloudiness (middle curves), and for different cloudiness with wind speed at 5 m s^{-1} and no precipitation (bottom curves).

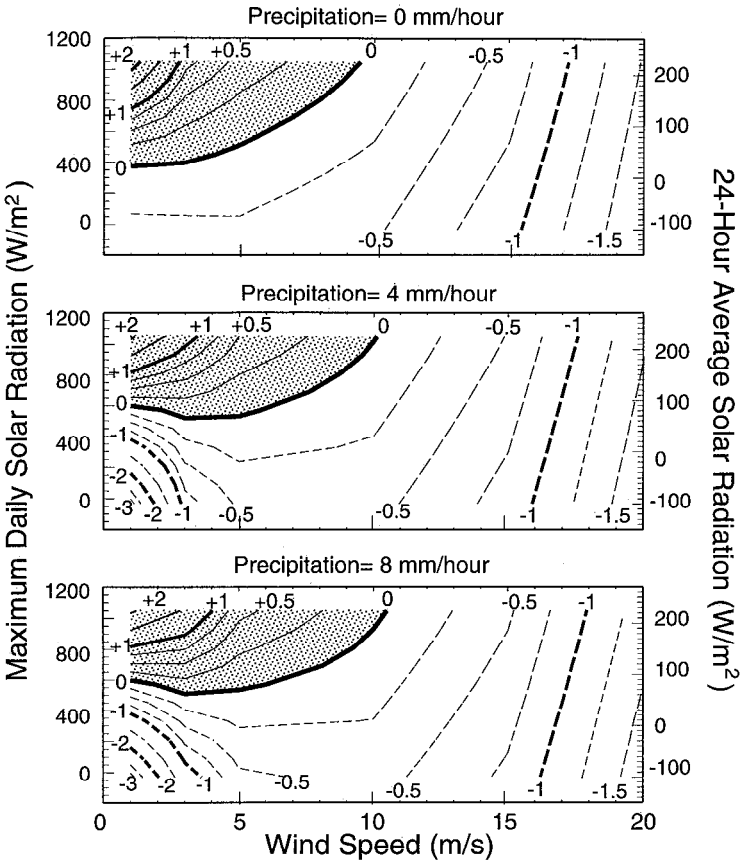

Figure 20c. The 5-day change in surface temperature as a function of solar radiation intensity (left ordinate, maximum daily value; right ordinate, 24-hour average solar radiation) plotted as a function of wind speed (in meters per second). Variations in radiation may be thought as a surrogate for cloudiness. Shaded areas indicate regions of increasing SST.

wind regime, mixing and evaporation tend to dominate over the radiative heating, irrespective of the magnitude of the freshwater flux. However, at low wind speeds, significant freshwater fluxes can create a fresh buoyant surface layer. With large solar radiation the surface layer will heat with values of order 2°C per 5 days. For low values of solar radiation, conditions that normally accompany heavy precipitation, the surface cools considerably. If the averaging time were increased, the cooling would eventually reach a limit when the column becomes gravitationally unstable. Also, winds are usually gusty and strong during periods of heavy rainfall so that it is unlikely that the fresh lens could become as cool as the figure indicates.

The magnitude of the diurnal variation of the SST was calculated as a function peak solar radiation for 3 and 5 m s^{-1} wind speeds. The results are shown in Figure 20d for precipitation rates of 0, 4, and 8 mm h^{-1}. In general, as insolation increases, the diurnal variability increases. However, as wind speed increases, the diurnal amplitude decreases. Finally, the larger the precipitation rate, the greater the amplitude. The model estimates compare well with the observed values along axis A in Figure 14.

Overall, the impacts of wind and cloudiness variation appear to be about the same order of magnitude. To put the effects into perspective, consider the vari-

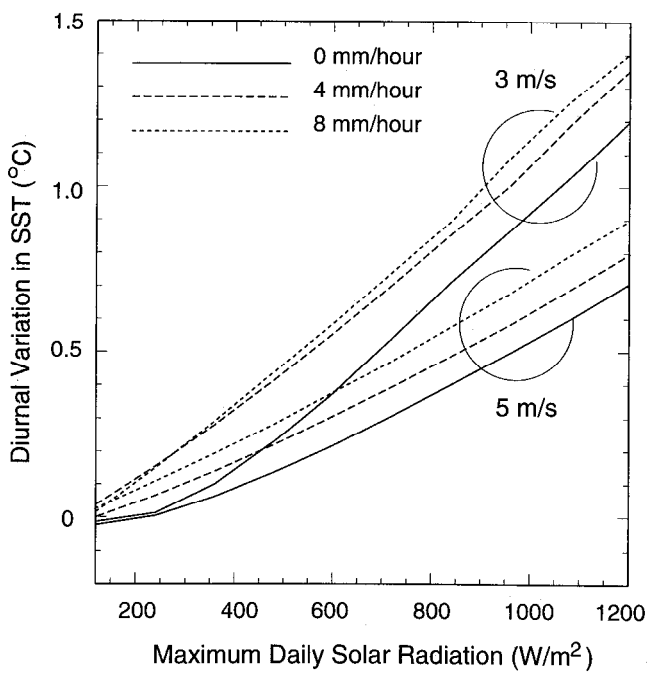

Figure 20d. The amplitude of the diurnal variation of the SST as a function of surface solar radiation for three precipitation rates (0, 4, and 8 mm h^{-1}). Results for wind speeds of 3 and 5 m s^{-1} are shown.

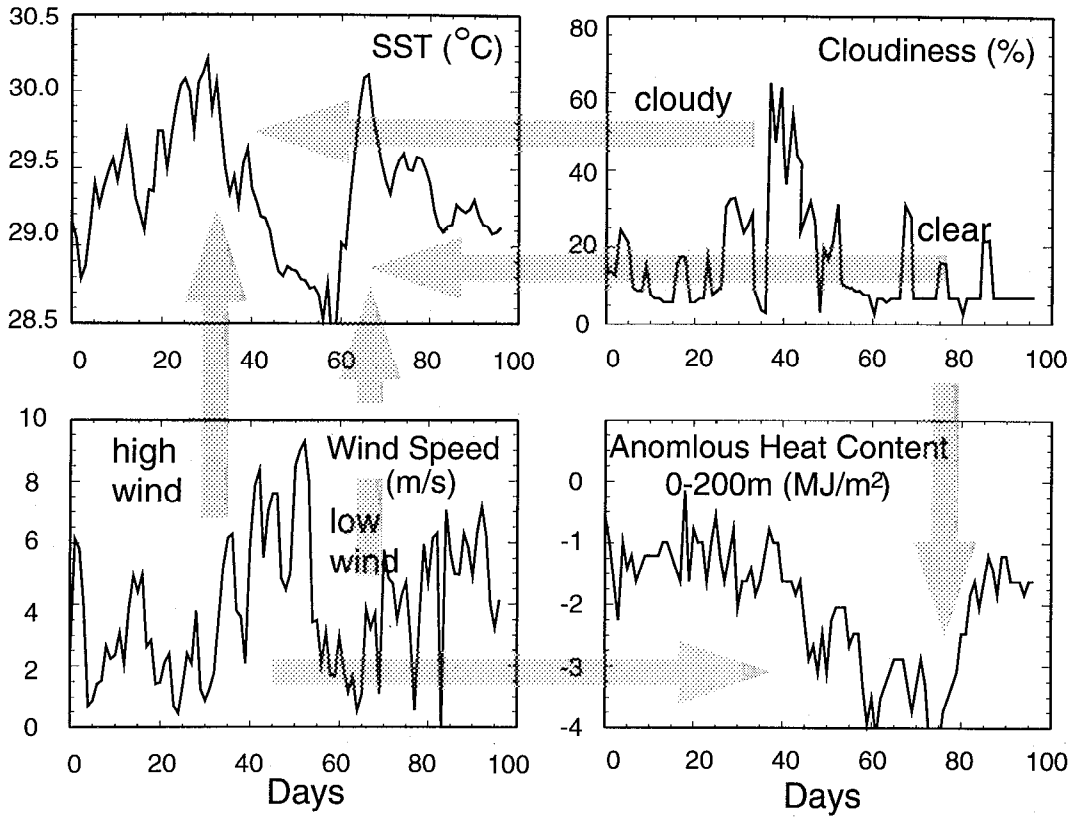

Figure 21. Example of ocean-atmosphere interaction during the western Pacific Tropical Ocean–Global Atmosphere Coupled Ocean-Atmosphere Response Experiment (TOGA COARE) held in the western Pacific Ocean, November 1992 to February 1993. Shown are the evolution of SST (in degrees Celsius; top left), wind speed (in meters per second; bottom left), a measure of cloudiness using outgoing longwave radiation (OLR < 235 K; top right), and the 0–200 m heat content (megajoules per square meter; lower right). The large arrows indicate the roles of wind (through deep mixing and evaporation) and insolation (heating) play in modifying the SST and the subsurface ocean structure.

ation of the two parameters over observed ranges. Winds vary between about 5 m s^{-1} and 10 m s^{-1}, excluding extreme events, and the total peak radiative flux varies between 400 and 800 W m^{-2}. If a precipitation rate of 4 mm hr^{-1} is assumed, insolation induced SST changes of about 0.3°C per 5 days are found. Wind effects, on the other hand, are slightly larger at 0.35°C per 5 days. For extremely strong wind events (15–20 m s^{-1}), wind-induced SST changes clearly dominate.

6.6.2. Observations of ocean-atmosphere interaction. From November 1992 through February 1993, a large-scale coupled ocean-atmosphere experiment was conducted in the western Pacific Ocean. TOGA COARE allowed, for the first time, for the tropical ocean and the atmosphere to be observed and diagnosed simultaneously on a multitude of scales. This coupled data set provides an unprecedented opportunity to test hypotheses of the basic processes that determine the SST and the state of the coupled ocean-atmosphere system.

Figure 21 shows daily averaged values of the SST, surface wind speed, the effective cloud cover, and the upper ocean heat content over a 20,000 km^2 area at the center of the TOGA COARE observing array in the western Pacific Ocean during the period November 10, 1992 to February 1, 1993. Heat content is defined as the integral of the enthalpy over an ocean layer (i.e., $\int_0^{200m} C_p T\, dz$) between the ocean surface and 200 m depth. Cloud cover (percent) is defined as the area possessing an OLR effective temperatures <235 K. As the downwelling radiation is almost independent of cloud amount (see Figure 15), high values of OLR indicate low net radiation at the surface. Low values, on the other hand, indicate high net radiation at the surface.

A correlation of −0.7 occurs between the SST and the wind speed as periods of strong wind speed are matched with rapid cooling of the SST. For example, the strong wind periods of mid-November, late December, and early February correspond to minima in SST. The steepest decline in SST (30°–28.5°C) occurs during a period of strong westerly winds in mid-December and early January. The cooling rate of 1.5°C per 10 days matches well the estimates from the one-dimensional model. For comparable conditions the

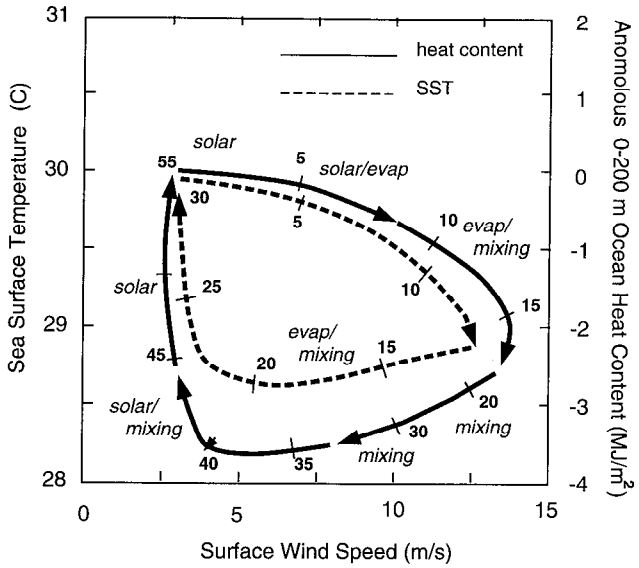

Figure 22. The evolution of the SST (dashed curve) and subsurface heat content (solid curve) as a function of time (numbers denote days) in SST surface wind space during a strong westerly burst case during TOGA COARE. The two quantities project hysteresis curves with the subsurface structure taking nearly twice as long as the surface to recover. Dominant processes are indicated on the diagram.

cooling rate in Figure 20c is about 0.5°C per 5 days. On the other hand, strong insolation (i.e., low OLR%) corresponds to SST warming but only when the wind speed is light. Thus, while solar radiation is very important in heating the upper ocean, so is the strong wind-induced evaporation and deep turbulent mixing. In addition, there is cooling throughout the column. Starting at the time of the late December strong winds, the heat content between the surface and 200 m decreases by nearly 5 MJ m^{-2}.

The results from Figure 21 can be summarized as follows. Concentrating on the principal strong wind period (late December to early January), the SST returns to preburst values in about 10 days. During the relatively light wind conditions following the burst, a shallow near-surface warm layer overlaying the cooled subsurface layer is produced by solar heating. Subsequent wind events will mix down this warm layer and eventually reestablish the heat content of the upper ocean but over a much longer period. The change in heat content is very large and is equivalent to the heat loss associated with "turning off" solar radiation for about 15 days.

The loss of upper ocean heat content in the TOGA COARE region is associated with two local basic processes: heat loss by enhanced evaporation and enhanced turbulent mixing throughout the ocean column which entrains cooler subthermocline water up from below. However, it is interesting to note that the loss of heat content continues for some period after the winds have diminished. This lag indicates that other, perhaps remote, features are important. Quite possibly, the strong winds have produced a dynamic response in the ocean, and the lag in the decrease in heat content is being produced by the upwelling of cold subthermocline water occurring behind a large-scale Kelvin wave propagating toward the east. Evidence of such waves was first noted in the eastern Pacific by *Knox and Halpern* [1982]. Following the westerly wind burst, warming occurred in the eastern Pacific about 2 months later, which is consistent with the 2 m s^{-1} propagation speed expected of the ocean Kelvin wave [*Philander*, 1990]. Thus at this time it is difficult to attribute exactly the proportion of heat content change due to local heat flux changes, enhanced mixing, or the propagation of dynamic modes through the ocean column.

A summary of the processes involved in changing the SST and the heat content of the upper ocean during the strong wind event during TOGA COARE is shown in Figure 22. Heat content and SST are plotted against surface wind speed. The evolution of the SST and the heat content both follow hysteresislike curves. The hysteresis period for the evolution of the heat content of the upper ocean (60 days) is much slower than that of the SST (30 days). Both are slower than the 24-hour relaxation time of the atmospheric boundary layer following convection noted in Figure 15.

7. HYDROLOGICAL PROCESSES AND LARGE-SCALE OCEANIC AND ATMOSPHERIC CIRCULATIONS

Up till this point, the main concentration has been on developing a background for the role of hydrological processes in climate and understanding the specific processes involved in ocean-atmosphere interaction. Here an attempt is made to relate these processes to the climate system in general.

7.1. The Ocean Thermohaline Circulation

The ocean thermohaline circulation that appears in nature takes on a far more complicated structure than the simple prototype developed in section 5.1. There are many reasons for this, but probably the most important are the finiteness of the ocean basins, the interconnections of the basins, and the spatially and temporally varying forcing from the atmosphere.

Stommel [1958] first established the existence of a coherent, deep (abyssal) ocean current pattern that linked the ocean basins. He showed that given deep-water generation in the northern Atlantic Ocean, an abyssal circulation flows southward along the western boundary to the southern oceans. In a sense the flow appears as a deep countercurrent beneath the major wind-driven western boundary currents of the upper ocean. The flow moves eastward around Africa to form a deep circumpolar current. Deep flows also move northward along the western Indian and Pacific

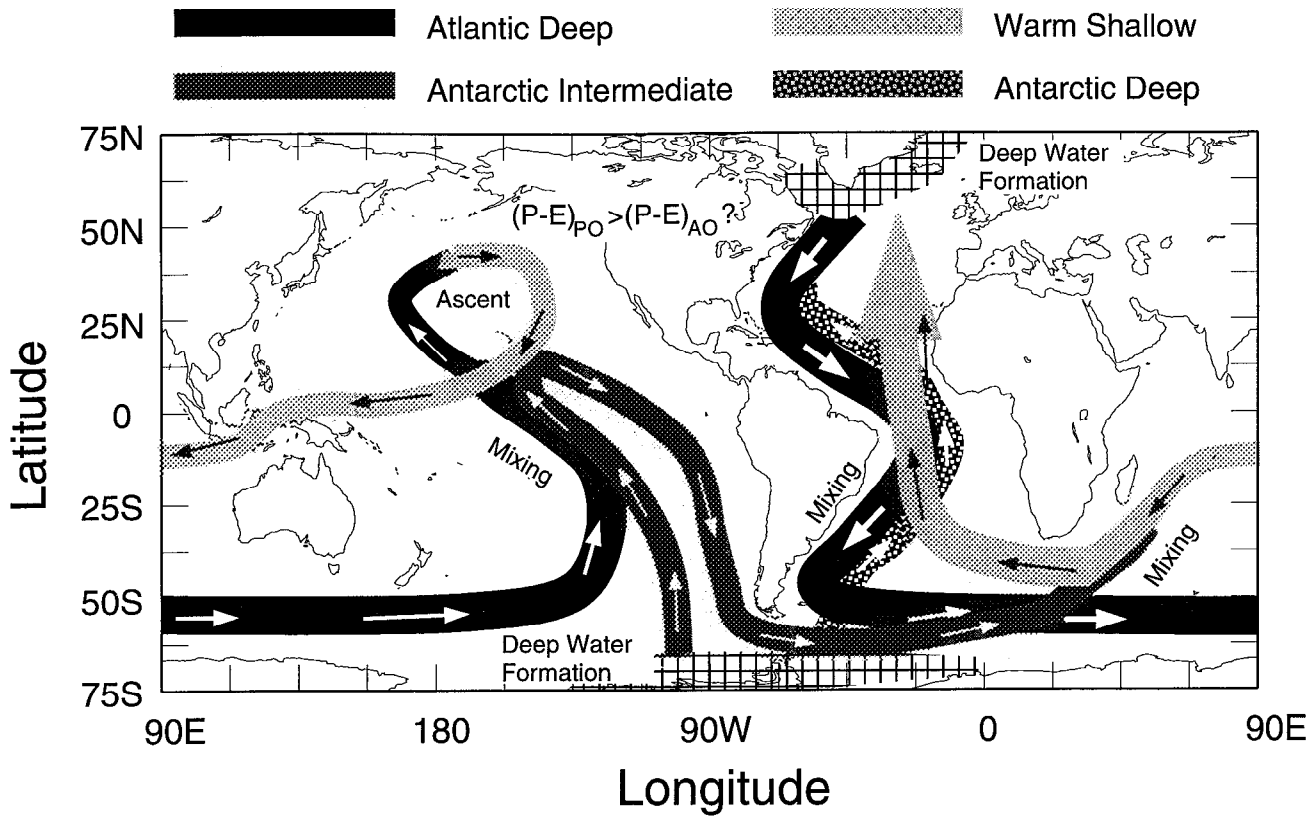

Figure 23. A simplified schematic view of the ocean thermohaline "conveyor belt." Current major deepwater sources are shown as hatched areas in the North Atlantic and the Weddell Sea. Atlantic Deep Water (black curves) flows southward as an abyssal current reminiscent of *Stommel* [1958] that eventually reaches the North Pacific Ocean. The return flow to the Atlantic Ocean is accomplished by two processes. The Atlantic Deep Water intermingles with the Antarctic Intermediate Water (dark gray curves) with which it returns to the South Atlantic Ocean through the Drake Passage. The remaining 30% of the flow rises in the North Pacific Ocean and flows through the Indonesian Archipelago and the South Indian Ocean as a warm surface current (light gray curve). There it intermingles with the returning Antarctic Intermediate Water with which it forms a general northward flow as it completes the ocean circuit. Deep water from the Weddell Sea (the Antarctic Deep Water; hatched curve) underflows the Atlantic Deep Water with which it probably mixes. It is suggested that the reason there is no deep water formation in the North Pacific Ocean is that the Pacific is more stable than the Atlantic because of a higher freshwater flux.

basins. A second deepwater source in the Weddell Sea joins the flow from the North Atlantic in the circumpolar current.

Gordon [1986] and *Broecker* [1991] took *Stommel*'s [1958] abyssal circulation, extended it into three dimensions, and completed the circuit through the world's oceans by making connections with the surface currents. Figure 23 illustrates the extension. Referred to by Broecker as a "conveyor belt," the thermohaline circulation starts with the same major deepwater sources as Stommel and remains consistent with the abyssal circulation (black curves) until the flow reaches the northern Pacific Ocean. Mass continuity insists that there must be a return flow to the North Atlantic Ocean. *Gordon* [1991] suggests that during its northward flow in the Pacific Ocean, the Atlantic Deep Water mingles with the Antarctic Intermediate Water (deep gray curves) which forms in the southern oceans. Most of the Atlantic water leaves the Pacific Ocean through the Drake Straits. The remaining 30% of the Atlantic water rises in the North Pacific and returns as an upper ocean circulation through the Indonesian archipelago to the Indian Ocean. *Gordon* [1991] shows evidence that this warm surface flow mixes with the returning Antarctic Intermediate Water that has passed through the Drake Passage. Together, the combined water flows into the South Atlantic where it flows northward to the original source region in the North Atlantic. It is thought that the deep water formed in the Weddell sea (the Antarctic Deep Water) moves northward beneath the Atlantic Deep Water with which it intermingles. Gordon and Broecker, for the first time, pieced together a complete circuit of the ocean circulation. The timescale of the circuit was estimated to be of the order of 10,000 years or on the timescales of ice ages.

It seems certain that the Stommel-Gordon-Broecker circulation is very important in the maintenance of the present climate and in climate variability on the long timescale. *Bryan* [1986] showed that the thermohaline circulations account for the global-scale heat and freshwater balances and transports. There are also suggestions that the thermohaline circulation may vary with time. Analysis of paleoclimatology data by *Broecker et al.* [1985] and *Broecker and Denton* [1990] suggests that the form and strength of the interbasin thermohaline circulations have changed considerably over the timescales of the ice ages. Such variability is probably tied to the variation of salinity, perhaps through the influence of a variable freshwater flux from the atmosphere. Whether the freshwater flux is a stochastic process or the result of ocean or coupled forcing through some feedback route remains to be determined.

There are a number of vexing problems that still remain even with regard to the present state of the thermohaline circulation. Critical questions remain: Why are the deepwater sources so localized? Why is there not deepwater formation in the northern Pacific Ocean? Does the lower salinity of the Pacific Ocean [*Worthington*, 1981] translate into a more stable upper ocean and account for the lack of deep water formation in that basin? Why is there a difference in the salinities between the two oceans? Are the very long-term average values of $(P - E)$ different between the two oceans? What promotes variability of the thermohaline circulation as suggested by Broecker and Denton? It is questions such as these that have placed the long-term circulation of the oceans at the forefront of climate research.

7.2. Convection-SST Relationships and the Scale of Tropical Motions

There are three basic peculiarities of the major atmospheric circulation systems. First, the vertical scales of the circulations are extremely deep. The Walker Circulation along the equator and the interhemispheric monsoons extend throughout the entire troposphere [e.g., *Webster*, 1983b]. Near the equator the circulations can be identified at 16–17 km above the surface. Second, the principal circulation systems are driven and defined by heating gradients associated with hydrological processes. Third, the convection associated with the circulations is either over the continents, as in the case of the monsoon, or in the warm pools of the tropical ocean.

Classical fluid dynamics do not predict the correct scale height of convective motion in the tropics. For example, *Jeffries* [1923] anticipated that the vertical scale of the monsoon circulation should be 3–4 km using Laplace's tidal equations. Jeffries's estimate was made prior to the existence of an atmospheric sounding network that would have allowed him to check his predictions. Jeffries's failure came from an incorrect heating formulation. He assumed that the monsoon was driven by heating at the surface and not also by convective heating in the middle troposphere. *Chang* [1977] was able to show that very deep and slowly evolving solutions existed if heating was included appropriately. Clearly, the form of heating and its distribution in the vertical is important in determining the vertical scale of tropical motions.

Based on long periods of observations, *Riehl* [1954] made a key association. He noticed that tropical storms and disturbances, and deep convection in general, tend to occur within the 28°C SST isotherm. This observation is corroborated in Figure 7. However, after half a century of deliberation, the basic processes that produce the association between convection and SST remain a mystery. The predominant theory assumes that 28°C is a threshold temperature at which some coupled ocean-atmosphere instability occurs [e.g., *Lau and Chan*, 1988].

It will be argued here that the reconciliation of Jeffries's estimate of the depth of tropical circulations with observations and the juxtaposition of convection with the warmest SST have the same root. The solutions lie with dynamical arguments modulated by Clausius-Clapeyron effects.

A physical basis can be established by considering two atmospheric columns with SSTs of T_1 and T_2, where $T_2 > T_1$. The columns represent, for example, the western and eastern equatorial Pacific Ocean or the tropical warm pool and the subtropics. Panel I of Figure 24 shows the Clausius-Clapeyron relationship (from equation (2)) with the saturation vapor pressure e_s plotted as a function of SST. If we take representative SSTs of the western and eastern Pacific to be 29°C and 22°C, we find that $e_s(29°C)/e_s(20°C) \approx 1.7$, suggesting that moist processes will be considerably more important in the warm pools than in the colder regions of the tropics or elsewhere on the globe. This is merely a restatement of the results shown in Figure 4.

The implications of the differences in vapor pressures of the warm and cold columns can be seen by calculating the equivalent heat content in surface parcels in each column assuming they were to completely condense their water vapor and use that heat to raise an air parcel vertically. The convective penetration height of a moist parcel is defined as the level at which a saturated parcel, lifted through the atmosphere, will finally expend its latent heat, or, equivalently, the level at which its lapse rate asymptotes to a dry adiabatic lapse rate. At this convective penetration height the parcel will lose its buoyancy and become neutrally buoyant (Figure 24b). Assuming that the parcels are initially saturated near the surface, the convective penetration height must be a strongly nonlinear function of the SST. Figure 24c plots the convective penetration height as a function of SST. Furthermore, the magnitude of the latent heat release in each column

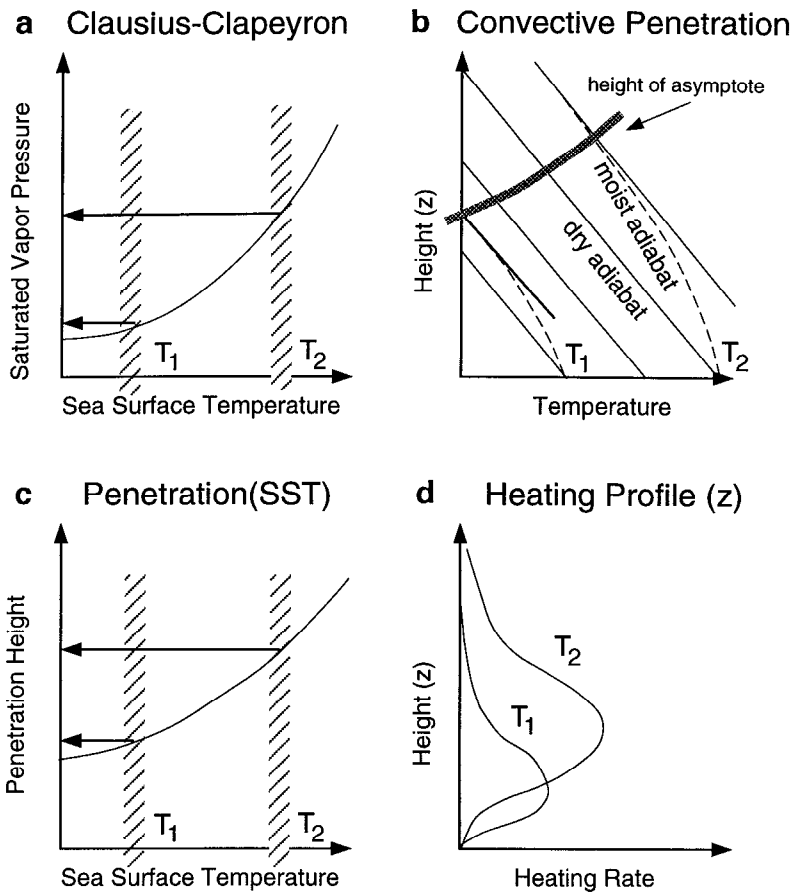

Figure 24. Schematic diagram relating the distribution of organized convection over the oceans with the SST. Two columns with temperatures T_1 and T_2 ($T_2 > T_1$) represent, for example, the eastern and western Pacific Ocean, respectively, or the tropics and the subtropics. Figure 24a shows the Clausius-Clapeyron relationship (i.e., $e_s = e_s(T)$) and its relation to the convective penetration height of a saturated parcel (Figures 24b and 24c) over the ocean. Assuming the same vertical distribution of relative humidity in each column and that convection has occurred, the magnitude of the heating in the warm column will be greater and will occur exponentially higher (Figure 24d) than in the cold column through the Clausius-Clapeyron relationship.

must also be a function of the SST and the vertical distribution of the heating will be determined by the convective penetration in each column. Thus the warmer and moister column (T_2) will have a higher and larger maximum latent heating rate than its cooler, dryer neighbor (T_1). Figure 24d shows a schematic representation of the heating profiles in the warm and cold columns. To first approximation at low latitudes, the heating is almost exactly balanced by adiabatic cooling. Such cooling can only be accomplished by rising motion [*Charney*, 1969; *Webster*, 1983b]. Thus the vertical heating profiles in Figure 24d may also be thought of as vertical motion profiles such that where the heating is positive, the vertical motion will be upward, and vice versa. In summary, over the warm pools of the tropics (and over the major convective regions of the tropical continents during the summer), the magnitude of the heating and the associated vertical velocity will be stronger and at a higher elevation than over other regions of the globe.

How do the convective penetration heights compare with the observed scales of atmospheric circulations? Assuming that atmospheric parcels have surface relative humidities of 85%, the convective penetration heights for SSTs of 30°C, 25°C, and 20°C are 17, 15, and 12 km, respectively. These compare with observed tropopause heights of 17, 15, and 13 km from *Peixoto and Oort* [1992].

So far, the two atmospheric columns have been considered in isolation. As air cannot rise at all points on the globe simultaneously (unless, of course, the planet is uniformly heated), it is reasonable to expect that regions of rising motions will become dominant over others. Figures 25a and 25b show the dynamic response to differential heating between the two columns. In an atmosphere represented by each column, the principal dynamic modes excited will be the same. In the equatorial region the modes would be a Kelvin-Rossby wave combination [*Gill*, 1980] and the mode closest to resonance would be the gravest (i.e., largest) horizontal mode [*Webster*, 1972]. Thus if forcing has a white noise spectrum (i.e., heating occurring with equal magnitude on all scales), the maximum response occurs at the largest horizontal scale [*Webster*, 1973]. Also, the magnitude and vertical scale of the response depend on the amplitude and vertical scale of the forcing [*Chang*, 1977]. Thus even though the horizontal scales of the response in atmospheres represented by the two columns of different temperatures may be the same, the vertical scale will be very different as the heating profile is much higher in the warmer column than in the column over the colder water. Therefore the convective circulation in the cooler column must grow within a strongly subsident region formed by the stronger and deeper circulation centered in the warm column. In other words, the circulation associated

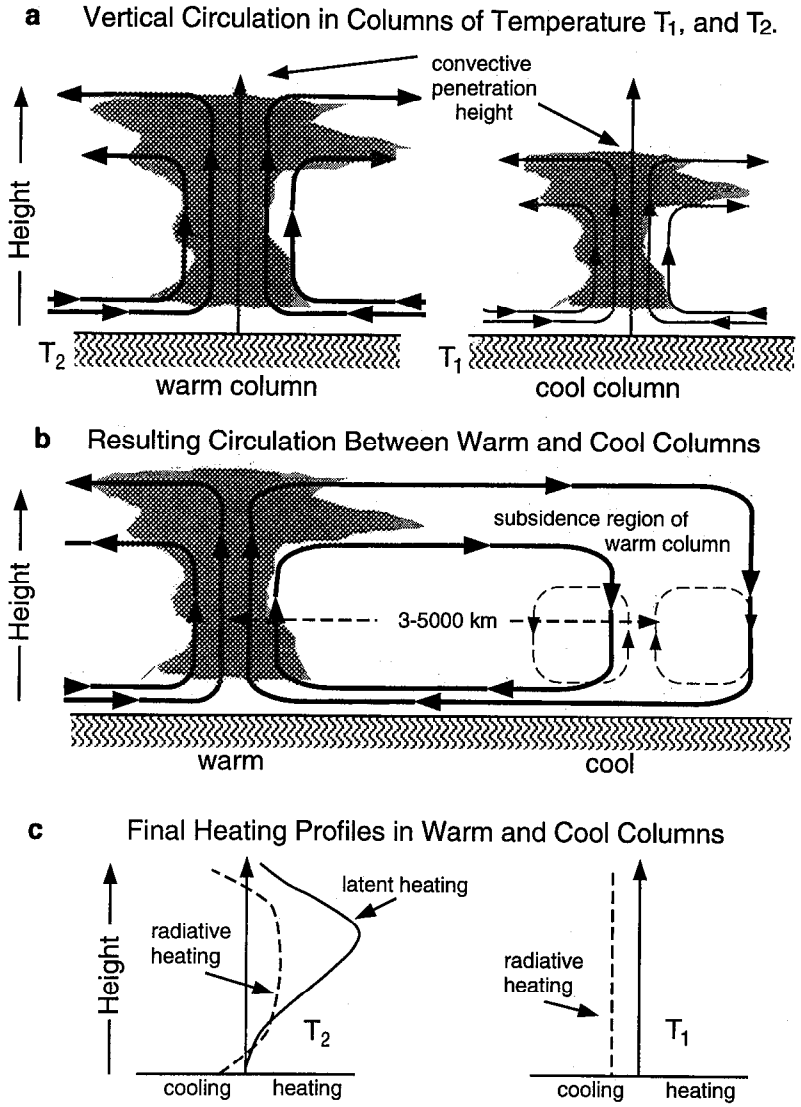

Figure 25. (a) The consequences of the higher and stronger heating profile in the warm column will be to produce a stronger and deeper dynamic response than that produced in the cooler column each with a large longitudinal scale. (b) Thus the warm region response may dominate over incipient convection elsewhere as the "cool" convection must develop in the subsident region created by the stronger and higher "warm" convection. (c) The final configuration of the heating rates.

with the warmest SST regions will dominate over all other circulation systems. This situation is shown in Figure 25b. Figure 25c shows the final radiational and latent heating profiles.

The juxtaposition of convection with the warmest SSTs comes directly from Clausius-Clapeyron moist thermodynamics and the physics of forced dynamic response. The moist thermodynamics associated with the tropical warm pools defines a heating profile which forces a very deep vertical structure. The rotational dynamics produces a very large scale horizontal response. The circulation associated with the warmest SST controls weaker and shallower convective circulations in colder regimes by producing a subsident environment that is not conducive to convective growth. Convection occurring within the dynamic length scales of the warm water convection will be subdued. In summary, the only special feature of the 28°C SST isotherm is that it is close to the maximum ocean temperature observed on Earth and thus is associated with the deepest convection.

7.3. Fundamental Atmospheric Circulation Systems

The annual cycle of the global atmospheric circulation is made up of three major components: the monsoon, the Walker circulation in the tropical-subtropical regime, and the band of migratory cyclonic storms and anticyclones in the extratropics. The Walker circulation is generally symmetric about the equator with ascending motion in the warm pool regions of the Indian and Pacific Oceans and the Indonesian archipelago and descent in the western Indian Ocean and the eastern Pacific Ocean. The monsoon is a global circulation pattern which is asymmetric about the equator and has its focus and basic forcing in the land/ocean distribution of the eastern hemisphere. Both the monsoon and the Walker circulation are characterized by strong hydrological signatures.

To help study the Walker and the monsoon circulation, cross sections have been constructed. The sections show vectors composed of the vertical and divergent part of the horizontal wind component in the direction of the section. A total wind vector may be

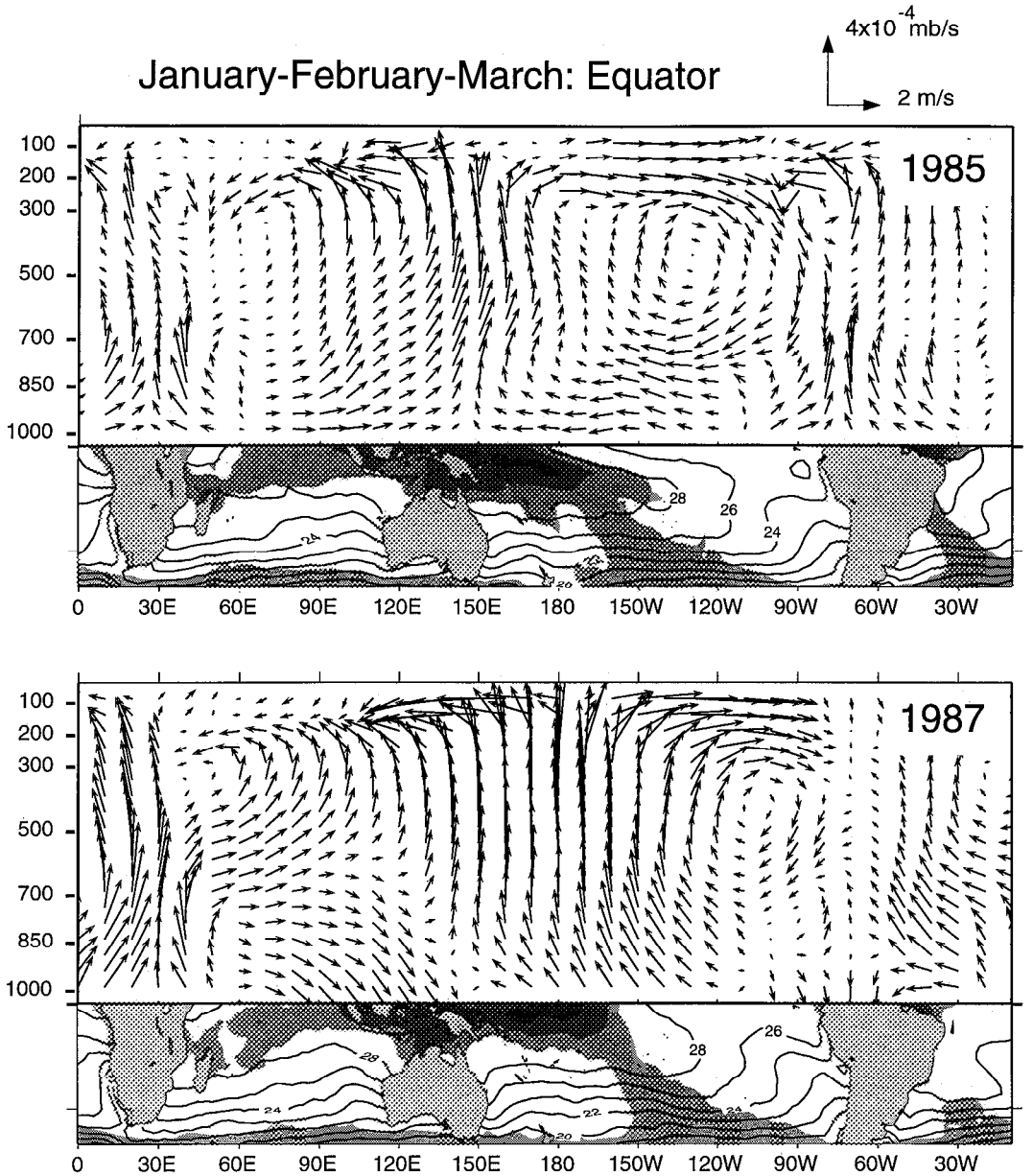

Figure 26a. Vertical sections along the equator of mean winter (January–March) flow vectors made up of the divergent part of the zonal wind component and the vertical velocity. Sections for 1985 and 1987 are shown. The latter year is an El Niño year. Panels below the sections show the geography, the SST (in degrees Celsius), and the OLR fields. The 240, 220, and 200 W m^{-2} OLR levels are shown in ascending shades of gray. Vector scale is shown at upper right. Data are from the European Centre for Medium-Range Weather Forecasts, Reading, England.

broken down into two parts: the rotational part that is essentially the geostrophic part of the flow that is parallel to the isobars and the divergent part which is the cross-isobaric flow. The divergent part is considered here as it describes flow into and out of the heat sources and sinks. The vertical cross sections are shown for the boreal winter (January–March, Figure 26) and the boreal summer (July–September, Figure 27). Sections are shown around the equator, at 25°N, and from pole to pole along the 90°E meridian. To illustrate the interannual variability that occurs at different phases of the El Niño cycle on the Walker and monsoon circulations, each panel shows sections for 1985 and 1987. The first year was considered to be average. During the second year a moderate El Niño occurred. Below each panel are maps that show the geography of the section, the SST fields, and the distribution of the OLR.

7.3.1. The Walker circulation. The equatorial vertical sections (Figures 26a and 27a) show ascending air over the warm pool regions of the Indian and Pacific Oceans in both seasons. With the rising air over Africa and South America, a series of east-west cells

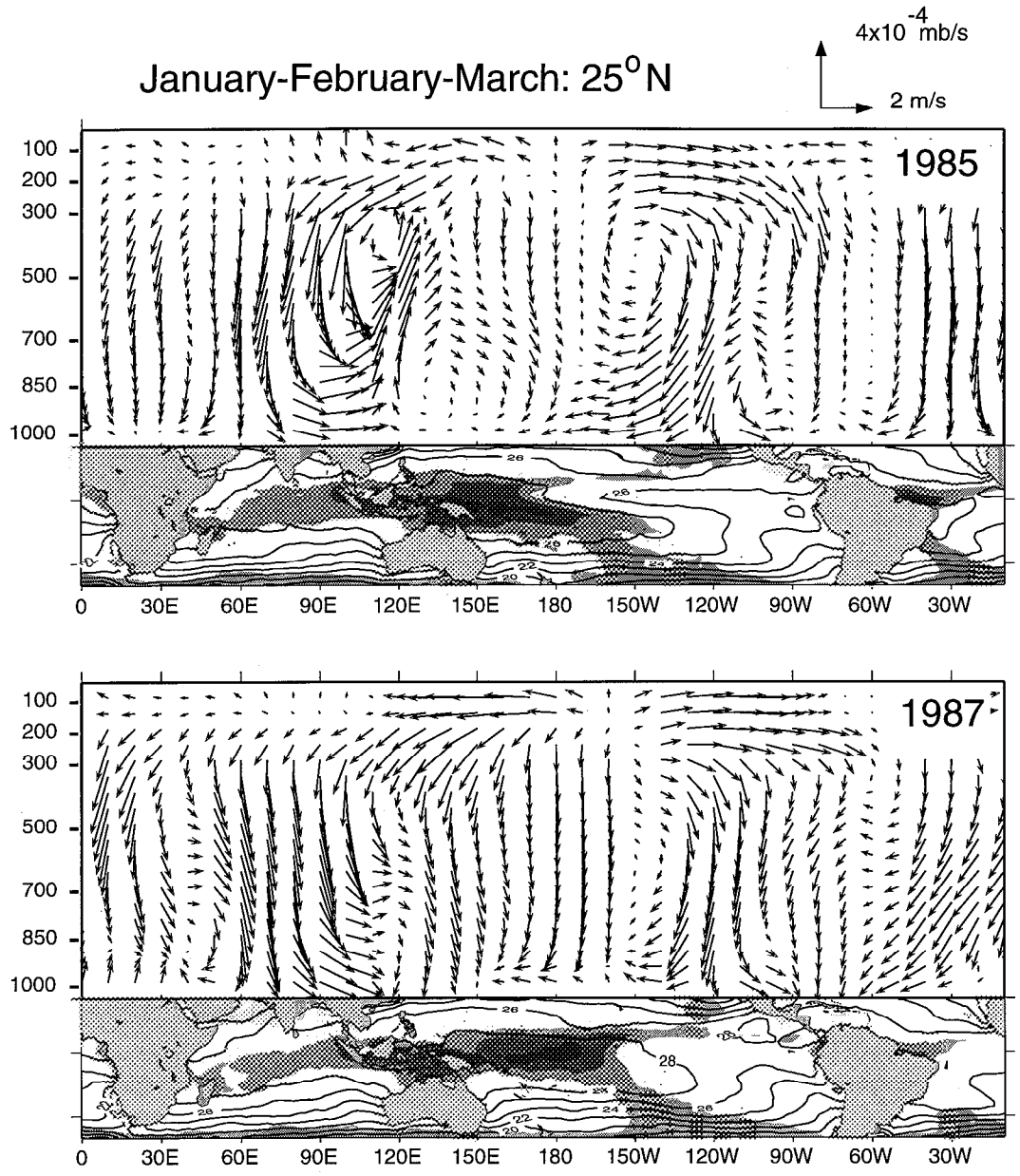

Figure 26b. Same as Figure 26a except for a winter section along 25°N.

are formed along the equator. Initially, the cell over the Pacific Ocean was referred to as the Walker circulation [*Bjerknes*, 1969]. However, the term has been broadened to include the companion cell over the Indian Ocean. The term Walker circulation celebrates the pioneering work of Sir Gilbert Walker who inferred the existence of a circulation from correlations of surface-observed quantities. It is the interannual variations of these circulations that cause the "great east-west swayings" [*Walker*, 1923, 1925] that Walker could only view statistically. The structure of the Walker circulation can be explained in terms of the dominant normal modes of the equatorial waveguide [*Webster*, 1972; *Gill*, 1980] responding to thermal forcing associated with the SST distribution in the tropical regions.

The common characteristic of the equatorial sections for the 1985 and 1987 periods is that the rising motion over the Pacific Ocean is still situated over the region of warmest water, even though the warm water has extended well eastward to the central Pacific. However, over Indonesia and the warm waters of the eastern Indian Ocean, there is now subsidence. The subsiding air, and the consequent reduction in convection, are the reason for the drought that accompanies El Niño over Indonesia and Australia. Figures 26a and 27a portray the limits of interannual variability of the near-equatorial flow. In fact, they display Walker's "great east-west swayings" [*Walker*, 1923].

The juxtaposition of the maximum upward motion of the Walker circulation and the SST maxima underlines the importance of the warm pools of the tropical oceans to the atmosphere. Their significance requires

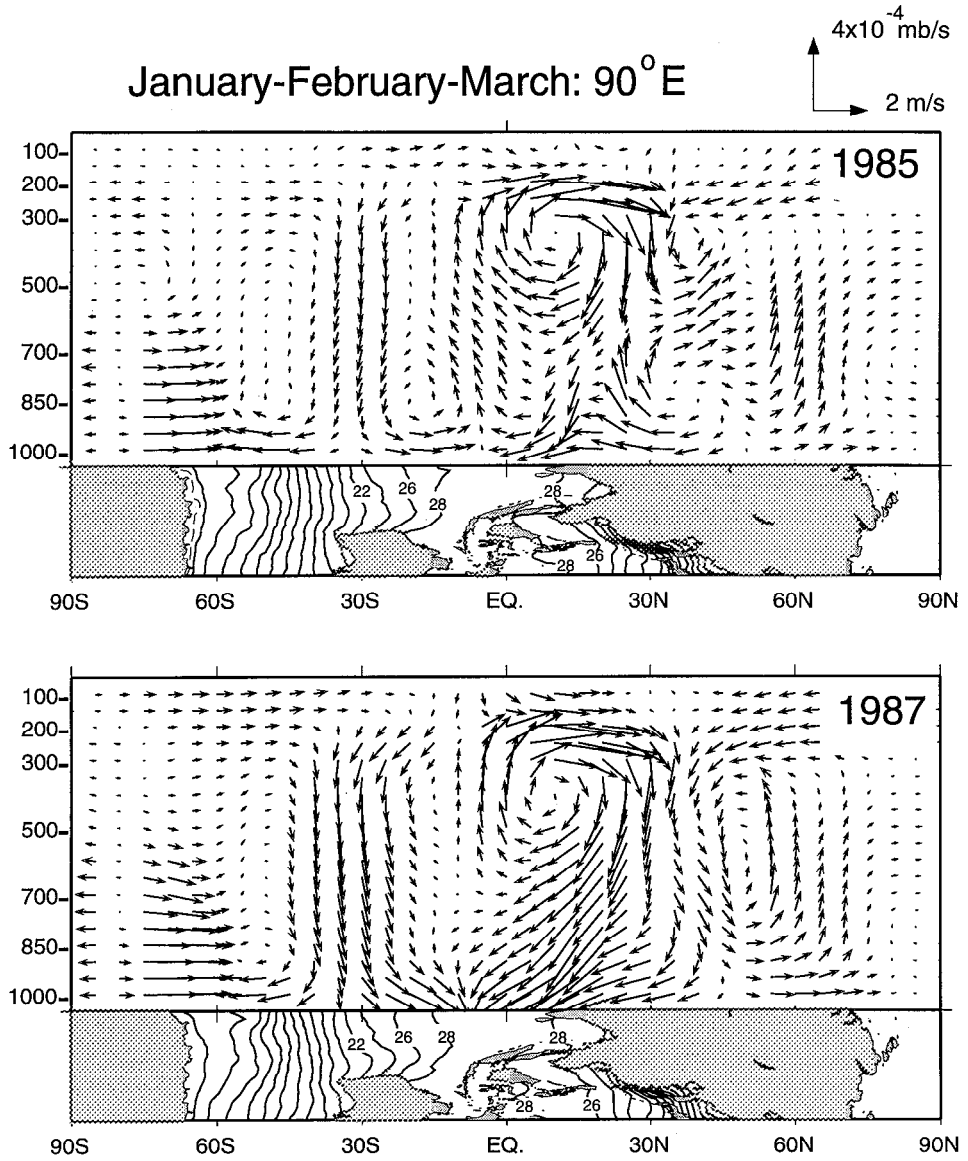

Figure 26c. Same as Figure 26a except for a winter section along the 90°E meridian between the south and north poles. The meridional (i.e., north-south) horizontal wind component is used with the vertical velocity component in compiling the vectors.

an understanding of why warm pools are located where they are. Why, for example, are the warm pools located in the western Indian Ocean and the eastern Pacific Ocean? Why should there be east-west SST asymmetries at all? The answer probably lies with the existence and distribution of the continents. If there were no tropical continents and the ocean continued completely around the equator, a general low-latitude SST maximum with no preferred longitudinal bias would be expected. Furthermore, there would be no monsoons. The equator itself would have local minima in SST (note the eastern Pacific, Figure 7) resulting from upwelling along the equator forced by an easterly wind stress. However, because of continents the general wind circulations are far more complicated.

Consider, first, the land asymmetry between the hemispheres which produces the monsoon circulation. As a result of the continental distribution and the dynamics that control the wind, the flow from the southern hemisphere to south Asia during the boreal summer is strongly biased toward the western Indian Ocean. There, the stronger winds cool the ocean by mixing and evaporation while leaving the eastern Indian Ocean relatively undisturbed. The result is an Indian Ocean with warmer water in the east than in the west and a corresponding increase in convection toward the east. In addition, there is substantial heating of the atmosphere from the Indonesian archipelago. Together with the warm eastern Indian Ocean, the island heating (latent and sensible) creates a relative low-pressure regime in the Indonesian region producing a low-level confluence from both the Indian and

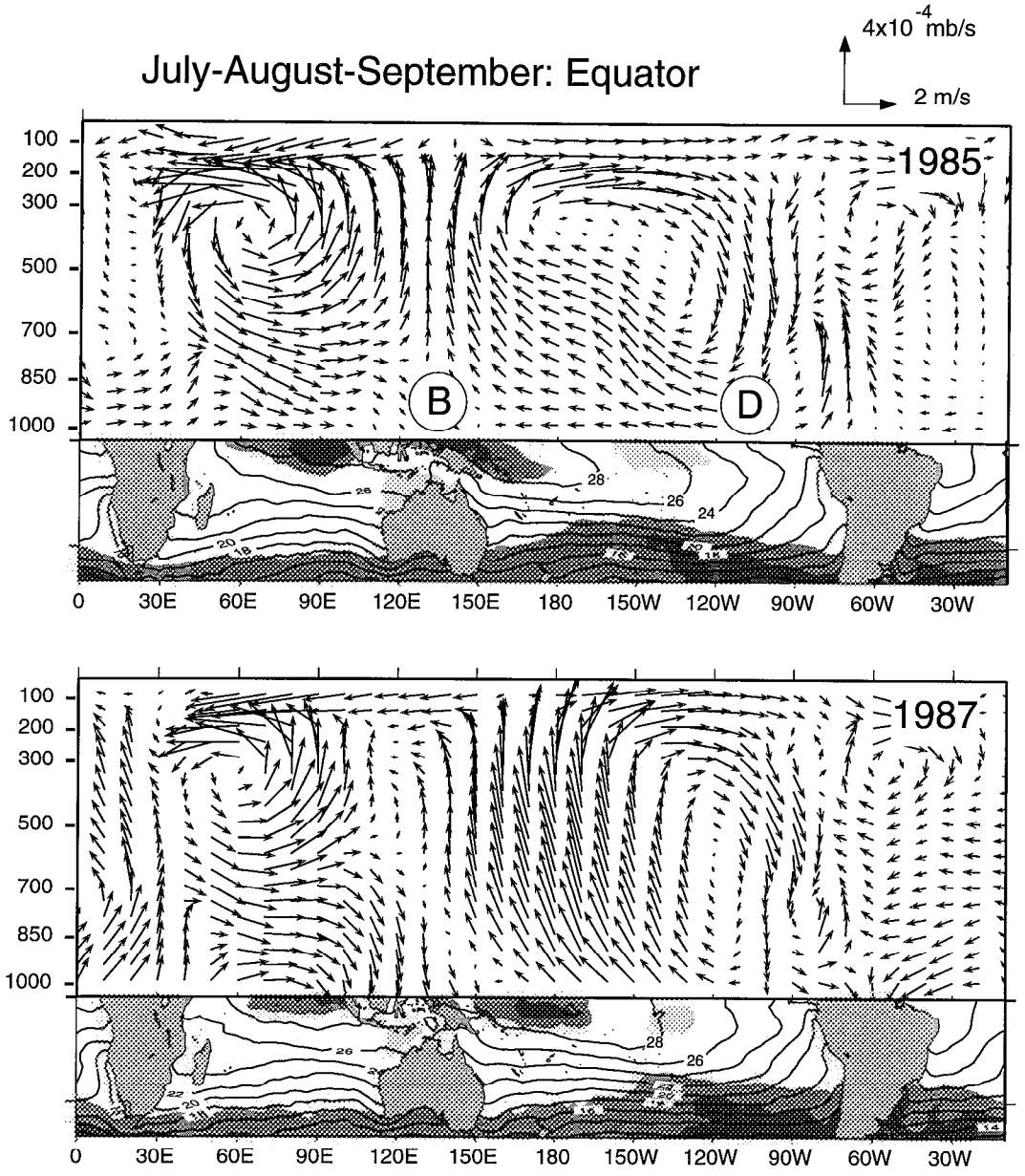

Figure 27a. Same as Figure 26a except for the boreal summer (July–September). The letters denote locations referred to in section 6.5.

Pacific Oceans. The decreased magnitude in the winds in the western Pacific and eastern Indian Oceans reduces the equatorial upwelling and surface cooling. Thus the western Pacific is relatively undisturbed. In the eastern Pacific Ocean the Andes act as a barrier and do not permit low-level flow toward the heating in the Amazon region. Flow toward the western Pacific, on the other hand, creates cold upwelling and a reduction of the eastern basin SST. All of these factors conspire to produce the observed tropical warm pools which span the Indonesian archipelago.

The Walker circulations also produce regions where direct interaction can occur between the extratropics and high latitudes. Extratropical waves have great difficulty in propagating through regions of easterlies [*Charney*, 1969]. However, the strong direct Walker circulations produce regions of westerlies. For example, in the upper troposphere of the eastern Pacific Ocean (see Figures 26a and 27a), a broad region of upper tropospheric westerlies occurs as the outflow region from the convection in the western Pacific Ocean. With the addition of the rotational component of the winds, they have magnitudes exceeding 20 m s^{-1} during the boreal winter. *Murakami and Unninayer* [1977] and *Webster and Holton* [1982] noted that the westerlies extended from one hemisphere to the other during most of the year. *Webster and Holton* [1982] termed these westerlies the "westerly duct" as only in these regions can atmospheric waves propagate from one hemisphere to the other.

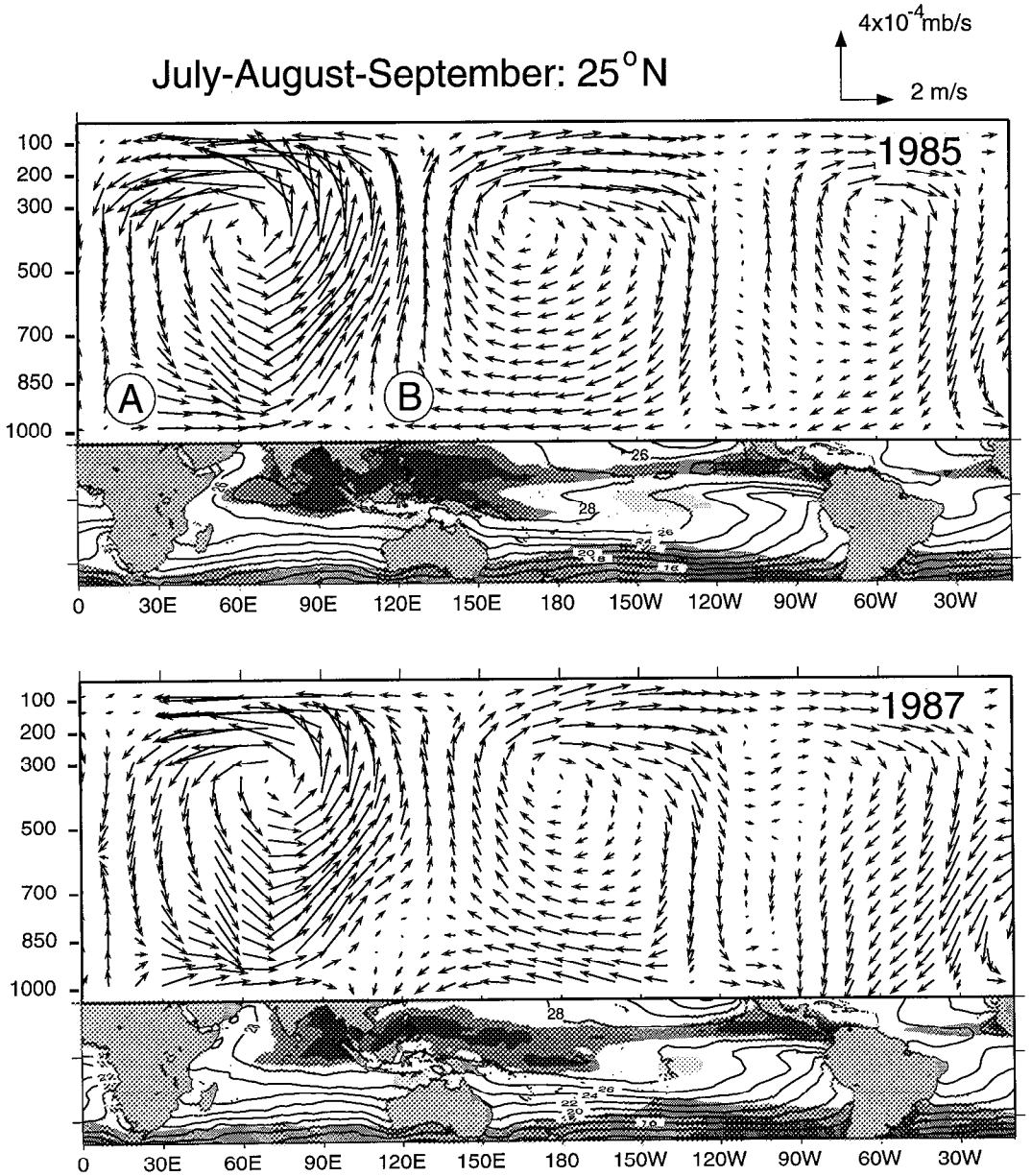

Figure 27b. Same as Figure 26b except for the boreal summer along 25°N.

A number of observational studies corroborate the westerly duct theory. For example, *Magaña and Yanai* [1991] show evidence of wave propagation through the westerly duct. *Hsu and Lin* [1992] and *Tomas and Webster* [1994] have created composites of clear teleconnection patterns from the northwest Pacific Ocean, through the westerly duct and into the southern hemisphere. *Prinn et al.* [1992] have found indirect evidence that the westerly duct is a region of mass transport. Tracing chemical species with known northern hemisphere sources, they found that the concentrations were high in the southern hemisphere when the westerly duct is strong but low during El Niño periods when the westerly duct is weak. Thus the mass flux between the two hemispheres depends on the strength of the westerlies in the duct region or, alternatively, on the strength of the Walker Circulation or the phase of the El Niño cycle.

7.3.2. The monsoon. Figures 26b and 26c and 27b and 27c show cross sections through the south Asian monsoon system during the winter and summers of 1985 and 1987 along 25°N and 90°E, respectively. The first cross sections plot the vertical velocity with the zonal component of the divergent horizontal wind. The second section shows the vertical velocity with the meridional component of the divergent wind.

A comparison of the winter and summer sections along 25°N indicates the extreme seasonality associated with the monsoon. During winter, almost the entire zone resides under descending air. In summer, on the other hand, strong rising motion dominates the south Asian region. The lower panel indicates that the

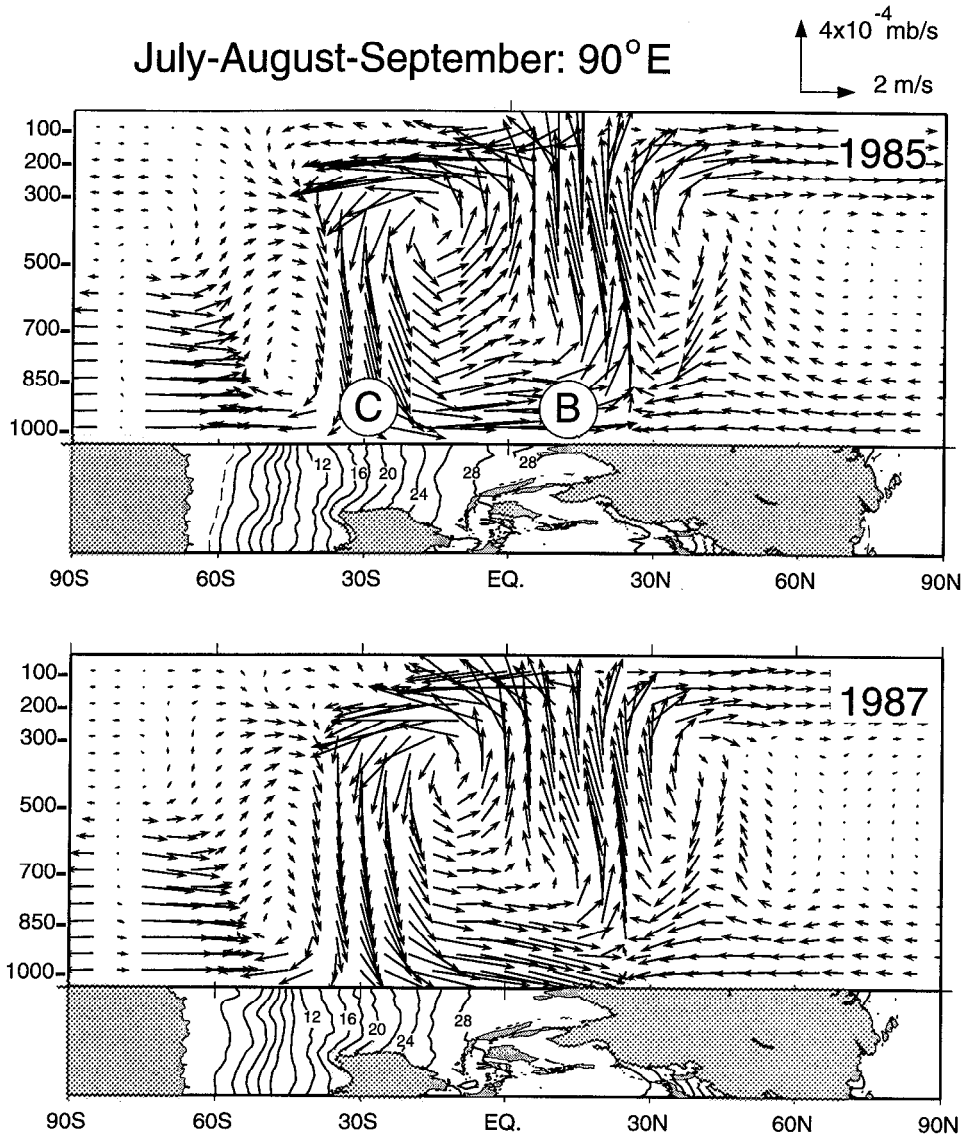

Figure 27c. Same as Figure 26c except for the boreal summer along 90°E.

rising motion is associated with cold OLR and hence deep cold clouds and precipitation. Over the desert regions of the middle east and north Africa, there is strong subsidence which turns eastward near the surface to provide inflow into the monsoon pluvial regions. Descent over the deserts exists at all times of the year but is strongest in summer.

The north-south sections (Figures 26c and 27c) exhibit the same seasonal variability. During winter, ascent occurs just south of the equator. In the northern hemisphere, subsidence extends all the way to northern Asia. The ascent is a westward extension of the winter monsoon that has maximum precipitation over south Indonesia and north Australia. During summer, at the height of the monsoon, the vigorous upward motion dominates south Asia. In the upper troposphere the circuit is completed with a strong southward flow across the equator.

These meridional cross sections describe the traditional picture of the monsoons. *Ramage* [1971], for example, describes the monsoon as primarily a cross-equatorial cell. Here, though, a much more complicated situation is found. The summer zonal sections along 25°N show an east-west cell that is almost as strong as the cross-equatorial cell. This lateral linkage between the deserts and south Asia is caused by the intense radiation loss to space over the deserts. As the desert columns are dry, the local greenhouse effect is small and descent (and adiabatic warming) is needed to compensate for the cooling of the column.

The interannual variability of the monsoon can be gauged by comparing the meridional cross sections of the two years, 1985 and 1987. During winter the normal ascent just south of the equator is replaced by broadscale subsidence. This circulation feature is consistent with drought that accompanies El Niño over Indonesia and north Australia. On the other hand, there is little difference between the two summer mon-

soons except for a slight downward trend of the vectors over India in 1987. Although it is not definitive, this may account for why 1987 was a weak monsoon year in terms of the precipitation over India.

The reasons for these particular configurations of the monsoon are rather straightforward. In the simplest sense, there are three components to monsoon forcing: differential heating between the ocean and land areas during the annual cycle of solar heating, the planetary rotation, and moist processes [*Webster*, 1983b, 1987]. The latter processes account for the majority of the vigor of the monsoon circulation [*Srinivasan et al.*, 1993]. *Webster and Chou* [1980a, b] conducted a series of model experiments with and without moist processes. Only when moist processes were included did the model wind speeds and surface temperatures correspond well with the meridional panels of Figures 26 and 27.

Moist processes are also responsible for the generation of vigorous intraseasonal transients in the monsoon system. *Sikka and Gadgil* [1980] noted that the established summer monsoon over south Asia was marked by periodic latitudinal migrations of bands of disturbances between the ocean and the continent. The time period of the migrations is between 15 and 30 days. *Webster* [1983a] and *Srinivasan et al.* [1993] were able to use models to generate variance that was very similar in magnitude and phase. The variance was introduced into the model by hydrological processes that bind the land and ocean surface with the atmosphere. Figure 28 shows how the intraseasonal variability of the monsoon is controlled by ground hydrology. Ground hydrology offsets the total heating of an atmospheric column and the vertical velocity, such that the system is not in local equilibrium, thus forcing a poleward migration of the convection.

The importance of ground hydrology also appears to be of importance on longer timescales and greater spatial scales. *Charney* [1975] and *Charney et al.* [1977] showed that albedo effects associated with the biosphere and the hydrological cycle provide feedbacks that affect drought in arid regions. A number of studies (see *Shukla and Mintz* [1982] for review) proposed that the long-term average rainfall over the continental regions could not be modeled properly without an adequate treatment of land hydrological processes including plant evapotranspiration.

7.4. Speculations on Ocean-Atmosphere Synergies

Heating in the tropics and cooling in the polar regions drive and govern the circulation patterns of the Earth's climate system in order to maintain a global heat balance. Poleward heat transports are a combined effort between the atmosphere and the ocean [*Trenberth and Solomon*, 1994]. The question is now raised about how the ocean and the atmosphere work together to perform the balancing of the global heat budget and how, through this effort, they maintain the stability of the climate system.

A hypothesis is proposed that describes the entire Earth system as a robust interactive entity. Robustness refers to a resilient configuration of the climate state. Interaction refers to an interdependency of the various spheres of the climate system that maintain the robust system. Within this scheme, the hydrology cycle, so important on fairly short timescales, is hypothesized to impart a powerful constraint on the overall climate on very long timescales. To develop this hypothesis, a very simple model of Earth is used where the planet is assumed to be ocean covered. Clearly, this is an oversimplification as the division of the ocean into ocean basins is critically important for the explanation of the thermohaline circulation. However, the simplification is made to elucidate some very basic interactions and controls. The simple model will suggest linkages over long timescales and remotely located geographical regions of the coupled system.

7.4.1. The notion of interactive zones. The ocean and the atmosphere have very different timescales. In turn, within each sphere, there are regions of markedly different temporal variation. The atmosphere possesses a rapidly evolving troposphere and the more slowly evolving stratosphere. The ocean possesses an upper ocean and a deep ocean demarked by relatively fast and slow timescales, respectively. Thus, as a working hypothesis, suppose that the regions of most rapid variability of the ocean and the atmosphere are those which interact together, namely, the upper region of the ocean and the troposphere. This interactive zone, so defined, is demarked by stippling in Figure 29a. Note that the interactive zone has a marked latitudinal structure. The deepest part of the atmospheric interactive zone exists at low latitudes, while the deepest region of interaction in the ocean lies at high latitudes. Latitudinally, the interactive zones of the ocean and the atmosphere are completely reversed.

The reasons for the structural reversal are rather straightforward. The tropopause separates the slow dynamics of the stratosphere from the rapid dynamics of the troposphere. Similarly, the thermocline separates the slow deep ocean from the more rapid upper ocean. In that sense the tropopause and the thermocline fulfill the same roles. The tropopause lies at about 15–17 km in the tropics and at less than 10 km in the high latitudes. The depth of the troposphere is determined by the degree of convective penetration, with the tropopause demarking the mean free convective height of the moist convection, which, in turn, is determined by the SST (see section 7.2). In the tropics the thermocline is the clear demarcation of the rapid and slow regions of the tropical ocean. At higher latitudes the demarcation between timescales can be expected to be much deeper. The wind-driven circulation, less constrained by the thermocline, which is not as strong as in the tropics, extends to greater

depths [*Niiler*, 1992]. Furthermore, the higher latitudes are regions of penetrative convection, or subsidence, caused by radiative cooling of the upper surface and salt rejection during the freezing process. Figure 29a suggests a reversed mirror image between the atmosphere and the ocean where the tropical troposphere and the high-latitude oceans play very similar roles. Both accomplish deep mixing into their respective interiors. Both are dominated by the same physical process: gravitational instability.

The conceptualization of the coupled system in such a simple manner now allows the processes of ocean-atmosphere interaction to be placed on a global-scale perspective. In the next section the simple model will be extended to show how hydrological processes bind the interactive zones and the noninteractive zones together.

7.4.2. A hypothesis for a stable global interactive system. Figure 29b provides a synthesis of the codependence of the ocean-atmosphere couplet. The broad arrows represent the circulations in the ocean and the atmosphere between the equator and the poles. These circulations are clearly a response to the imposed radiational heating gradient (section 6.5). The circulation patterns in the real system, of course, would be much more complicated as discussed in section 7.1. The existence of continents would add a very strong longitudinal structure to the atmospheric circulation as shown, for example, in Figures 26 and 27. Continents would also form bounded ocean circulation, and the abyssal circulation would have a more complex nature than depicted here (see Figure 23).

In this simple system, major convection takes place in two locations: in the tropical atmosphere (upward) and the polar ocean (downward). The convective (gravitational) instability in the atmosphere is a result of very moist air rising over the warmest SST (section 7.2). The convective instability in the polar oceans is caused by the negative buoyancy flux related to the intense radiational cooling at the surface of the ocean during winter, ice formation, and an effective negative buoyancy flux as salinity increases during the freezing process. Similar effects occur in the subtropics, where strong evaporation causes ocean descent and the subduction of cool saline water under the equator. The tropical ocean mixed layer is very stable with rising cold water beneath a warm upper layer creating a gravitationally stable layer in the upper ocean. Similarly, the polar atmospheric circulation is stable with descending and warming air producing a low-level inversion. The warm SST and the tropical atmosphere determine the state of the upper atmosphere, and the polar mixed layer in the ocean determines the deep-water characteristics.

Can this simple model be used to tie together the many seemingly disparate parts of the ocean and the atmosphere? With reference to Figure 29b, the tropical warm pool is chosen as a starting point.

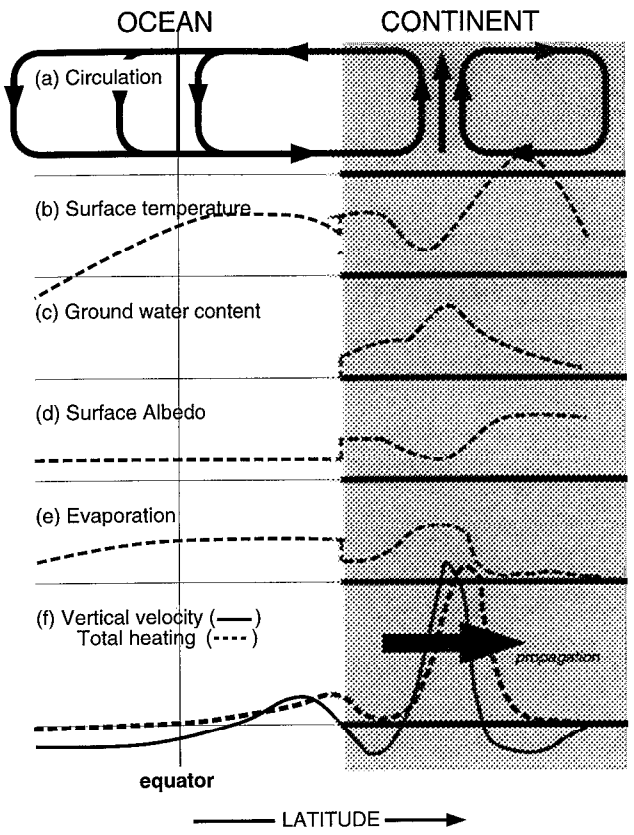

Figure 28. Schematic diagram of the interactive hydrology cycle over tropical land masses. Results from a simple monsoon model are used to indicate the degree of interaction between the atmospheric and surface hydrological processes. The figure shows the values of certain quantities as a function of latitude during the poleward propagation of a monsoon convective event. The quantities are (a) typical monsoon circulation with maximum ascending motion over the continent, (b) the surface temperature, (c) the groundwater contained in the land surface, (d) surface albedo, (e) the evaporation, and (f) the total heating and vertical velocity in the atmospheric column. *Srinivasan et al.* [1993] contend that the impact of the ground hydrology is to slightly offset the vertical velocity and total heating which cause poleward propagation of the convection.

7.4.2.1. The tropical circulation: Driven principally by gradients of SST [e.g., *Lindzen and Nigam*, 1987], warm, moist air converges into the equatorial regions, especially into the warm pool regions of the tropical oceans. Along trajectories up the SST gradient, continual evaporation increases the moisture content of the column. Over the warm pools, in the region of maximum surface convergence, the air is forced to rise producing deep penetrative moist convection, precipitation, and large releases of latent heat in the middle troposphere (see section 7.2). The large-scale circulations that feed the tropical convection act as a form of solar heat collector. Solar energy is stored in the evaporated water vapor picked up as the winds converge toward the equator across the ocean basins. The effect is emphasized by the exponential increase

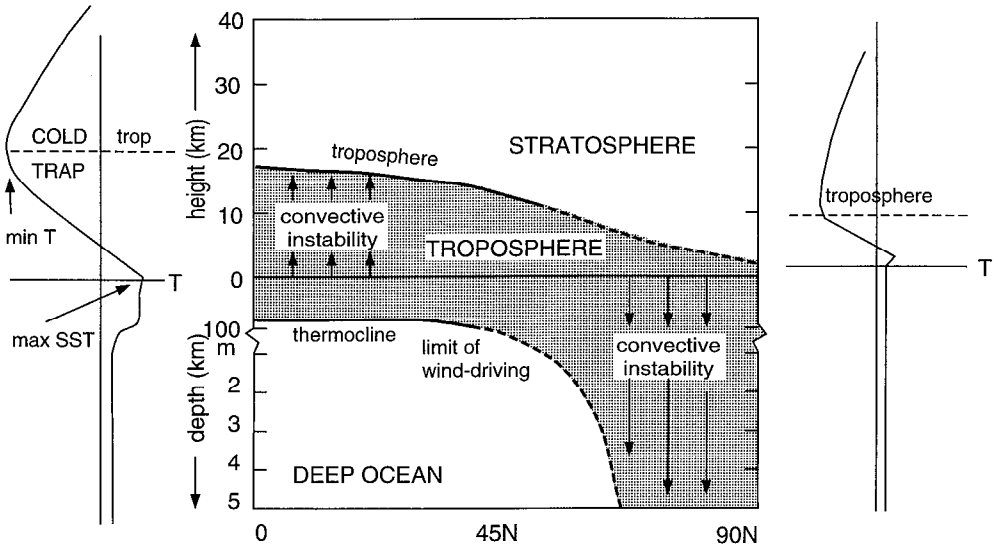

Figure 29a. Schematic diagram of the interactive zones of the ocean and the atmosphere. Interactive zones are defined as regions in the ocean and the atmosphere that have comparable timescales and thus directly influence each other. Vertical temperature sections through the atmosphere and the ocean are shown for (left) the tropics and (right) the polar regions. The interactive zones encompass the most rapidly evolving regions of the two spheres such as the troposphere, the upper ocean, and the entire ocean at higher latitudes where deep water is formed. The deep ocean and the stratosphere evolve on much longer timescales; note the reversed mirror image of the ocean and the atmosphere. Convective instability occurs in the tropical atmosphere and the high-latitude oceans. Both regions are responsible for the formation of deep penetrative circulations or currents.

in the saturated vapor pressure of the parcels as their temperature increases toward the equator (see section 3). The collected solar energy is released in a relatively small volume over the warm pool driving vigorous upward motion. The vertical limit of convection, demarked by the tropopause, is determined principally by the magnitude of the SST (section 7.2). Furthermore, the higher the SST, the greater the convection and vertical penetration and the greater the adiabatic cooling. Thus there is a strong inverse relationship between the magnitude of the SST maximum and the coldness of the tropopause. Over the tropical warm pools (e.g., 29°–30°C) the air temperature at the tropopause (17–18 km) is less than 190 K. Above the tropopause in the stratosphere, the temperature increases.

7.4.2.2. Determination of the state of the stratosphere: The atmospheric Lagrangian circulation (i.e., the path a parcel of air would actually follow), driven by the equator-to-pole heating gradients, is similar to a large Hadley-type cell with equatorial motion in the troposphere and poleward motion in the stratosphere. Thus all of the moist air ascending through convection (the shaded area in Figure 29b) must pass through the cold tropical troposphere [*Danielson*, 1968, 1993]. Except for the oxidation of methane (CH_4), the injection is the only source of water vapor in the stratosphere. The temperature of the tropopause T_T must then define the maximum vapor pressure in the stratosphere. Indeed, observations indicate that the warmer stratosphere is unsaturated with a vapor pressure of $e_s(T_T)$ or, roughly, a constant vapor pressure of 4 ppm. *Danielson* [1993] argued that the cold tropopause acts as a moisture "cold trap" where tropospheric water vapor of higher vapor pressure than $e_s(T_T)$ will be "freeze dried" at the troposphere. The excess water, in the form of ice crystals, precipitates back into the tropical troposphere. *Potter and Holton* [1994] offer an alternative explanation of how the lower stratosphere remains so dry. The envisaged buoyancy waves, generated by tropospheric convection, producing ice clouds through local lifting in the stratosphere. The ice crystals formed in the clouds precipitate downward as in the Danielson model. Thus two plausible theories of how the stratosphere remains dry have been advanced.

7.4.2.3. The return atmospheric flow between the tropics and the poles: The stratospheric air, dried efficiently by the equatorial cold trap, moves poleward down the pressure gradient. Nearer the pole, the dry air subsides and warms adiabatically, creating a stable inversion over the poles. As the air is always unsaturated while in the stratosphere and as it warms as it subsides, the formation of clouds is very difficult. Thus the stratospheric air, when it arrives over the higher latitudes, has a very low water vapor content. The dry, clear stratosphere allows efficient radiational cooling of the surface and the atmosphere to outer space.

7.4.2.4. The polar ocean-atmosphere interface and the formation of deep water: Intense radiational cool-

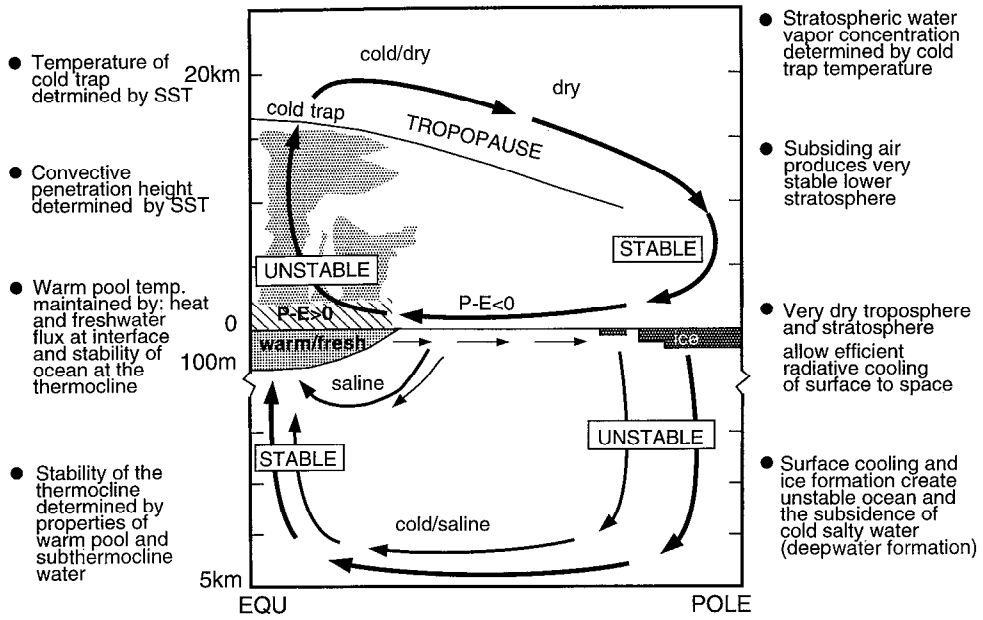

Figure 29b. A schematic sequence of the role of hydrological processes in maintaining the general circulation of the coupled ocean-atmosphere system. In the tropics, complicated ocean-atmosphere fluxes together with high insolation and the very stable ocean configuration hold the SST in rather narrow bounds. The deep penetrative atmospheric convection produces a very cold tropopause which provides a "cold trap" for moist air passing through to the stratosphere, thus assuring that the stratosphere remains dry at least to the saturated vapor pressure of the temperature of the cold trap. A cold, dry stratosphere assists the rapid surface cooling in the polar regions, the formation of sea ice, and the formation of cold saline deep water. The slow equatorial encroachment of the polar water and the subduction of saline water from the subtropics below the equatorial warm pools enhance the stability of the upper ocean structure at low latitudes and thus help maintain the high temperature of the tropical water. In this manner the ocean-atmosphere system, with a strong involvement of the hydrology cycle, maintains a long-term balance and stability.

ing of the polar ocean surface during the winter causes the formation or extension of sea ice. Cooling and ice formation (through salt ejection) produce an unstable density gradient in the upper ocean allowing the dense water (cool and saline) to mix downward convectively. Just as the tropical ascent is the rising part of the atmospheric direct circulation (i.e., warm air rising), the sinking motion of the ocean is the thermally direct part of the ocean circulation (i.e., cold water sinking). A thermodynamically direct circulation converts potential energy into kinetic energy. These processes constitute the formation of the deep ocean waters.

7.4.2.5. The return ocean flow between the poles and the equator: An oceanic meridional circulation (the thermohaline circulation) spreads out away from the poles until it slowly ascends toward the equator. The cold, saline ascending water mass has characteristics that are in sharp contrast to the warm surface layers of the tropics and the warmer, though very saline, water sinking from the subtropics. The intersection of the water masses produces an extremely stable stratification at the base of the tropical thermocline. This part of the ocean circulation is analogous to the descending branch of the atmospheric Lagrangian circulation.

7.4.2.6. Maintenance of the warm pool: In section 4.2 it was shown that water warmer than 28°C occupied less than 0.05% of the total ocean water mass and that this water lay as a thin skin over a much colder body of water. Conflicts exist at the tropical thermocline that are critical for the maintenance of this thin layer of warm water. The cold ascending deep ocean water rises up under the warm, fresh tropical waters. Given the difference between the temperature and salinity of these water masses, an extremely stable interface develops. The stability of the upper ocean is further increased by the flux of freshwater from the copious precipitation over the warm pools. The stability of the thermocline severely restricts the mixing of the two water masses which helps maintain the temperature of the tropical upper ocean. Maintenance of the warm pool temperature is important in order to continue the convective processes discussed in section 7.4.2.1.

The model presented above is an extremely simple interpretation of a very complicated meshing of ocean and atmospheric processes. The longitudinal variations related to the finite basin sizes of the ocean, including the complications introduced by the finite basins to the abyssal circulation, have been ignored. However, despite the simplicity of the model, it shows how the coupled ocean-atmosphere system conspires

to maintain the SST gradient between the equator and thus the stability of the system. The arguments also help identify a keystone for the global coupled ocean-atmosphere system: the warm pool temperatures of the tropical ocean and the hydrological processes with which it is associated.

7.4.3. Maintenance of water on Earth. If water is an essential aspect of the stability of the global climate, the question of how water is maintained on Earth must be addressed. The question arises because the Earth is sufficiently close to the Sun and has a small enough mass that hydrogen should not be retained on the planet [*Goody and Walker*, 1972]. Loss of hydrogen to space would occur when H_2O is photodissociated in the upper atmosphere by ultraviolet radiation. A continual loss of hydrogen would lead to the eventual deprivation of water on the planet. The rather paradoxical hypothesis is proposed that the loss of water by the planet is minimized because of the high temperature of the tropical ocean warm pools. In other words, the existence of water within the particular climatic configuration found on the planet insists that water will be maintained or, at least, lost at an extremely slow rate.

Photodissociation of water requires that water vapor is transported to the upper atmosphere where ultraviolet radiation is in abundance. If the processes discussed in the last section are valid, water vapor will only be transported into the stratosphere through the tropical tropopause. Furthermore, the stratospheric water vapor pressure will be determined by the temperature of the tropopause cold trap. Consequently, the warmer the tropical SST, the colder the trap and the lower the concentration of water vapor residing in the stratosphere. Conversely, the cooler the SST, the lower the tropopause and the warmer the trap. Thus cooler SSTs correspond to higher water vapor concentrations in the stratosphere. Therefore the warmer the SST, the less water vapor is available to be disassociated and less hydrogen loss to space.

There are other sources of water vapor in the stratosphere. Methane is a gas of tropospheric origin. When methane is advected into the stratosphere, it is oxidized producing water vapor [*Rind et al.*, 1993; *McCormick et al.*, 1993]. As the process is most efficient in the upper stratosphere, the water vapor concentration tends to increase with height above the lower stratospheric minimum (Figure 30, bottom). The cold trap plays no role in this source of stratospheric water vapor as methane concentration appears independent of tropospheric temperature.

In summary, the processes that maintain the warm tropical SSTs on Earth also minimize the loss of water from the planet. Therefore on very long timescales hydrological processes maintain themselves. As long as coupled ocean-atmosphere processes conspire to maintain the tropical SSTs at their present high value, the mainstay of climate stability, water, will remain in its present abundance. Figure 30 provides a schematic representation of the water maintenance.

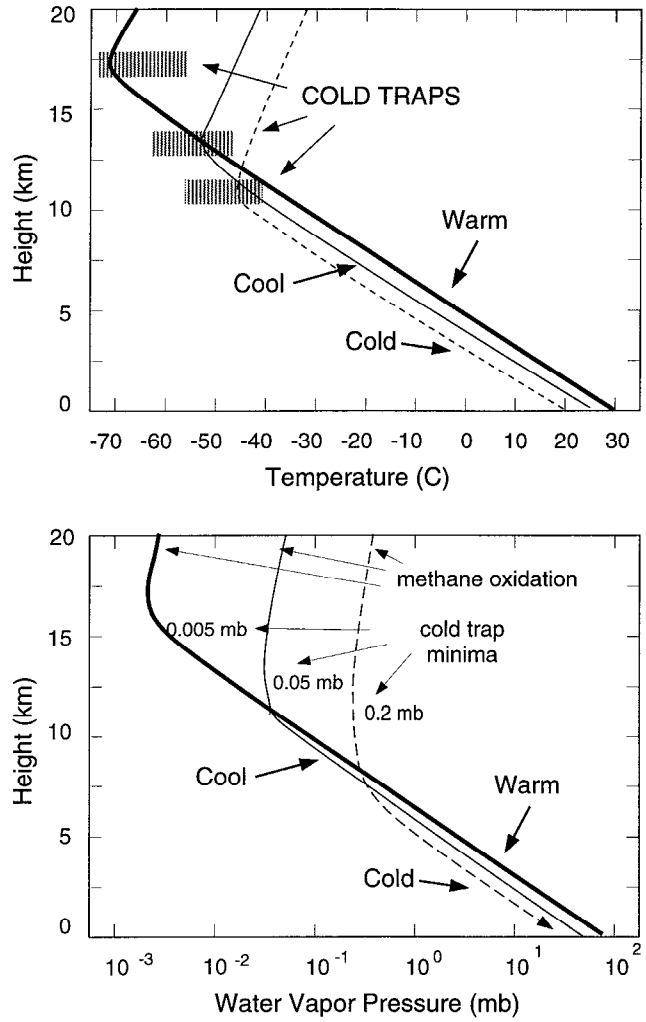

Figure 30. The impact of SST on the moisture content of the stratosphere. (top) The vertical structure associated with SSTs of 30°C (warm), 25°C (cool), and 20°C (cold). (bottom) As the SST decreases, the convective penetration is less and the tropical troposphere is lower and warmer. Assuming that all water vapor resident in the stratosphere must pass through the tropical tropopause, the tropopause acts as a cold trap and determines the moisture content of the stratosphere. The warmer the SST, the colder the cold trap and the less the water vapor content of the stratosphere. In the text it is argued that the reason that Earth retains its hydrogen (and thus water) is because of the inverse relationship between SST and the temperature of the cold trap. That is, the warm SSTs in the warm pool inhibit the loss of H_2O. The increase in water vapor with height in the stratosphere is due to the oxidation of methane. Methane thus acts as a further source of water vapor in the stratosphere but one that is independent of the temperature of the troposphere.

8. CONCLUSIONS

The major purpose of this review has been to indicate the importance of hydrological processes in cli-

mate variability ranging from days to millennia. It has been argued that Earth is unique within the solar system because of the planet's location on the water phase diagram (Figure 2). Where a planet is placed on the diagram early in the planet's history depends on such fundamental factors as the planetary distance from the Sun, the planetary mass, and the early atmospheric chemistry of the planet. The planet's final and permanent location depends primarily on the evolution of the atmosphere, the development of an absorbing atmosphere, and the development of an offsetting planetary albedo that will balance the increases in absorption by greenhouse gases. Such balances depend on the location of the mean structure of the planet relative to the triple point of water.

Another key point appears to be the Clausius-Clapeyron nonlinearity. The nonlinear relationship between saturation vapor pressure and temperature, discussed in section 3, produces a strong regionality in the importance of the hydrology processes. Saturation vapor pressure (e_s) at temperatures of 0°C, 10°C, 20°C, and 30°C increases in the ratio of 1:1.5:3:10, respectively, relative to the saturation vapor pressure at 0°C. Thus latent heat fluxes will grow exponentially with increasing SST following the exponential increase in the saturation vapor pressure. The principal implication of the nonlinearity is to inject a very strong latitudinal gradient into moist processes. For example, for the same amount of work in moving a saturated parcel vertically upward, the realization in terms of latent heat release will be exponentially larger depending on the initial temperature of the parcel given, usually, by the SST.

The nonlinearity of water phase changes imparts a very strong latitudinal bias on the impact of clouds on the surface of the planet (Figure 17). Because of the latitudinal differences in water vapor concentration, especially in the planetary boundary layer, clouds modulate the total surface radiative flux reaching the surface differently in the tropics than in higher latitudes. Because of these differences, clouds exert a greater influence in the tropical regions in terms of net energy loss at the surface than at higher latitudes. One implication of the impact of clouds in the tropics is that the tropical ocean is considerably more sensitive to cloud amount than elsewhere simply because the solar radiation losses are uncompensated by increased downwelling infrared radiation.

One of the more important conclusions is the phase locking that occurs between latent and radiative heating of an atmospheric column. Once convective modes are established over the warm pool regions or the heated continents, latent heating gradients are set up between the precipitating and remote dry regions. Simultaneously, gradients of net radiative flux convergence in a column occur with magnitudes of about one third to one half of the magnitude of the latent heating. The two forms of heating gradients must always have the same sign. However, the convergence of radiational flux in a cloudy region (i.e., radiative warming of a column) means that there will be a heating deficiency in the ocean column below. Thus, once the latent and radiative heating gradients are established in the atmosphere, ocean cooling immediately commences below the cloudy region while heating occurs in the clear regions. *Ramanathan and Collins* [1991] place considerable importance on the radiative feedbacks between cloud increase and SST decrease which form the basis of their "natural thermostat" hypothesis. However, it has been argued that a fuller set of hydrological processes is probably required to understand more fully the regulation of the tropical SST.

A process of considerable importance is freshwater flux between the ocean and the atmosphere. The tropical warm pools are one of the few regions where precipitation exceeds evaporation by a large amount. For example, in the western Pacific in regions within the 28°C SST isopleth, $(P - E)$ is greater than 2 m (Figure 12). The positive buoyancy flux into the ocean associated with the precipitation excess very effectively stabilizes the upper ocean producing a shallow mixed layer in a region of maximum solar heating. The increased stability reduces mixing in the upper ocean and allows rapid surface heating (Figure 9b) which, in turn, enhances the stability of the near-surface layer. A positive feedback may ensue that allows the warm pool SST to increase substantially. Only if the wind is very strong during, for example, equatorial westerly wind bursts, will the turbulent mixing in the upper ocean be sufficient to erode through the stable fresh surface layer.

Finally, the role of hydrological processes on very long timescales was considered. It was suggested that there are linkages between low-latitude hydrological phenomena and the stability of global climate. That is, a simple regulatory role for moist processes was suggested. A final speculation was that the hydrological cycle itself is chiefly responsible for the maintenance of water on the planet. These speculations appeared from the development of a conceptual model of the planetary climate. Unstable and stable regions of the atmosphere and the ocean were identified and also zones of interaction. Both the tropical atmosphere and the polar oceans were shown to be convectively unstable whereas the polar atmosphere and the tropical oceans are gravitationally stable. It was argued that the stable and unstable parts of the spheres are linked hydrologically to produce a very resilient and stable climate system. In this scheme the warm water of the tropical oceans is of particular importance (section 7.3).

The advancement and testing of some of these ideas will require a combination of observational programs and the subsequent analysis of the data, theoretical reasoning, and numerical modeling. Clearly, the most straightforward assessment of the ideas discussed in this paper is through numerical experimentation and

through comparison of the results with observations. In that sense, in situ observations from field experiments or remote observations from space go hand in hand with the development of the coupled models.

In order to improve modeling schemes, considerably more data on the water budget of the Earth system is necessary. Currently, the quantities such as area-averaged precipitation are only known to within 25–50%. Surface energy fluxes which couple the ocean and the atmosphere are not known well either. Ultimately, the solution to many of these questions will lie with observations from satellite. Active and passive microwave radiometers will have to provide estimates of area-averaged rainfall to within a few percent averaged over one month. Furthermore, the satellite will have to measure cloud structure and hydrometer distribution on a global basis to provide data to determine subcloud layer radiation fluxes.

The modeling and observing efforts are probably very worthwhile. Not only may they lead to a better understanding of the most basic component of the Earth system, the hydrology cycle, but there may also be the practical benefit of increasing the predictability of climate.

ACKNOWLEDGMENTS. The research has been supported by the National Science Foundation under grants ATM-9214840 and ATM-9223150, the National Oceanic and Atmospheric Administration under grant NA266PO12201, and NASA under grant NAG8-876. Much of the initial research was undertaken at the European Centre for Medium Range Weather Forecasting during a sabbatical period. I would like to thank Roger Lukas of the University of Hawaii for the many discussions regarding the mutual dependency of the ocean and the atmosphere. Special thanks are due to Judith Curry for her suggestions regarding the manuscript and to Xubin Zeng and Graeme Stephens for their erudite comments. I would like to thank Stuart Godfrey, George Young, and Chris Fairall for making their oceanographic data available for this paper and L. Kantha and Carol Ann Clayson for the use of their ocean mixed layer model. Chidong Zhang kindly made his OLR data available. Victor Magana generously provided Figures 25 and 26. Finally, the patient reviewers of the manuscript were extremely helpful in rendering the paper into a more palatable form.

I would like to dedicate this paper to Joachim Kuettner whose insight and thoughtfulness has encouraged and inspired a generation of scientists to seek a clearer view of the atmosphere and the ocean.

Ann Henderson-Sellers and Alan Chave were the editors responsible for this paper. They thank Neville Smith and other anonymous persons for technical reviews and Tracy Vallier for a cross-disciplinary review.

REFERENCES

Anderson, D. L. T., and J. P. McCreary, Slowly propagating disturbances in a coupled ocean-atmosphere model, *J. Atmos. Sci.*, *42*, 615–629, 1985.

Arkin, P., and B. Meisner, The relationship between large-scale convective rainfall and cold cloud cover over the western hemisphere during 1982–1984, *Mon. Weather Rev.*, *115*, 51–74, 1987.

Bjerknes, J., Atmospheric teleconnections from the equatorial Pacific, *Mon. Weather Rev.*, *97*, 163–172, 1969.

Broecker, W. S., The great ocean conveyor, *Oceanography*, *4*, 79–84, 1991.

Broecker, W. S., and G. Denton, What drives glacial cycles?, *Sci. Am.*, *262*(2), 51–54, 1990.

Broecker, W. S., D. M. Peteet, and D. Rind, Does the ocean have more than one stable mode?, *Nature*, *315*, 21–26, 1985.

Bryan, K. A., High latitude salinity effects and interhemispheric thermohaline circulations, *Nature*, *323*, 301–304, 1986.

Cane, M. A., and S. E. Zebiak, A theory of El Niño and the Southern Oscillation, *Science*, *228*, 1085–1097, 1985.

Chahine, M., The hydrological cycle and its influence on climate, *Nature*, *359*, 373–380, 1992.

Chang, C. P., Viscous internal gravity waves and low frequency oscillations in the tropics, *J. Atmos. Sci.*, *34*, 901–910, 1977.

Charney, J. G., A further note on the large-scale motions in the tropics, *J. Atmos. Sci.*, *20*, 607–609, 1969.

Charney, J. G., Dynamics of deserts and droughts in the Sahel, *Q. J. R. Meteorol. Soc.*, *101*, 193–202, 1975.

Charney, J. G., W. J. Quirk, S. Chow, and J. Kornfield, A comparative study of the effects of albedo change on drought in semi-arid regions, *J. Atmos. Sci.*, *34*, 1366–1385, 1977.

Danielson, R. E., Stratospheric-tropospheric exchange based on ozone and potential vorticity, *J. Atmos. Sci.*, *25*, 502–518, 1968.

Danielson, R. E., In situ evidence of rapid, vertical, irreversible transport of lower tropospheric air into the lower tropical stratosphere by convective cloud turrets and by larger-scale upwelling in tropical cyclones, *J. Geophys. Res.*, *98*, 8665–8681, 1993.

Fu, R., A. D. Del Genio, W. B. Rossow, and W. T. Liu, Are cirrus clouds a "thermostat" for tropical sea surface temperatures?, *Nature*, *358*, 394–397, 1992.

Garwood, R. W., An ocean mixed layer model capable of simulating cyclic states, *J. Phys. Oceanogr.*, *17*, 1507–1524, 1977.

Gill, A., Some simple solutions for heat induced tropical circulations, *Q. J. R. Meteorol. Soc.*, *106*, 447–462, 1980.

Gill, A., *Atmosphere-Ocean Dynamics*, *Int. Geophys. Ser.*, vol. 30, 662 pp., Academic, San Diego, Calif., 1982.

Godfrey, J. S., A strategy for TOGA salinity monitoring, in Proceedings of the Workshop on Japanese Coupled Ocean-Atmosphere Response Experiments, 23–24 October, 1989, *Meteorol. Res. Rep. 90-2*, Div. of Meteorol., Geophys. Inst., Univ. of Tokyo, Tokyo, 1989.

Goody, R. M., *Atmospheric Radiation*, vol. I, *Theoretical Basis*, Oxford University Press, New York, 1964.

Goody, R. M., and J. C. G. Walker, *Atmospheres*, 150 pp., Prentice-Hall, Englewood Cliffs, N. J., 1972.

Gordon, A. L., Interocean exchange of thermohaline water, *J. Geophys. Res.*, *91*, 5037–5046, 1986.

Gordon, A. L., The role of the thermohaline circulation in global climate change, *Annu. Rep. 1990–1991*, pp. 44–51, Lamont-Doherty Earth Obs., Columbia Univ., Palisades, N. Y., 1991.

Greenwald, T. J., G. L. Stephens, T. H. Vonder Haar, and D. L. Jackson, A physical retrieval of cloud liquid water over the global oceans using Special Sensor Microwave/Imager (SSM/I) observations, *J. Geophys. Res.*, *98*, 18,471–18,488, 1993.

Hartmann, W. K., *Moons and Planets*, 509 pp., Wadsworth, Belmont, Calif., 1983.

Hartmann, D. L., and M. L. Michelsen, Large scale effects on the regulation of tropical sea surface temperature, *J. Clim.*, *6*, 2049–2062, 1993.

Hsu, H.-H., and S.-H. Lin, Global teleconnections in the 250-mb streamfunction field during the northern hemisphere winter, *Mon. Weather Rev.*, *120*, 1169–1190, 1992.

Jeffries, H., On the dynamics of geostrophic winds, *Q. J. R. Meteorol. Soc.*, *52*, 85–104, 1923.

Kantha, L. H., and C. A. Clayson, An improved mixed layer model for geophysical applications, *J. Geophys. Res.*, in press, 1994.

Kastings, J. F., How climate evolved on terrestrial planets, *Sci. Am.*, *258*(2), 90–112, 1988.

Keen, R. A., Equatorial westerlies and the Southern Oscillation, in Proceedings of the U.S. TOGA Western Pacific Air-Sea Interaction Workshop, Honolulu, edited by R. Lukas and P. J. Webster, *U.S. TOGA Rep. USTOGA-8*, pp. 121–140, Univ. Corp. of Atmos. Res., Boulder, Colo., 1988.

Knox, R. A., and D. Halpern, Long range Kelvin wave propagation of transport variations in the Pacific Ocean equatorial currents, *J. Mar. Res.*, *40*, 329–339, 1982.

Kraus, E. B., and J. A. Turner, A one-dimensional model of the seasonal thermocline: The general theory and its consequences, *Tellus*, *19*, 98–105, 1967.

Lau, K.-M., and P. H. Chan, Intraseasonal and interannual variations of tropical convection: A possible link between the 40-day mode and ENSO, *J. Atmos. Sci.*, *45*, 950–972, 1982.

Levitus, S., Climatological atlas of the world ocean, *NOAA Prof. Pap. 13*, 163 pp., U.S. Govt. Print. Off., Washington, D. C., 1982.

Lewis, J. S., and R. G. Prinn, *Planets and Their Atmospheres: Origin and Evolution*, 470 pp., Academic, San Diego, Calif., 1984.

Lindzen, R. S., and S. Nigam, On the role of sea surface temperature gradients in forcing low level winds and convergence in the tropics, *J. Atmos. Sci.*, *44*, 2418–2436, 1987.

Liou, K.-N., *An Introduction to Atmospheric Radiation*, *Int. Geophys. Ser.*, vol. 26, 392 pp., Academic, San Diego, Calif., 1980.

Lukas, R., On the role of the western Pacific air-sea interaction in the El Niño Southern Oscillation Phenomena, in Proceedings of the U.S. TOGA Western Pacific Air-Sea Interaction Workshop, Honolulu, edited by R. Lukas and P. J. Webster, *U.S. TOGA Rep. USTOGA-8*, pp. 43–69, Univ. Corp. of Atmos. Res., Boulder, Colo., 1988.

Lukas, R., The role of salinity in the dynamics and thermodynamics of the western Pacific warm pool, in Proceedings of the International TOGA Conference, 16–20 July, 1990, Honolulu, Hawaii, *Rep. WCRP-43, WMO/TD. 379*, pp. 73–81, World Meteorol. Org., Geneva, 1990.

Lukas, R., and E. Lindstrom, The mixed layer of the western equatorial Pacific ocean, in Proceedings of the 'Aha Huliko'a Hawaiian Winter Workshop on the Dynamics of the Oceanic Surface Mixed Layer, Honolulu, Hawaii, edited by P. Muller and D. Henderson, special publication, pp. 67–94, Hawaii Inst. of Geophys., Honolulu, 1987.

Lukas, R., and E. Lindstrom, The mixed layer of the western equatorial Pacific Ocean, *J. Geophys. Res.*, *96*, 3343–3357, 1991.

Magaña, V., and M. Yanai, Tropical-midlatitude interaction on the time scale of 30 to 60 days during the northern summer of 1979, *J. Clim.*, *4*, 180–201, 1991.

McCormick, M. P., E.-W. Chiou, L. R. McMaster, W. P. Chu, J. C. Larsen, D. Rind, and S. Oltmans, Annual variations of water vapor in the stratosphere and upper troposphere observed by the Stratospheric Aerosol and Gas Experiment II, *J. Geophys. Res.*, *98*, 4867–4874, 1993.

Murakami, T., and S. Unninayer, Atmospheric circulation during December, 1970 through February, 1971, *Mon. Weather Rev.*, *105*, 1024–1038, 1977.

Neumann, G., and W. J. Pierson Jr., *Principals of Physical Oceanography*, 545 pp., Prentice-Hall, Englewood Cliffs, N. J., 1966.

Niiler, P. P., The ocean circulation, in *Climate System Modeling*, edited by K. E. Trenberth, pp. 117–148, Cambridge University Press, New York, 1992.

Oberhuber, J. M., An atlas based on the COADS data set: The budgets of heat, buoyancy and turbulent kinetic energy at the surface of the global ocean, *Rep. 15*, 20 pp., Max-Planck Inst., Hamburg, Germany, 1988.

Paltridge, G. W., and C. M. R. Platt, *Radiative Processes in Meteorology and Climatology*, *Dev. Atmos. Sci.*, vol. 5, 318 pp., Elsevier Science, New York, 1976.

Peixoto, J. P., and A. H. Oort, *Physics of Climate*, 520 pp., American Institute of Physics, New York, 1992.

Philander, S. G. H., *El Niño, La Niña and the Southern Oscillation*, 283 pp., Academic, San Diego, Calif., 1990.

Pond, S., and G. L. Pickard, *Introduction to Dynamical Oceanography*, 2nd ed., 329 pp., Pergamon, New York, 1983.

Potter, B. E., and J. R. Holton, The role of monsoon convection in the dehydration of the lower tropical stratosphere, *J. Atmos. Sci.*, in press, 1994.

Prinn, R., et al., Global average concentration and trend for hydroxyl radicals deduced from ALE/GAGE trichloroethane (methyl chloroform) data for 1978–1990, *J. Geophys. Res.*, *97*, 2445–2461, 1992.

Ramage, C., *Monsoon Meteorology*, *Int. Geophys. Ser.*, vol. 15, Academic, San Diego, Calif., 1971.

Ramanathan, V., Atmospheric general circulation and its low frequency variance: Radiative influences, *J. Meteorol. Soc. Jpn.*, *65*, spec. vol., 1512–1576, 1987.

Ramanathan, V., and W. Collins, Thermodynamic regulation of ocean warming by cirrus clouds deduced from observations of the 1987 El Niño, *Nature*, *351*, 27–32, 1991.

Randall, D., Harshvardhan, D. A. Dazlich, and T. G. Corsetti, Interactions among radiation, convection and large-scale dynamics in a general circulation model, *J. Atmos. Sci.*, *46*, 1943–1970, 1989.

Rasool, S. I., and C. de Bergh, The runaway greenhouse and the accumulation of CO_2 in the Venus atmosphere, *Nature*, *266*, 1037–1039, 1970.

Riehl, H., *Tropical Meteorology*, 392 pp., McGraw-Hill, New York, 1954.

Rind, D., E.-W. Chiou, W. Chu, S. Oltmans, J. Lerner, J. Larsen, M. P. McCormick, and L. McMaster, Overview of the Stratospheric Aerosol and Gas Experiment II water vapor observations: Method, validation, and data characteristics, *J. Geophys. Res.*, *98*, 4835–4856, 1993.

Shukla, J., and Y. Mintz, Influence of land-surface evapotranspiration on the Earth's climate, *Science*, *214*, 1498–1501, 1982.

Sikka, D., and S. Gadgil, On the maximum cloud zone and the ITCZ over Indian longitudes during the Southwest Monsoon, *Mon. Weather Rev.*, *108*, 1840–1853, 1980.

Simpson, J. J., and T. D. Dickey, The relationship between downward irradiance and upper ocean structure, *J. Phys. Oceanogr.*, *11*, 309–323, 1981.

Srinivasan, J., S. Gadgil, and P. J. Webster, Meridional

propagation of large-scale convective zones, *Meteorol. Atmos. Phys.*, *52*, 15–36, 1993.

Stephens, G. L., Radiative properties of extended water clouds, II, Parameterizations, *J. Atmos. Sci.*, *35*, 2133–2142, 1978.

Stephens, G. L., The relationship between water vapor over the oceans and sea surface temperatures, *J. Clim.*, *3*, 634–645, 1990.

Stephens, G. L., and A. Slingo, An air-conditioned greenhouse, *Nature*, *358*, 369–370, 1992.

Stephens, G. L., and P. J. Webster, Sensitivity of radiative forcing to variable cloud and moisture, *J. Atmos. Sci.*, *36*, 1542–1556, 1979.

Stephens, G. L., and P. J. Webster, Cloud decoupling of surface and upper radiation balances, *J. Atmos. Sci.*, *40*, 681–686, 1983.

Stommel, H., The abyssal circulation, *Deep Sea Res.*, *5*, 80–82, 1958.

Tomas, R., and P. J. Webster, Horizontal and vertical structure of cross-equatorial wave propagation, *J. Atmos. Sci.*, *51*, 1417–1430, 1994.

Trenberth, K., and A. Solomon, The global heat balance: Heat transports in the atmosphere and the ocean, *Clim. Dyn.*, in press, 1994.

Untersteiner, N., The cryosphere, in *The Global Climate*, edited by J. T. Houghton, pp. 121–137, Cambridge University Press, New York, 1984.

Walker, G. T., Correlations in seasonal variations of weather, III, A preliminary study of world weather, *Mem. 24*(4), pp. 75–131, Indian Meteorol. Dep., New Dehli, 1923.

Walker, G. T., Correlations in seasonal variations of weather, IV, A further study of world weather, *Mem. 24*(9), pp. 275–332, Indian Meteorol. Dep., New Dehli, 1925.

Wallace, J. M., and P. V. Hobbs, *Atmospheric Science: An Introductory Survey*, 467 pp., Academic, San Diego, Calif., 1977.

Webster, P. J., Response of the tropical atmosphere to local steady forcing, *Mon. Weather Rev.*, *100*, 518–540, 1972.

Webster, P. J., Temporal variation of low latitude zonal circulations, *Mon. Weather Rev.*, *101*, 803–816, 1973.

Webster, P. J., The low-latitude circulation of Mars, *Icarus*, *30*, 626–664, 1977.

Webster, P. J., Mechanisms of monsoon low-frequency variability: Surface hydrological effects, *J. Atmos. Sci.*, *40*, 2110–2124, 1983a.

Webster, P. J., The large scale structure of the tropical atmosphere, in *Large Scale Dynamical Processes in the Atmosphere*, edited by B. J. Hoskins and R. Pearce, pp. 235–276, Academic, San Diego, Calif., 1983b.

Webster, P. J., The elementary monsoon, in *Monsoons*, edited by J. S. Fein and P. L. Stephens, pp. 1–32, Wiley-Interscience, New York, 1987.

Webster, P. J., and L. Chou, Seasonal structure of a simple monsoon structure, *J. Atmos. Sci.*, *37*, 354–367, 1980a.

Webster, P. J., and L. Chou, Low frequency transition of a simple monsoon system, *J. Atmos. Sci.*, *37*, 368–382, 1980b.

Webster, P. J., and J. R. Holton, Cross equatorial response to midlatitude forcing in a zonally varying basic state, *J. Atmos. Sci.*, *39*, 722–733, 1982.

Webster, P. J., and R. Lukas, TOGA COARE: The Coupled Ocean-Atmosphere Response Experiment, *Bull. Am. Meteorol. Soc.*, *73*, 1377–1416, 1992.

Webster, P. J., and S. Yang, Monsoon and ENSO: Selectively interactive systems, *Q. J. R. Meteorol. Soc.*, *118*, 877–926, 1992.

Woods, J. D., The upper ocean and air-sea interaction in global climate, in *The Global Climate*, edited by J. J. Houghton, pp. 141–178, Cambridge University Press, New York, 1984.

World Climate Research Program (WCRP), Scientific plan for the Tropical Ocean Global Atmosphere Programme, *WCRP Publ. 3*, 146 pp., World Meteorol. Org., Geneva, 1985.

Worthington, L. V., The water masses of the world ocean: Some results of a fine scale census, in *Evolution of Physical Oceanography*, edited by B. A. Warren and C. Wunch, pp. 42–69, MIT Press, Cambridge, Mass., 1981.

Yang, S., and P. J. Webster, The effect of summer tropical heating on the location and intensity of the extratropical westerly jet streams, *J. Geophys. Res.*, *95*, 18,705–18,721, 1990.

Young, G. S., D. V. Ledvina, and C. W. Fairall, Influence of precipitating convection on the surface energy balance observed during a Tropical Ocean Global Atmosphere pilot cruise in the tropical western Pacific Ocean, *J. Geophys. Res.*, *97*, 9595–9603, 1992.

P. J. Webster, University of Colorado, Campus Box 311, Boulder, CO 80309. (e-mail: pjw@willywilly.colorado.edu)